PHOTOIONIZATION IN GASES

by

A.J.Blake B.Sc.(Hons.)

Department of Physics

A thesis
submitted for the degree of
Doctor of Philosophy
in the
University of Adelaide

August,1966

20th March, 1967

The Registrar,
University of Adelaide.

Dear Sir,

I hereby consent to my thesis 'Photoionization in Gases' being available for loan and for photo-copying.

Yours faithfully,

Alastair J. Blake

AJB/BJM

CONTENTS

SUMMARY

This thesis describes the measurement of partial photoionization cross-sections for processes which lead to the formation of the ion in a particular quantum state. Partial cross-sections for oxygen, nitrogen and water vapour have been measured.

Previous determinations of photoionization cross-sections have been limited to measurements of the total cross-section for a multiplicity of processes corresponding to transitions to any one of a number of quantum states of the ion. Two examples of total cross-section measurements are presented in this thesis. Total cross-sections of molecular oxygen have been measured in the region from 1050 Å to 1250 Å. This region includes the wavelength of hydrogen Lyman-α, an important emission line in the solar spectrum. A double parallel plate ion chamber has been used to measure total photoionisation cross-sections of nitric oxide in the region 1150 Å to 1350 Å. This chamber has also been used with argon to measure absolute beam intensities according to the method of Samson.

The partial photoionization cross-sections have been determined by recording the energy spectra of the photo-electrons. The spectrometer, which was of the

retarding potential type, consisted of three concentric cylindrical electrodes: a collimating electrode, an analysing grid, and an anode. A one-metre near normal incidence monochromator has been used with a slit width corresponding to a resolution of 10 Å. The monochromator has been equipped with a helium capillary discharge lamp powered by a condensed spark discharge.

Electron energy spectra have been recorded by differentiating the output of the electrometer which measured the electron current at the anode, and applying this signal and the retarding voltage to the Y and X axes respectively of an X-Y co-ordinate plotter. Smoothed spectra have been obtained by digitising the spectra and using the memory storage of a multichannel analyser to add several scans of the spectrum.

Interpretation of the spectra has been aided by a study of the spectra of argon and hydrogen, which contain a single line and a single band respectively in the range of wavelengths used. The peak in the argon spectrum had a width at half height of 0.4 eV under the best conditions.

Spectra have been obtained over a wavelength range from the threshold for the first excited state of the ion to 584 Å for oxygen, nitrogen and water vapour.

The relative area associated with each peak has been measured, and this information combined with the total photoionization cross-section data of Cook and Metzger to produce partial cross-sections.

The partial cross-sections of oxygen show the thresholds of the $b^4\Sigma_g$ and $a^4\Pi_u$ states of O_2^+; the $A^2\Pi_u$ and the $a^4\Pi_u$ states are not properly resolved. The continua are seen to have the form of a step function modified by competition between the continua, and by autoionizing processes. At wavelengths longer than the $a^4\Pi_u$ threshold the spectra have a large peak at low energy as well as the peak corresponding to the $^2\Pi_g$ ground state. It is suggested that fluorescence occurs from a highly excited level of O_2 before autoionization to the $X^2\Pi_g$ state of O_2^+.

The nitrogen results show the thresholds of the $B^2\Pi_u^+$ and $A^2\Pi_u$ states of N_2^+. All the continua have a maximum just below the threshold. The $B^2\Sigma_u^+$ continuum has a maximum value which is less than half the maximum values of the $A^2\Pi_u$ and $X^2\Sigma_g^+$ continua.

The water vapour results show the continua corresponding to the $^2B_1$ and $^2A_1$ levels of H_2O^+, and another corresponding to dissociative ionization. These continua have little structure, and the onset is more

gradual than in the case of oxygen and nitrogen.

The partial photoionisation cross-sections have been used in calculations of the energy distribution of primary photoelectrons in the ionosphere, and in calculations of the overhead intensities of various fluorescent band systems emitted in the ionosphere.

PREFACE

This thesis contains no material which has been accepted for the award of any other degree or diploma in any University. To the best of the author's knowledge and belief it contains no material previously published or written by another person, except where due reference is made in the text.

A. J. Blake

August, 1966

ACKNOWLEDGEMENTS

The measurements of the total absorption coefficients of molecular oxygen were carried out in co-operation with Mr.G.N.Haddad.

The author would like to thank Dr.M.H.Lokan for helpful discussion during the writing of this thesis, and to acknowledge helpful discussion with other members of the Physics Department.

Thanks are also due to the Workshop staff for the construction of the apparatus, and to Dr.R.L.Murray and the Electronics Technicians for assistance with the electronic circuits.

Finally, the author would like to thank his supervisor, Professor J.N.Carver, most sincerely for his guidance throughout the course of this work.

This investigation was carried out while the author was holding a Senior Postgraduate Studentship granted by the Commonwealth Scientific and Industrial Research Organization.

CHAPTER I

REVIEW OF THE PROCESSES OF PHOTOIONIZATION

I.1 Introduction

The term photoionization is applied to photon induced transitions to an unbound energy state of a gaseous atom or molecule, where the unbound state is that of a positively charged ion and a free electron. Several early attempts to observe photoionization produced in gases by ultraviolet radiation (Wilson 1899; Henry 1897; Lenard 1900) were not successful, but in 1910 Hughes (Hughes 1910) found that ultraviolet radiation entering an air filled chamber through a fluorite window produced positively charged ions, which had the same mobility as those produced by X-rays.* Wood (Wood 1911) observed the absorption spectrum of sodium vapour, and found that it consisted of a series of absorption lines, and a region of continuous absorption which extended from the limit of the line series towards shorter wavelengths.

---

*It must be noted that Hughes could not have observed the direct photoionization of any of the components of air, since a fluorite window ceases to be transparent at a wavelength longer than the ionization thresholds of these gases. Weissler (Weissler 1957) has suggested that Hughes may have observed the photoionization of dissociation products.

The nature of this spectrum was explained by Bohr (Bohr 1913) in terms of transitions between a quantised energy state, and an unquantised energy state of the atom.

The absorption spectrum observed by Wood may be understood by reference to the energy level diagram shown in Fig.1. The levels on the left hand side of the diagram indicate the energy states of the neutral atom, and those on the right hand side indicate the energy states of the positive ion. The absorption lines correspond to photon induced transitions between the ground state of the atom and higher bound levels of the atom. The absorption of a photon with an energy greater than the difference between the ground state of the atom and the ground state of the ion, may result in a transition to an unbound state. This energy difference, which is the amount of energy required to remove the least firmly bound electron from the atom, is of course the ionisation potential of the atom.

Because the final state in a photoionisation process is unbound, absorption may occur over a continuous range of wavelengths. The excess of the photon energy over the amount of energy required to produce the ion in its final state, appears as kinetic energy of the photo-ionisation products. Since the mass of the electron is much less than that of the atom, virtually all of the excess energy is carried away by the electron. Kunz and

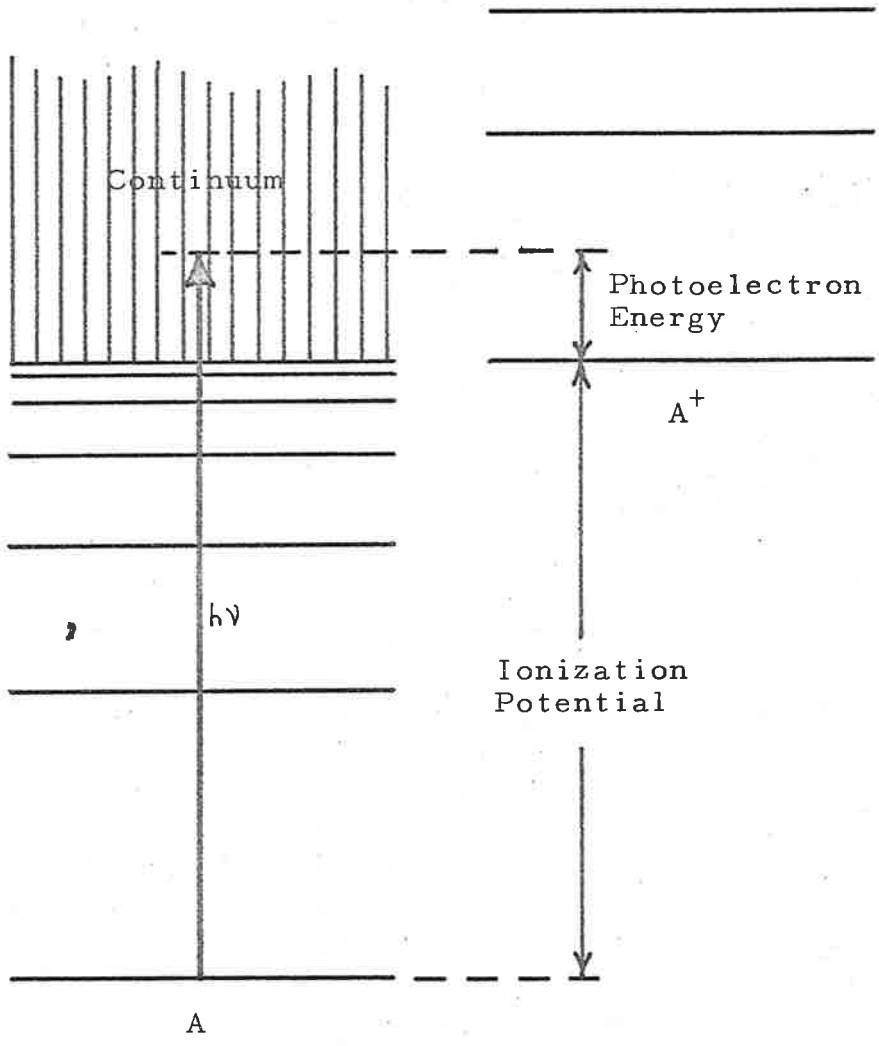

Fig.1. Energy levels of an atom A and the ion A^+, showing a photoionizing transition.

Williams (Lunz and Williams 1920, 1923) detected photoionization in caesium vapour over a continuous range of wavelengths shorter than a threshold at 3180 Å. This threshold agreed well with the ionization potential determined from the series limit of the lines in the absorption spectrum of caesium vapour.

Measurement of the cross-section for photoionization as a function of wavelength is a means of acquiring information about the energy states of the atom or molecule, and the nature of the photon induced transitions between these states. The cross-sections for the photoionization of many atomic gases have been calculated theoretically. In most cases many approximations are involved in the calculations, and a comparison of the theoretical cross-sections with the experimental measurements allows an evaluation of the various approximations to be made.

Recently the processes of photoionization have been studied experimentally in considerable detail. Absolute values of total photoionisation cross-sections have been measured as a function of wavelength (Weissler 1956) for many gases. The presence of line and band structure in these cross-sections led to the discovery of the process of auto-ionization (see Sec.1.3.2). When photoionization occurs, the residual ion may in general be formed in any of its energy states which are separated from the ground

state of the neutral atom or molecule by less than the photon energy. Thus the total cross-section represents the sum of many competing photoionizing processes, and provides no information about which of these are occurring. For molecular gases the cross section may also include a contribution from dissociative ionisation; dissociative photoionization has been distinguished from the former process by identifying the ionization products with a mass spectrometer. (Hurzeler et al 1957). Some information about the nature of the photoionization process has been gained from the study of the threshold behaviour of the cross-section. (Morrison 1962).

Although a knowledge of the energies of the various states is sufficient to decide in which states it is energetically possible for the ions to be formed, the existing experimental data provides very little information about the final states of the ions produced by photo-ionization. It is therefore desirable that experiments should be conducted to measure the partial photoionization cross-sections for the formation of ions in particular states. Partial photoionization cross-sections are also required for application to ionospheric problems. Photo-ionization of atmospheric gases by solar ultraviolet radiation makes an important contribution to the formation of the ionosphere. (Hinteregger et al 1964). Total

photoionization cross-sections are sufficient to account for the production of these electrons, but their subsequent behaviour cannot be predicted without a knowledge of their initial energy distribution, and this can only be determined if the partial photoionization cross-sections are known. (Dalgarno et al 1963). Partial cross-sections are also required in order to predict the intensity and spectral distribution of fluorescent radiation emitted in the ionosphere when ions produced in an excited state return to the ground state. (Dalgarno et al 1965).

Both of the ionospheric problems indicate methods of measuring partial photoionization cross-sections. The determination of the intensity of fluorescent radiation (Judge et al 1963) provides a measure of the number of ions produced in the higher of the states involved in the transition, but the method is not very satisfactory because of the experimental difficulties. A more satisfactory source of information is provided by a measurement of the energy distribution of the photoelectrons. Partial photoionisation cross-sections have been obtained by Schoen, (Schoen 1964), but his measurements contain insufficient detail to make a detailed interpretation. The object of the present work has been to obtain more accurate and more detailed partial photoionization cross-sections,

particularly in the atmospheric gases. A photoelectron spectrometer of moderate resolution is also a powerful tool for the investigation of the process of autoionisation. (See Chapter IV).

I.2 Calculation of Photoionization Cross-sections.

The experimental determination of photoionisation cross-sections have in many cases been preceded by theoretical calculations of the cross-sections. In all but the simplest cases these calculations involve many approximations, and a comparison of the theoretical and the experimental cross-sections provides a test of the approximations used in the calculations.

I.2.1 The dipole approximation

The theory of quantum electrodynamics provides an explicit formulation of the problem of photoionization in terms of the initial and final state wavefunctions. (Bethe and Salpeter 1956). Let Φ_0 be the wavefunction of the initial bound state of the atom, and Φ_n be the continuum wavefunction, normalised to unit energy range, of the system consisting of the ion and the free electron. If radiation with frequency ν such that $h\nu > I$ is incident on the gas, where I is the ionisation potential of the gas, then the cross-section for the absorption of a photon is:

$$\sigma_\nu = \frac{2\pi e^2 \hbar^2}{m^2 c\nu} \left| R_{n0} \right|^2 \qquad (1)$$

In (1) R_{n0} is the matrix element:

$$R_{n0} = \int \Phi_n^* \sum_i e^{i\underline{k}\cdot\underline{r}_i} \text{grad}_i \Phi \, d\tau \qquad (2)$$

where r_i is the position of the i^{th} electron, and the integral extends over the configuration space of all electrons. It must be remembered that the final state refers to absorption processes which lead to the ejection of the electron with specific values of the quantum numbers ℓ and m. To obtain the total cross-section the equation must be summed over all possible values of ℓ and m for the electron.

For the absorption of ultraviolet radiation by gases, $\underline{k}.\underline{r} \leq 10^{-3}$, and equation (2) may be simplified by replacing the exponential term by unity. Physically, this corresponds to assuming no change in the phase of the electric field over the dimensions of the atom, which is the situation for a classical oscillating dipole. Thus only 'electric dipole' transitions need to be considered. With this approximation the matrix element becomes:

$$R_{n0} = \frac{2\pi m\nu}{h} r_{n0} \qquad (3)$$

where r_{n0} is the dipole length matrix element:

$$r_{n0} = \int \Phi_n^* \sum_i \underline{r}_i \, \Phi_0 \, d\tau \qquad (4)$$

Two other exactly equivalent forms of the dipole matrix element may be found: the dipole velocity, and the

dipole acceleration matrix elements. Each of these matrix elements places a different emphasis on the wavefunctions, and the degree of agreement between cross-sections calculated using the three forms of the matrix element indicates the accuracy of the wavefunctions used in the calculations. (Cooper 1962).

I.2.2 The hydrogen atom

Unfortunately the expressions of the previous section can be applied exactly only to the case of atomic hydrogen, since only in this case can analytic expressions for the wavefunctions be obtained. The expression for the total cross-section for the absorption of radiation of frequency ν by a hydrogen-like atom is: (Ditchburn and Opik 1962)

$$\sigma(\nu,n) = g(32\pi^2 e^6 RZ^4)/(3^{\frac{3}{2}} h^3 \nu^3 n^5) \qquad (5)$$

where R is the Rydberg constant, n is the principle quantum number of the initial state, Z is the nuclear charge, and g is a complicated factor depending on n and the energy of the final state, with a value close to unity.

In some circumstances the hydrogen atom type of calculation may be used as an approximation for other atoms. When the energy difference between the initial and final states is large, as in the case of X-ray absorption, the calculation is insensitive to the details of the initial state wavefunction, and therefore a

hydrogen atom treatment is sufficient. Also an atom in a highly excited initial state is very much like a hydrogen atom.

The absorption cross-section of equation (1) is related to the attenuation of the intensity of a beam of radiation as it travels through the gas by Beer's law:

$$I = I_0 e^{-\rho\sigma l} \qquad (6)$$

Beynon and Cairns (Beynon and Cairns 1965) have recently made an experimental determination of the absorption cross-section of atomic hydrogen at 850.6Å. The good agreement between their value and the theoretical value (Ditchburn and Opik 1962) indicates the validity of the assumptions on which the theoretical calculation is based.

It is interesting to note that in the case of the photoionisation of atomic hydrogen only one final state exists, and the cross-section does not consist of a number of overlapping continua corresponding to different states of the ion. For other atoms the ion has many excited states, and the total photoionization cross-section is the sum of many partial cross-sections.

I.2.3 Approximations to other wavefunctions.

The equation for the wavefunctions required for the calculation of photoionization cross-sections cannot be solved, except in the case of hydrogen-like atoms. However, there are various methods for obtaining approximate

wavefunctions which may be used to estimate the cross-sections. A mathematical model of the atom must be chosen which is good enough to make the results useful, but simple enough to be practicable. (Hartree 1957).

Most simple calculations are based on two general approximations. The first is that the electrons may be considered to move in a central potential V(r), which is not necessarily a Coulomb potential, when the Schroedinger equation has the form:

$$\nabla^2 \Phi + \frac{2m}{\hbar^2}\left[E - V(r)\right]\Phi = 0 \qquad (7)$$

When expressed in spherical polar co-ordinates this equation separates into an angular component, which is the same for all central potentials, and a radial component.

The other approximation is the assumption that each electron moves in a stationary state in the field of the nucleus and the other electrons. Wave mechanically this approximation is expressed in terms of separated wavefunctions:

$$\Phi = \psi_\alpha(1)\,\psi_\beta(2) \ldots\ldots \psi_\pi(p) \qquad (8)$$

where $\psi_\pi(p)$ is the wavefunction of the p^{th} electron in the π^{th} state. The wavefunction is made to conform to the Pauli principle by writing it in the form ofa Slater determinant. This also makes allowance for electron exchange, since it is not specified which electron is in

each of the single electron states.

The most commonly used wavefunctions are those calculated by the Hartee-Fock method (Hartee 1957). This method is based on the approximations outlined above, and the accuracy of the wavefunctions is optimised by using the variation principle to minimise the total energy of the system, calculated from the expression:

$$E' = \frac{\int \Phi^* H \Phi \, dt}{\int \Phi^* \Phi \, dt} \qquad (9)$$

Other more sophisticated wavefunctions which have been obtained include those in which a term is added to the potential to allow for polarization of the core of the atom. (Bates and Massey 1943).

Further approximations must be made in forming the continuum wavefunction. The final state is that of an unbound electron moving in the field of the ion, and there are two common approximations to the field in which the electron moves. In the unrelaxed core approximation, (Cooper 1962) it is assumed that of the N single electron wavefunctions of the initial state of the atom, N-1 remain unchanged after ionisation. That is, apart from the removal of one electron, the atom is unchanged, and the effect that the free electron has on the others is ignored.

The matrix element then involves only the spatial distribution of one electron before and after ionization:

$$r_{n0} = \int \psi_0 \, r \, \psi_n \, d\tau \qquad (10)$$

In the relaxed core approximation, (Seaton 1951) the continuum wavefunction is taken to be the anti-symmetrized product of a free electron wavefunction and the single electron wavefunctions of the ionic core. The effect of the outgoing electron on the ionic field is ignored. The best central field will, of course, be something between these two extreme cases. Close to the nucleus the field is probably like the unrelaxed core field, while near the edge of the atom the relaxed core is a good approximation. Thus, in low energy calculations, where the region near the edge of the atom is important, the relaxed core model offers the better approximation. (Cooper 1962).

I.2.4 Sum rules

The probability for a transition between two states may be expressed in terms of the oscillator strength, f_{n0}, defined by the expression:

$$f_{n0} = \frac{\epsilon}{3} \left| r_{n0} \right|^2 \qquad (11)$$

where ϵ is the energy difference between the two states, and r_{n0} is the dipole matrix element. Various moments of the oscillator strength distribution, defined by

$$\mu_p = \sum_n f_{n0} \epsilon^p \qquad (12)$$

may be evaluated to yield the sum rules:
(Dalgarno and Lynn 1957; Piecbe and Levinger 1964; and Lowry et al 1965)

$$\mu_{-2} = \sum_n f_{n0}\, \epsilon_{n0}^{-2} = \frac{\alpha}{4} \tag{13}$$

$$\mu_{-1} = \frac{1}{3} \sum_{i \neq j} \int \Phi_0^* \, \underline{r}_i \cdot \underline{r}_j \, \Phi \, dr - \frac{\chi}{2.64 \times 10^{-7}} \tag{14}$$

$$\mu_0 = Z \qquad \text{(Thomas-Reich-Kuhn sum rule)} \tag{15}$$

$$\mu_1 = \frac{4}{3} \left\{ E_0 + \frac{1}{2} \sum_{i \neq j} \int \Phi^* \underline{p}_i \cdot \underline{p}_j \, \Phi \, dr \right\} \tag{16}$$

$$\mu_2 = \frac{16\pi Z}{3} \sum_i \int \Phi_0^* \, \delta(r_i) \, \Phi_0 \, dr \tag{17}$$

where α is the atomic polarisability, and χ is the diamagnetic susceptibility. These sum rules are important because they relate the integrated oscillator strength to the static parameters without any knowledge of the final state wavefunctions.

The sum rules have been verified in the case of helium, (Migneron and Levinger 1965; and Samson 1964a) and neon.(Piech and Levinger 1964; and Samson 1965). They may be used to extrapolate cross-section data to wavelength regions which are experimentally inaccessable. (Cooper 1962).

I.3 Atomic Photoionisation Cross-sections

Measurement of the photoionisation cross-sections

of atomic gases provides a valuable method of studying photoionization processes because these gases have relatively simple absorption spectra. Theoretical cross-sections are available for many atomic gases, and a comparison of these with the experimental cross-sections allows an evaluation of the various methods of calculation to be made.

I.3.1 Comparison between experimental and theoretical cross-sections

There is good agreement between the cross-sections obtained by the theoretical methods outlined above, and the experimental results for the rare gases. (Po Lee and Weissler 1952; 1955; Axlerod and Givens 1959; Ditchburn 1960; Baker et al 1961; Huffman et al 1963a; Perry-Thorne and Garton 1960; Ederer and Tomboulian 1964; Rustgi 1964; Rustgi et al 1964; Matsunaga et al 1965; Metzger and Cook 1965; Samson 1964a, 1964b, 1964c, 1965; Cairns and Samson 1965a; and Lowry et al 1965). In the case of helium the agreement is excellent, and it is only recently that the scatter in the experimental data has been reduced sufficiently to choose between the various theoretical approaches. Samson (Samson 1964a) found that his results were in best agreement with the calculations of Stewart and Webb, (Stewart and Webb 1963) who used Hartree-Fock wavefunctions.

Calculations of the neon cross-section (Sewell 1965) predict an absorption jump of up to 18% at the L_1 absorption edge, which is the threshold for the ejection of 2s electrons. This jump has not been observed in the experimental results. (Samson 1965). This does not necessarily imply that the ejection of 2s electrons does not contribute to the cross-section at energies higher than the L_1 edge, but may indicate a redistribution of the total cross-section among the possible disintegration processes. Samson has suggested that the partial photo-ionization cross-sections of the rare gases at energies higher than the L_1 edge be determined. This could be achieved by measuring the relative numbers of electrons ejected with energies corresponding to the excess of the photon energy over the energies of the L_1 and L_3 edges respectively. The measurement was not made in the present work because a suitable light source was not available. The N_1 absorption edge of krypton is also interesting, since a negative absorption jump is observed. (Samson 1963).

The total absorption cross-section of atomic oxygen has been measured by Cairns and Samson. (Cairns and Samson 1965b). Their results tend to be higher than the theoretical results, (Dalgarno et al 1964) but because of the experimental difficulties the scatter in their results is too large to reveal any autoionized structure

which may be present.

I.3.2 Autoionization

While examining the absorption spectra of the rare gases, Beutler (Beutler 1935) identified members of two Rydberg series between the $^2P^o_{3/2}$ and $^2P_{1/2}$ limits of argon, krypton, and xenon. The unusual features of these lines were that they were very broad, and they were asymmetrical in shape, tailing off towards shorter wave-lengths.

The width of these lines was explained by assuming that an atom excited into one of the states indicated by the absorption lines subsequently underwent a transition into the $^2P^o_{3/2}$ ionization continuum, the excess energy being carried off by the photoelectron. If the lifetime of the intermediate state was very short, then the level would not be well defined. This interpretation was also indicated by the fact that the line structure appeared in the photoionization cross-sections of the rare gases. (Metzger and Cook 1965). The process was called auto-ionization, or sometimes, preionization. In Fig.2 the transitions involved in an auto-ionising process are illustrated.

The presence of auto-ionized lines in the absorption spectrum of helium (Madden and Codling 1963) indicates that both of the electrons in the helium atom are being excited to form a quasi-stable state, which decays into

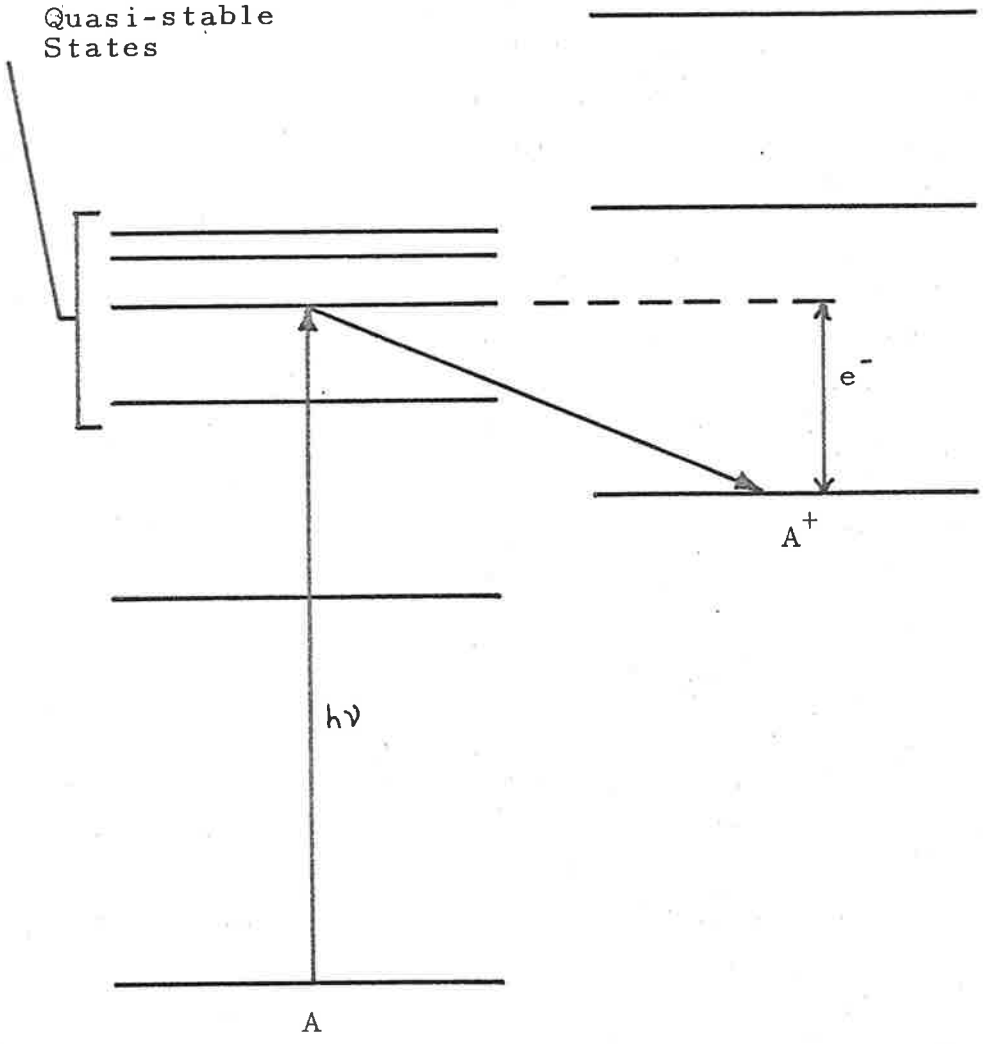

Fig.2. Energy levels of an atom A and the ion A^+, showing an auto-ionizing transition.

the ionization continuum when all of the excitation energy is transferred to one of the electrons. This is the simplest type of auto-ionizing transition which may occur. In more complex atoms other changes in the core may occur to produce a quasi-stable state which overlaps the continuum.

A simple explanation of the asymmetric shape of the absorption lines has been given by Morrison. (Morrison 1962). He considers the autoionization process to be intermediate between an excitation which gives a sharp absorption line, and a 'direct' ionization process which results in an ionization continuum extending below a threshold wavelength. These processes represent extreme values of the lifetime of the intermediate state.

A comprehensive analysis of the profiles of autoionized absorption lines has been given by Fano and Cooper. (Fano 1961; Fano and Cooper 1965). They considered the problem of the configuration interaction between a discrete state and an overlapping continuum, and found that the profiles of the autoionized lines may be represented by the formula:

$$\sigma(\epsilon) = \sigma_a \left[(q + \epsilon)^2 / (1 + \epsilon^2) \right] + \sigma_b \qquad (18)$$

where

$$\epsilon = (E - E_r)/\tfrac{1}{2}\Gamma$$

In this expression E_r is the unperturbed energy of the discrete state, E is the photon energy, and h/Γ is the mean life-time of the level with respect to autoionisation. The absorption co-efficient has two components, the second (σ_b) referring to direct ionisation. The line profile is characterised by the numerical index q, and profiles for several values of q are shown in Fig.3. Autoionized line profiles corresponding to a large range of values of q have been observed in the rare gases. (see for example Samson 1963; Madden and Codling 1963, 1964).

Experimental determinations of the photoionisation yield, which is defined as the number of ions produced per photon absorbed, have shown that the yield of the rare gases between the $^2P^0_{3/2}$ and $^2P^0_{1/2}$ limits is equal to unity. (Samson 1964d; Matsunaga et al 1965). This indicates that all of the atoms excited to the autoionizing levels in this region undergo transitions to the ionization continuum. The results of experiments with molecular oxygen which are presented in this thesis, (Sec.IV.1.6) indicate that a fluorescent transition from the autoionizing state to a lower autoionizing state may occur before the transition to the ionization continuum.

Structure due to autoionization has also been observed by electron impact, (Morrison 1964) and by positive ion bombardment. (Rudd 1964).

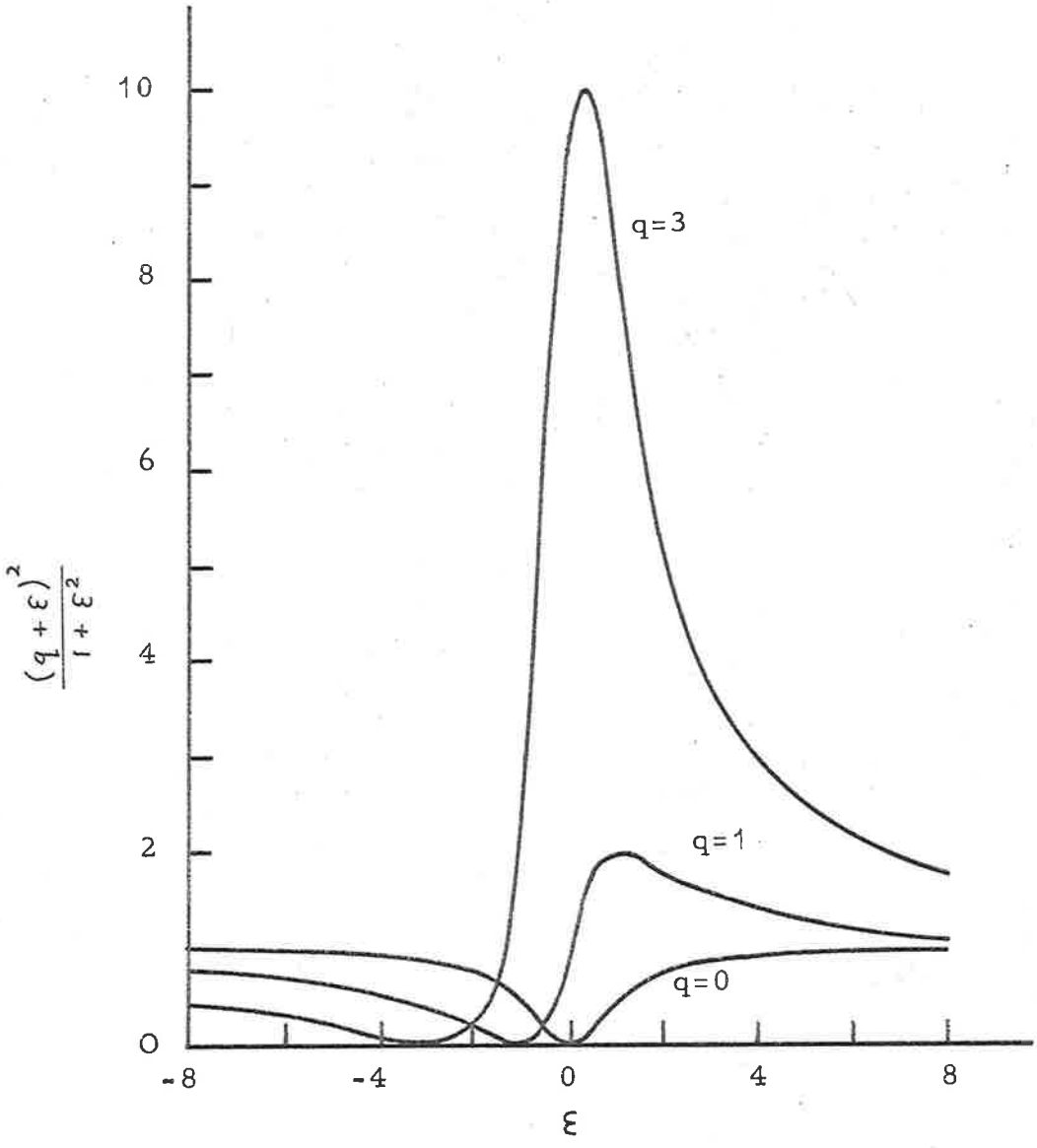

Fig.3. Autoionized line profiles for several values of q. (Fano 1961)

I.4 Molecular Photoionization Cross-sections

Molecular gases in general have absorption spectra which are far more complex than atomic absorption spectra, and for this reason they are less useful for studying the basic processes of photoionization. However, the photoionization of molecular gases in the atmosphere by solar ultraviolet radiation makes the study of these gases important.

I.4.1 Molecular spectra

The complexity of molecular spectra is a result of the vast number of molecular energy states which exist, each electronic level having fine structure due to vibration within the molecule, and rotation of the molecule. Instead of the absorption lines of the atomic spectra there are many absorption bands with rotational fine structure.

Occasionally a number of bands are observed which may be fitted to a Rydberg series converging to an ionization potential of the molecule. More often the bands form vibrational progressions, representing a series of transitions in which only two electronic states are involved. Such a series of bands tends towards a limit at a dissociation potential of the molecule, which is the energy required to split the molecule into its constituent atoms. The spectra of diatomic molecules have been reviewed by Herzberg. (Herzberg 1950).

The energy levels of a diatomic molecule may be pictured in terms of potential energy curves in which the potential energy of the molecule is plotted against the internuclear distance. A potential energy curve for a hypothetical state of a diatomic molecule is shown in Fig.4. This curve shows the equilibrium internuclear distance r_o of the state, the vibrational levels of the state, and the amount of vibrational energy D_o required to dissociate the molecule from the lowest vibrational level. The kinetic energy of the nuclei for a given separation is represented by the vertical distance between the appropriate vibrational level and the potential energy curve. Gilmore (Gilmore 1965) has reviewed the potential energy curves of several atmospheric molecules, and the curves for some of the states of molecular oxygen given by him are shown in Fig.5.

I.4.2 The Frank-Condon principle

If a transition occurs in a diatomic molecule between the lowest vibrational levels of two electronic states which have different equilibrium internuclear distances, then the relative positions or moments of the nuclei must change during the transition. The Frank-Condon principle states that such a transition is unlikely to occur, since electronic transitions occur in a time too short for the relatively massive nuclei to change their

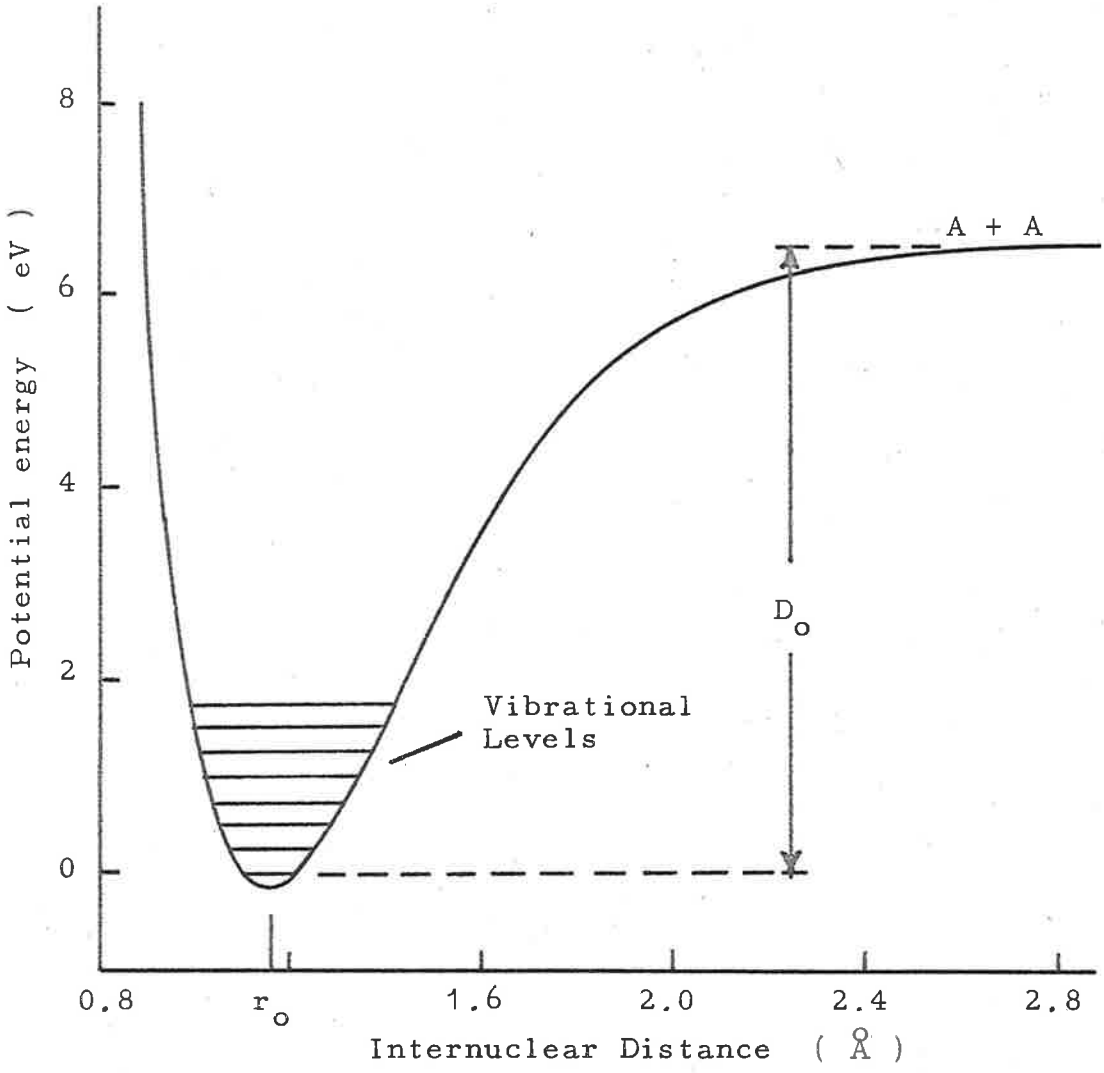

Fig.4 Potential energy curve for a hypothetical diatomic molecule A_2

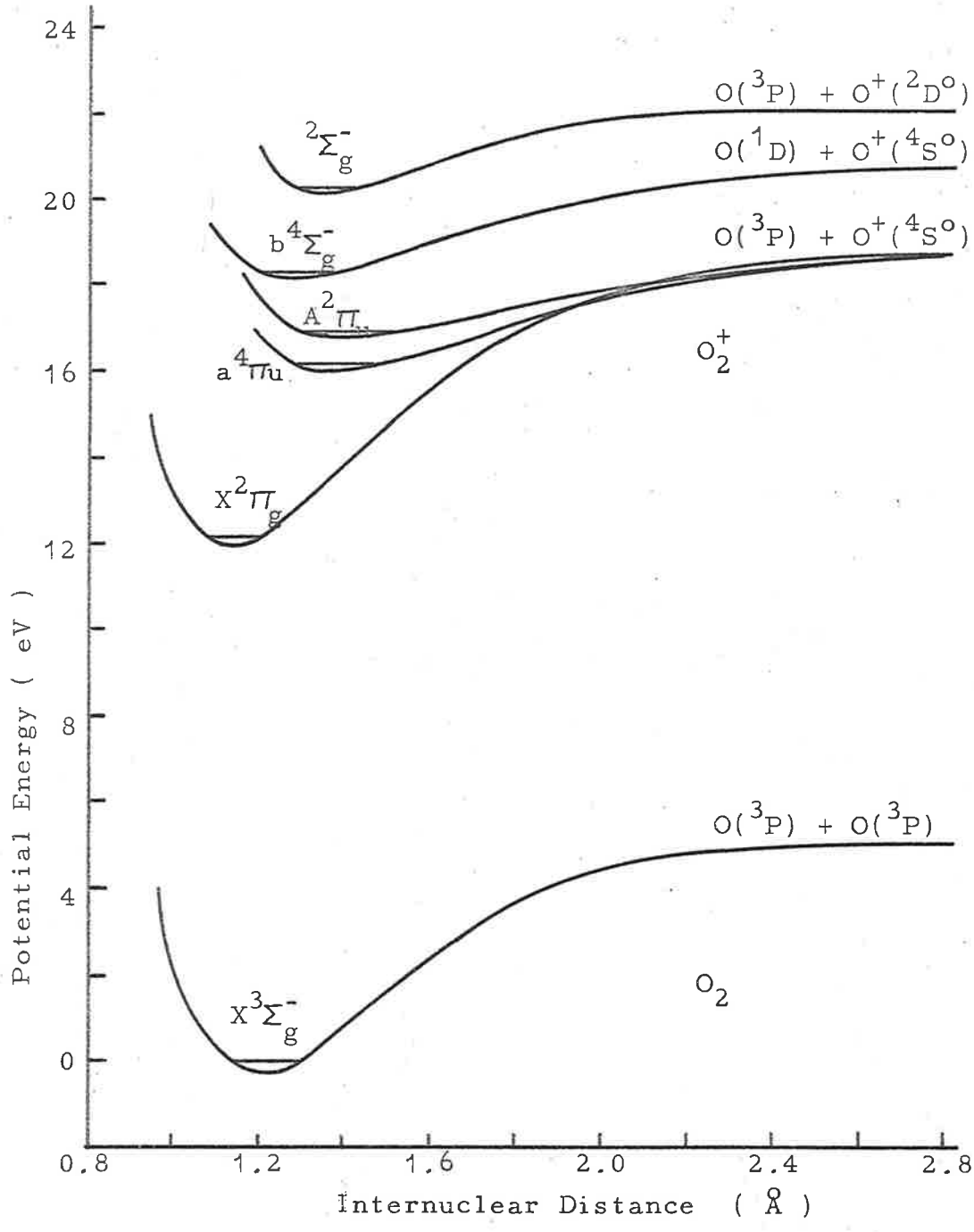

Fig.5. Potential energy curves for O_2 and O_2^+.
(Gilmore 1965)

positions, or their momenta.

The most probable transition is the one which is represented by the vertical line on the potential energy diagram in Fig.6, and the transition is to the vibrational level closest to the point of intersection of the vertical line and the potential curve. Such transitions, which satisfy the condition that neither the positions nor the momenta of the nuclei change, are often referred to as 'vertical' transitions. They correspond to transitions between two states with similar wavefunctions. The principle may be extended to estimate the distribution of intensity among the bands. (Herzberg 1950).

I.4.3 Ionization potentials of molecules.

The determination of the ionization potentials of atomic gases is relatively simple, since Rydberg series may be observed which converge to the ionization potential. However, in only a few cases have Rydberg series been found in molecular spectra.

Ionization potentials which cannot be determined by spectroscopic methods may be found by electrical methods. These methods depend on the observation of the onset of ionization in the gas as the wavelength of an incident monochromatic beam of radiation is swept past the threshold. There has been some dispute about the best method of interpreting the experimental data. In a simple experiment

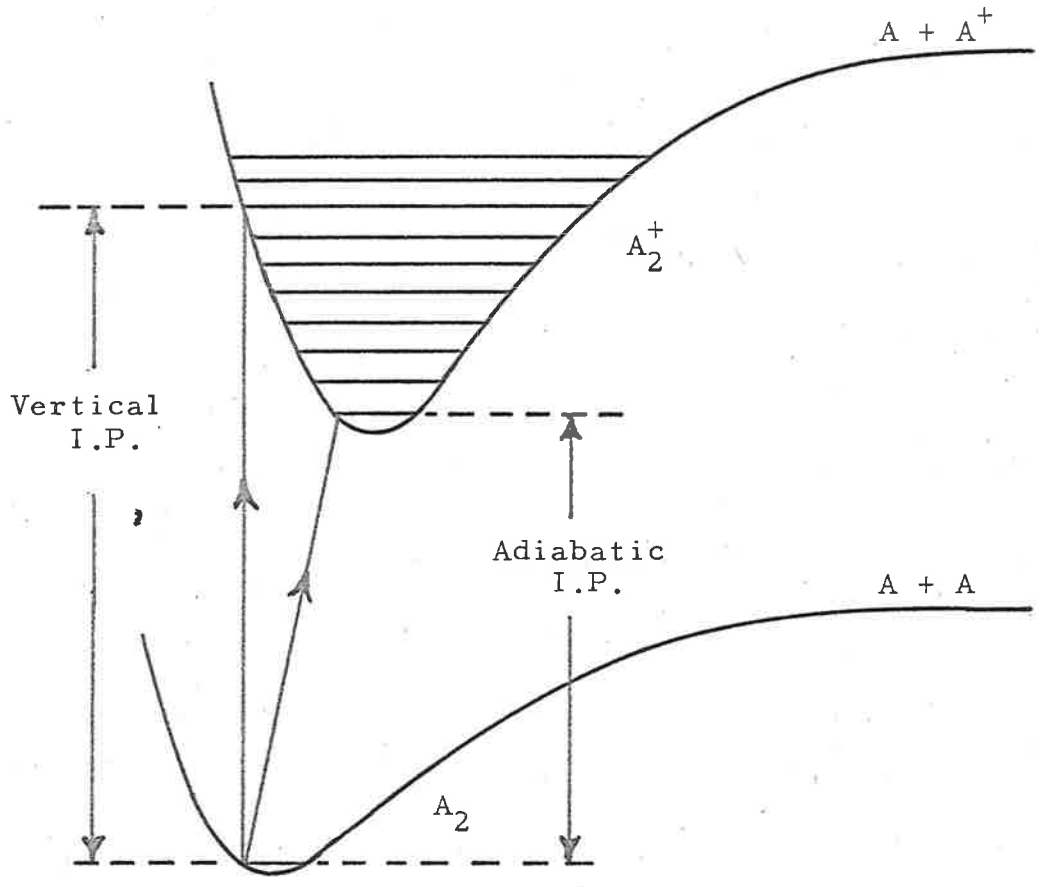

Fig.6 Potential energy diagram showing a vertical transition, and the vertical and adiabatic ionization potentials.

where only the wavelength of the onset of ionisation is measured, there is considerable difficulty in relating the measurement to a particular transition in the molecule, because of possible Frank-Condon effects. Since the onset of ionization in a molecular gas is often very gradual, the value obtained for the threshold wavelength will depend on the sensitivity of the experiment.

In most 'photoionisation' methods of determining ionization potentials the shape of the photoionization cross-section curve near the threshold is measured. Interpretation of this curve helps the experimenter to decide whether the 'vertical' or the 'adiabatic' ionisation potential is being measured. The 'vertical' ionization potential corresponds to a 'vertical' transition in the Frank-Condon sense, while the 'adiabatic' ionization potential refers to a transition between the lowest vibrational levels of the two states. Where the two electronic states concerned have different internuclear distances, the vertical and adiabatic values of the ionization potential are different, as shown in Fig.6.

Watanabe (Watanabe 1954, 1957) chose to associate the ionization potential with the point at which the experimental curve changed direction abruptly. Nicholson (Nicholson 1963) associated the ionization potential with the steepest part of the cross-section curve. These two

interpretations give results which are in good agreement, except when the energy spread in the beam is large, and then Nicholson's method is probably more accurate. Hurzeler et al (Hurzeler et al 1957) formed the first derivative of the photoionization cross-section curve near threshold, and interpreted this as the profile of the probability distribution among the vibrational levels. The vertical ionization potential was associated with the peak of this distribution, and the adiabatic ionization potential was associated with a sharp cutoff in the distribution. However, there is some uncertainty in all of these interpretations, and the most reliable values are obtained when the vertical and adiabatic ionization potentials are nearly the same. Another source of uncertainty in the photoionization method of determining ionization potentials occurs in cases where the ionization potential may be confused with the threshold of a dissociative ionization process. This uncertainty has been removed by the identification with a mass spectrometer of the ions produced by photoionization. (Hurzeler et al 1957).

I.4.4 Threshold behaviour of ionization

Theoretical cross-sections for the photoionization of molecular gases have not been calculated in most cases, because sufficiently accurate wavefunctions are not available. However, the way in which the cross-section increases from

threshold has been predicted with simple models.

Wigner (Wigner 1948) predicted that the threshold law for processes such as photoionization, where the products are oppositely charged, should be a step function. This is in good agreement with the increase of the total photoionization cross-section of nitric oxide from threshold, (Watanabe et al 1953b; Watanabe 1954; Nicholson 1963; and the present work, Sec. II.3.5) where a series of steps indicate the thresholds of excited vibrational states of the ion. The cross-section for the photoionization of helium, (Samson 1964a) where only a single ionizing process may occur for some 30 eV above the threshold, shows a sharp increase from threshold, and a gradual decrease towards shorter wavelengths.

It is interesting to compare the threshold behaviour of photoionization with that of ionization by electron impact. In an ionizing collision with a molecule, an electron may retain any amount of energy between zero and the excess of its initial energy over the ionization potential of the molecule. Comparing this with photo-ionization, where only a discrete amount of energy may be absorbed, the electron impact cross-section might be expected to be similar to the integral of the photoionization cross-section. If the photoionization cross-section increases from threshold like a step function, then the

electron impact cross-section should increase linearly from threshold. A linear increase from threshold has been predicted by Wannier. (Wannier 1956). Experimentally, electron impact cross-sections have been shown to increase linearly from threshold over a region of several electron volts. (Morrison 1962).

It is often found that values of ionization potentials measured by electron impact methods are higher than those measured by photoionization methods. The assumption has commonly been made that electron impact methods lead to the vertical ionization potential, and that the photoionization methods give the adiabatic value. Nicholson (Nicholson 1965) has suggested that this is only true to the extent that low resolution experiments would tend to give the vertical ionization potential, and that many electron impact experiments have had a low resolution. It would seem that a more fundamental difference between the methods arises from the fact that the electron is charged. The incident electron cannot lose all of its initial energy during a collision, but must retain sufficient to carry it away from the molecule. This is illustrated by Wannier's model. (Wannier 1956).

McGowan et al (McGowan et al 1964) have obtained a value for the ionization potential of molecular oxygen by electron impact which is in good agreement with values

obtained by photoionization, using the ionization potential of molecular nitrogen as a standard to calibrate the energy scale. They have also compared the derivative of their electron impact cross-section for oxygen with the photoionization cross-section obtained by Nicholson. (Nicholson 1963). Both curves have the same structure, indicating that similar autoionizing processes occur in each case.

I.4.5 Total photoionization cross-sections

Total photoionization cross-sections may be determined by measuring both the total absorption cross-section and the photoionization yield of the gas. These cross-sections provide information only about the total number of ions produced, and do not distinguish between the final states of the ions, or the various dissociative ionization processes which may occur. It might be expected that steps in the cross-section curve would indicate the thresholds of new ionizing processes, but rarely are well defined steps observed.

An example of such steps is provided by the total photoionization cross-section of nitric oxide. (Sec.II.3.5). These steps are associated with the vibrational levels of the ground state of the NO^+ ion. (Watanabe 1954). The relative heights of these steps indicate the relative probabilities of the transitions, and thus provide some information about the potential energy curves of the states

involved. (Morrison 1962).

The total photoionization cross-section of oxygen (Metzger and Cook 1964a) shown in Fig.7 is typical of molecular cross-sections. The complex autoionized band structure conceals most of the structure in the continuum. The broad, poorly defined maxima in the continuous part of the cross-section may indicate individual continua, corresponding to excited states of the ion. (Cook and Metzger 1964a). However, the results presented in Chapter IV indicate that because of the interaction between the continua, the individual continua are not indicated clearly by the total cross-section. The value of the photoionization yield of molecular gases is usually less than unity, indicating that dissociation processes also occur*. Measurements of the total photoionization cross-sections of molecular gases have been reviewed by Weissler**. (Weissler 1956).

I.4.6 Dissociative ionization

It was mentioned in section I.4.3 that the application of the mass spectrometer to the identification of

---

* Photon scattering may also occur, but these processes have cross-sections several orders of magnitude smaller than other absorption processes (Heddle 1962).

** See also Cook and Metzger 1964a, 1964b; Samson and Cairns 1964; Cook and Ogawa 1965; Nicholson 1963; Metzger and Cook 1964a; and Watanabe and Jursa 1964 for more recent measurements with atmospheric gases.

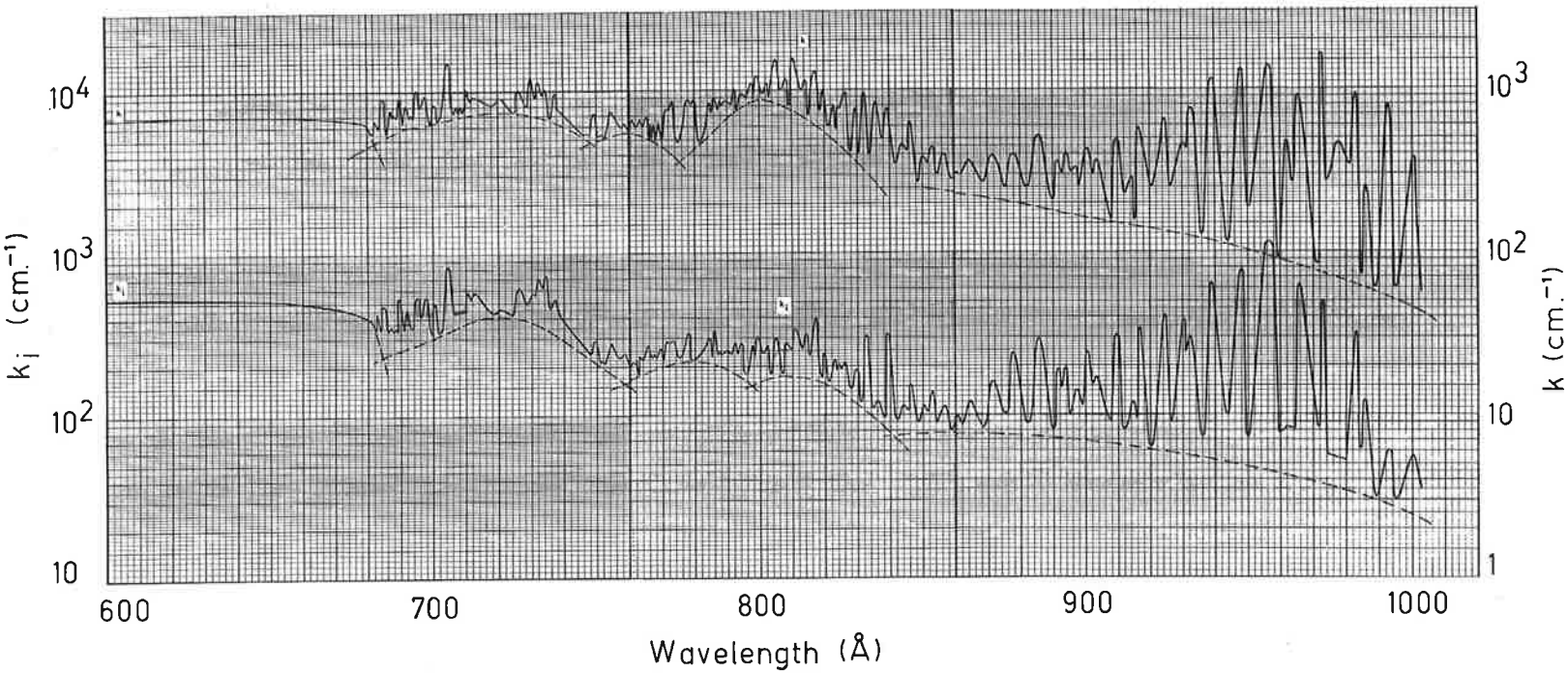

Fig. 7. Total photoionization coefficient (lower curve) and total absorption coefficient (upper curve) of O_2 (Cook and Metzger 1964a)

photoionization products allowed processes of dissociative ionization to be distinguished from other photoionization processes. This technique has been used to measure the relative cross-sections for the production of each particular ion fragment. The early results of Weissler et al (Weissler et al 1959) do not correspond well with measurements of the total photoionization cross-sections by other methods, but they show that for O_2, N_2, NO, and other diatomic and triatomic molecules, dissociative ionization accounts for less than ten percent of the total number of ions produced.

There are considerable difficulties in measuring the relative numbers of different ions, because of the effect of the ion mass and energy on the collecting efficiency of the apparatus. In most of the experiments of this type, it is the shape of the cross-section curve for the production of a particular ion that has been measured. Dibeler et al (Dibeler et al 1965a) have studied the structure due to autoionization in the cross-sections for the formation of H_2^+, HD^+, and D_2^+. Other molecules have been studied by: Dibeler and Reese 1964a, 1964b; Wacks and Krauss 1961; and Dibeler et al 1965b.

I.4.7 Thresholds of excited ionic states

The energies of some excited states have been determined directly from spectroscopic data. These levels

are determined to a typical accuracy of 0.001 eV. In many cases where no Rydberg series have been found, the energy of the state has been related to that of another state by the observation of fluorescent radiation emitted when transitions between the two states occur. Some levels have been related in this way to ionization potentials which have been determined by photoionization methods to an accuracy of about 0.01 eV. For some levels the best values available are those determined in electron impact experiments. (Frost and McDowell 1955, 1958). These states are identified with abrupt changes in the slope of the cross-section curve. The measurements have an accuracy of about 0.1 eV.

I.4.8 Partial photoionization cross-sections

If as a result of photoionization ions are produced in an excited state, fluorescent radiation is emitted when the ions return to the ground state, and the intensity of the fluorescent radiation is an indication of the number of ions produced in the particular state. Observation of fluorescent radiation therefore provides a method of measuring partial cross-sections for photoionization to those states of the ion from which allowed transitions to a lower state of the ion occur. Schoen et al (Schoen et al 1961) observed fluorescent radiation from several gases. They were unable to disperse the fluorescent radiation, but

they measured the total intensity as a function of the wavelength of the incident beam.

In a similar experiment Huffman et al (Huffman et al 1963b) placed a lower limit on the wavelength distribution of the flurescent radiation from nitrogen, by observing it through quartz and glass windows. They concluded that the first negative band system was being observed, but not the Meinel bands. This indicated that a considerable number of ions were produced in the $B^2\Sigma_u^+$ state of N_2^+. This result has been confirmed by Judge et al, (Judge et al 1963) who succeeded in dispersing the fluorescent radiation from several gases. The resolution was not good, but they were able to observe the profile of the first negative band system of nitrogen.

For oxygen, at a wavelength of 703 $\mathring{A}$, Judge et al observed the second negative band system, indicating the production of ions in the $A^2\Pi_u$ state of O_2^+. However, at an incident wavelength of 630 $\mathring{A}$ they observed the first negative band system, indicating that ions were produced in the $b^4\Sigma_g^-$ state in preference to the $A^2\Pi_u$ state. They also observed a delay in the fluorescence from oxygen, which they associated with the metastable $a^4\Pi_u$ state of O_2^+.

It is apparent that the observation of fluorescent radiation is far from ideal as a method of obtaining partial photoionization cross-sections. The radiation is difficult

to detect because of its low intensity, and the presence of metastable states makes the interpretation difficult. Also the number of ions produced in the ground state cannot be measured directly.

The alternative method of determining partial photoionization cross-sections is to measure the energy distribution of the photoelectrons, since the energy of the final state of the ion is uniquely determined by the difference between the photon energy and the photoelectron energy. Few experiments of this nature have been performed. Al-Joboury and Turner, (Al-Joboury and Turner 1963) and Frost and McDowell (Frost and McDowell 1965) have recorded the energy spectra of the photoelectrons produced in a number of gases by undispersed radiation from a helium discharge (584 Å). Vilesov et al, (Vilesov et al 1961) and Schoen (Schoen 1964) have obtained estimates of the photoelectron energy distributions at a number of wavelengths using a cylindrical retarding potential analyser. The partial photoionization cross-sections of molecular oxygen measured by Schoen are shown in Fig.8. These results are useful, but they contain little detail. The experiments which have been performed indicate that a more detailed investigation of partial photoionization cross-sections is possible. The method provides a powerful tool for investigating details of photoionization processes which have

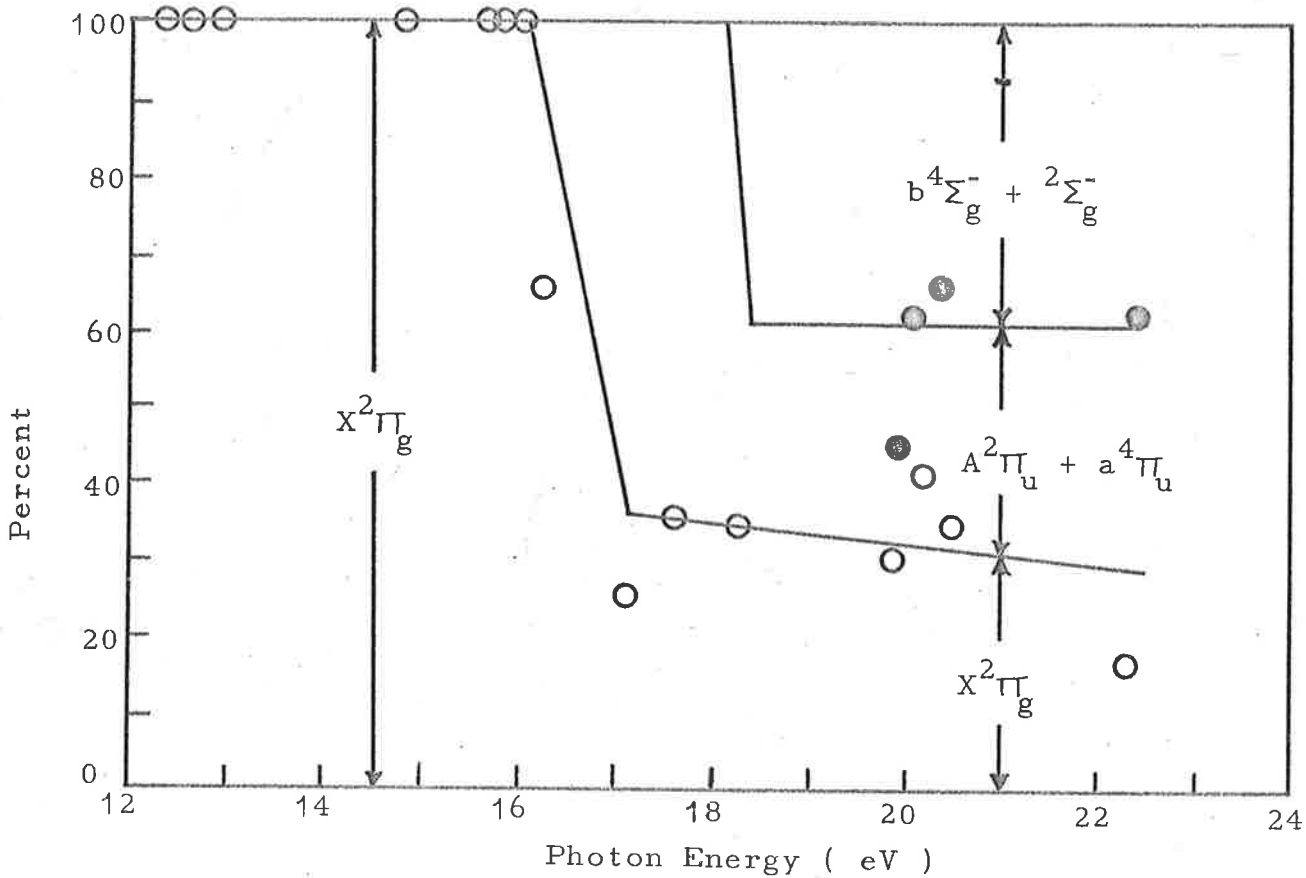

Fig.8. Percentage excitation to various states of O_2^+. (Schoen 1964)

previously been inaccessible.

In Chapters III and IV experiments are described in which the partial photoionisation cross-sections of oxygen, nitrogen and water vapour have been measured. A photoelectron spectrometer with better resolution than the one used by Schoen was used in the experiments, and a continuum light source allowed a detailed study of the partial cross-sections. Photoelectron energy spectra of oxygen are presented which indicate a new autoionizing process. As a background to this work, the measurement of total cross-sections is discussed in Chapter II. Also described in this Chapter are two experiments in which total absorption and total photoionization cross-sections are measured.

CHAPTER II

MEASUREMENT OF TOTAL PHOTOIONIZATION CROSS-SECTIONS

II.1 Light Sources for the Ultraviolet Region

An ideal light source for use in absorption measurements is one which emits a continuous range of wavelengths with a smooth intensity distribution. Radiation from an electron synchrotron provides an almost ideal light source for the ultraviolet region, (Madden and Codling 1965) but it is impracticable in most instances. A variety of ultraviolet light sources have been used, each being useful in a particular spectral region.

Most of the light sources used for the ultraviolet region consist of a gas discharge in which a high current density, and therefore a high intensity, is achieved by confining the discharge within a narrow tube. Power may be supplied to a capillary discharge in a number of ways. The discharge may be excited by microwave power, (Wilkinson and Byram 1965) and in this case the capillary tube is surrounded by a resonant microwave cavity. In the present experiments power was supplied to the light source in two different modes. The first of these was the A.C. mode, (Fig. 9a) in which the lamp was connected to a high voltage (15 kV) supply through a series resistance, which had the effect of stabilising the discharge. The spectrum from a

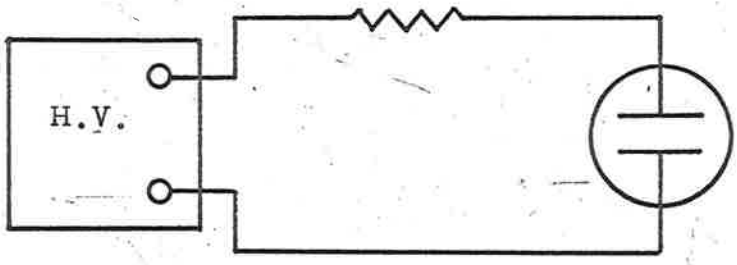

(a)

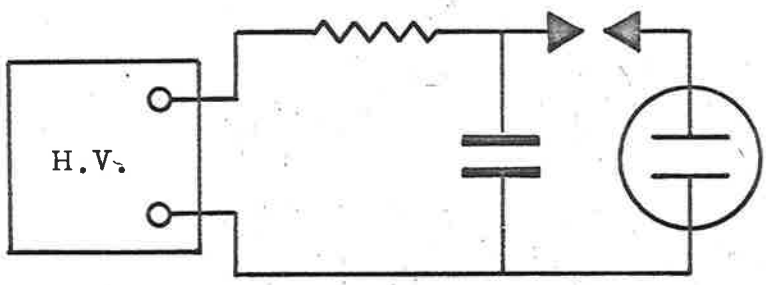

(b)

Fig.9. Circuits for supplying power to the capillary discharge lamp.
(a) A.C. mode
(b) condensed spark discharge mode

discharge through hydrogen shown in Fig.10 was obtained by this method with a discharge current of 60 mA. through 4 mm.Hg. of hydrogen. The 'many lined' spectrum of molecular hydrogen in the region 900 Å - 1500 Å provides a continuous range of wavelengths, but is far from being ideal because of the large fluctuations of intensity with wavelength. When this spectrum is used for absorption measurements, great care must be taken to ensure that false structure does not occur in the cross-sections because of the structure in the light source spectrum.

More satisfactory light sources have been obtained by exciting the emission continua of the rare gases. (Tanaka et al 1958; Huffman et al 1965; Tanaka et al 1962; Wilkinson and Byram 1965). The Hopfield continuum of helium (Hopfield 1930) has a useful intensity in the range 600 Å - 1000 Å. In a discharge through helium at high pressure (50 mm.Hg.) diatomic helium molecular ions are formed in their bound first excited state, (Tanaka 1942) and the continuum is due to transitions between this state and the unstable ground state of the ion. Corresponding continuous spectra have been excited in neon (740 Å - 1000 Å), argon (1070 Å - 1600 Å), krypton (1240 Å -1700 Å), and xenon (1470 Å - 1900 Å).

In order to produce ions in the gas discharge a very high current density is necessary. In the present

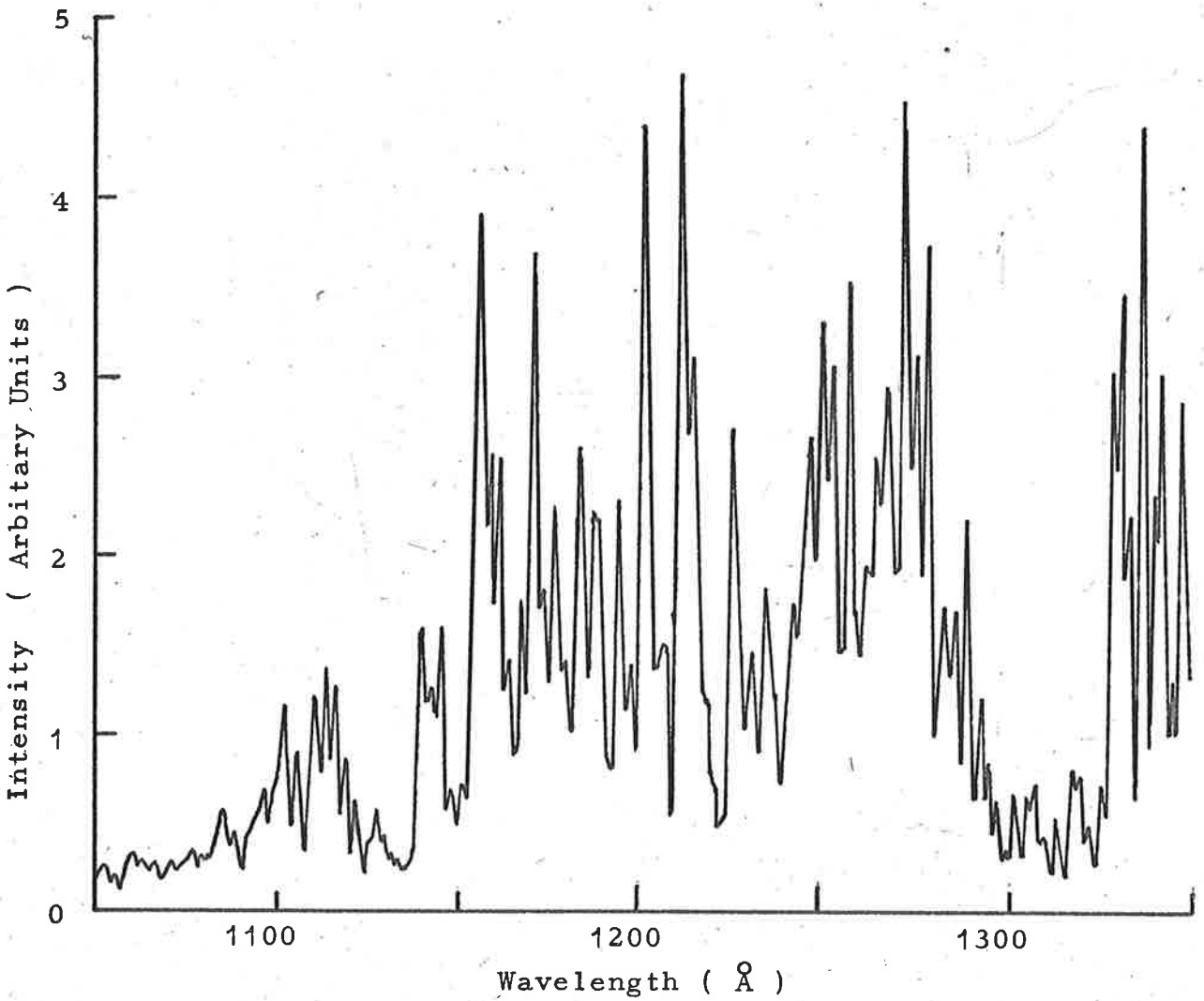

Fig.10. Emission spectrum from a discharge through hydrogen.

experiments this was achieved by using a condensed spark discharge, which was produced with the circuit shown in Fig.9b. A condensor bank was charged through a series resistance, and discharged through the lamp via a spark gap between two tungsten electrodes. The breakdown conditions of the spark gap were stabilized by illuminating the gap with ultraviolet radiation from a quartz mercury lamp, and by passing a jet of compressed air through the gap. The spectrum excited in helium in this manner is shown in Fig.11. The helium was purified (Newburgh et al 1962) by passing it through a trap containing a molecular sieve material which was cooled to liquid air temperature.

II.2 Absorption Measurements

Total absorption cross-sections can be determined by measuring the attenuation of a monochromatic beam of radiation as it passes through a cell filled with the gas under study. The usual experimental arrangement (e.g. Huffman et al 1963c) consists of an absorption cell placed behind the exit slit of a vacuum ultraviolet monochromator, and an ultraviolet detector at the end of the cell. The ratio of intensities I/I_o is measured by taking readings from the detector both with the cell filled with gas to a known pressure, and with the cell evacuated.

II.2.1 Detectors for the ultraviolet region

In an absorption experiment it is only necessary

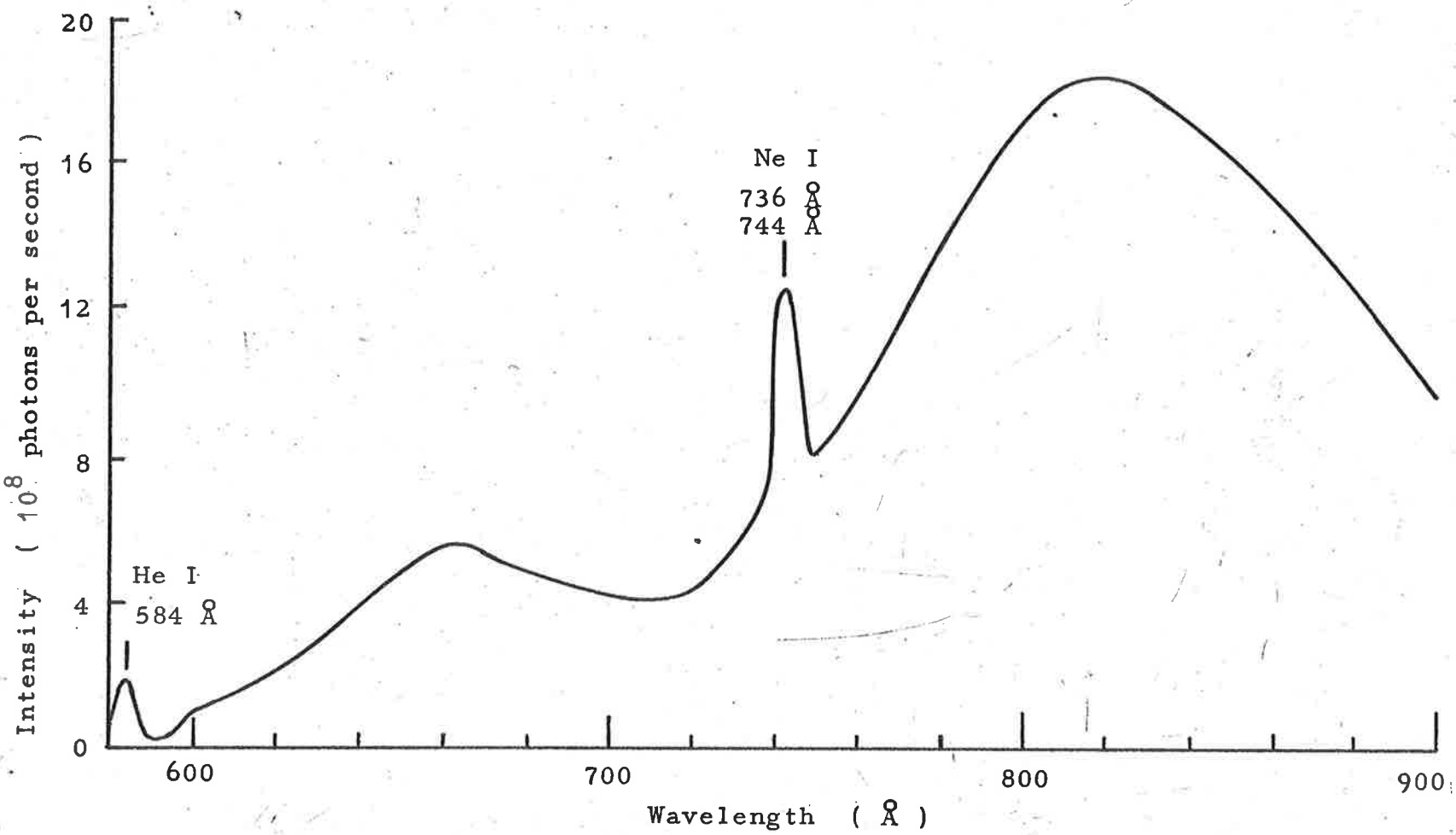

Fig.11. Hopfield continuum excited by a condensed spark discharge in 50 mm. Hg. of helium.

to measure relative beam intensities, and absolute calibration of the detector is not needed. The most convenient form of detector consists of a photomultiplier tube made sensitive to ultraviolet radiation with a coating of sodium salicylate, which is a fluorescent material. (Johnson et al 1951). The spectral distribution of the fluorescent radiation from sodium salicylate has a maximum at about 4250 Å, which corresponds well with the spectral sensitivity of S-type photomultiplier cathodes. (Allison et al 1964).

Sodium salicylate has an absolute quantum efficiency of 94% at wavelengths near 1200 Å. (Allison et al 1964). The relative quantum efficiency as a function of wavelength is reasonably constant over a range of wavelengths from 500 Å - 3000 Å, (Johnson et al 1951; Watanabe and Inn 1953; Smith 1961; and Samson 1964d) although there is some increase in the efficiency from 1000 Å to 1600 Å. A further advantage of sodium salicylate is its stability under vacuum, since the fluorescent coating must be placed within the absorption cell.

Cook and Metzger (Cook and Metzger 1964a) used a platinum photocathode as an alternative detector for making absorption measurements. This detector had the advantages of a stable sensitivity over a period of time, making it suitable for absolute calibration, and of being

insensitive to long wavelength scattered light from the monochromator. In the region above 1050 Å, which is the transmission limit of lithium fluoride, gas filled ionization chambers may be used as ultraviolet detectors. (Carver and Mitchell 1964). These chambers also have the advantage of being sensitive only to a limited spectral range, and a number of different spectral responses may be obtained by using different combinations of window and filling gas.

II.2.2 Procedure for measuring molecular oxygen absorption cross-sections

A diagram of the experimental arrangement which was used to measure the absorption cross-section of molecular oxygen is shown in Fig.12. The monochromator was of the Seya-Namioka type (McPherson model 235) with a half-metre grating blazed for 1500 Å. Slit widths of 30μ gave a resolution of 1 Å. The light source was a hydrogen discharge in a windowless lamp, which gave the spectrum shown in Fig.10.

A number of absorption cells, ranging in length from 0.13 cm. to 15 cm., were used. All the cells were of demountable construction, using O-ring sealed flanged joints. The construction of the short cell, shown in Fig.13, was such that the length of the cell was determined by a spacer which was easily interchanged.

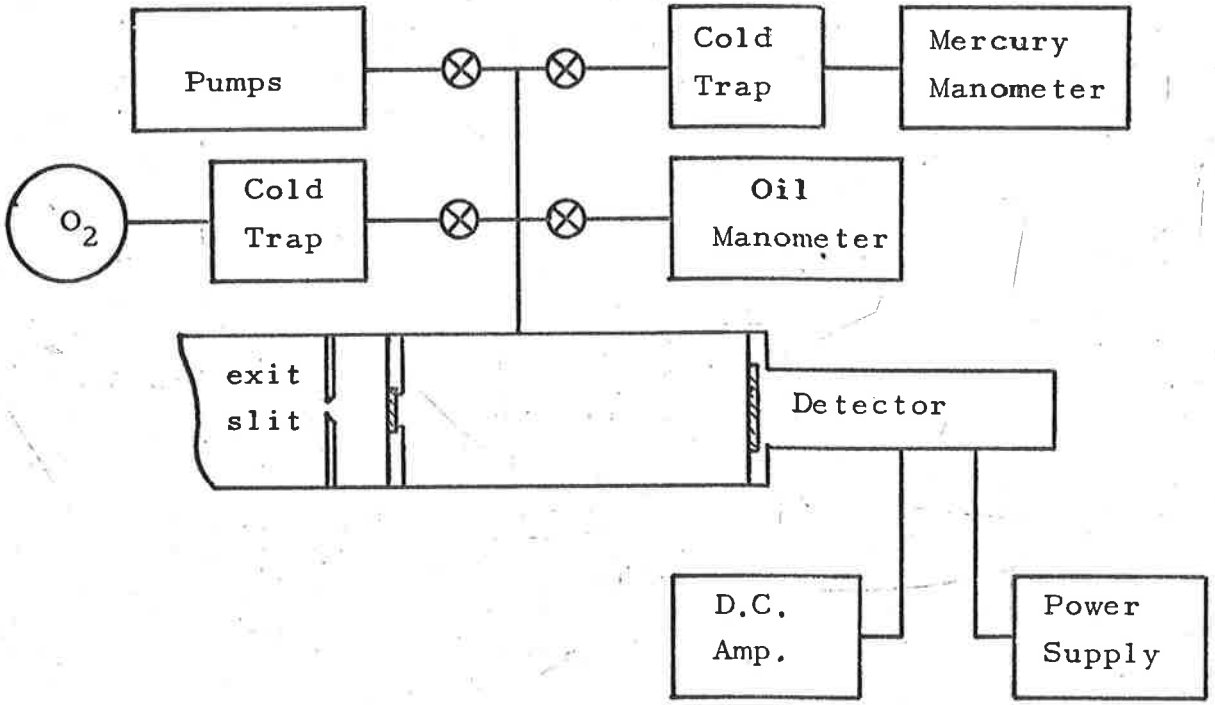

Fig.12. Experimental arrangement for measuring the total absorption cross-section of molecular oxygen.

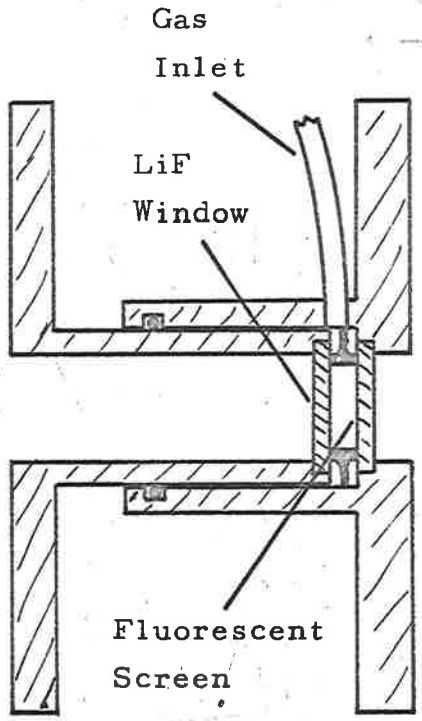

Fig.13. Short cell for determining the total absorption cross-section of molecular oxygen.

The cells were fitted with a lithium fluoride window at the end nearest to the exit slit of the monochromator, and a sodium salicylate coated glass plate at the other end. The current from the photomultiplier tube (E.M.I. 95143), which was placed behind the fluorescent screen, was fed into a d-c amplifier (Hewlett-Packard model 425A).

The length of the cell and the gas pressure were adjusted for each measurement so that about half of the beam was absorbed in the cell. Absolute measurements of the gas pressure to an accuracy of about 5% were made with two manometers. Pressures greater than 2 cm. Hg. were measured with a mercury manometer. A liquid air cooled trap was placed between the mercury manometer and the absorption cell to prevent contamination of the cell with mercury vapour. Pressures between 1 mm. Hg. and 20 mm. Hg. were measured with a manometer filled with Apiezon C oil, which has a specific gravity of 0.875. The oil was outgassed by heating it while the manometer was evacuated.

The gas used was 'medical grade' oxygen supplied by Commonwealth Industrial Gases. It was purified by condensing a quantity of the gas in a liquid air cooled trap, and allowing the liquid oxygen to boil under vacuum for some time before being allowed to evaporate into the absorption cell through a needle valve. Before being filled the absorption cell was evacuated to a pressure of

less than 10^{-6} mm. Hg. with a two inch oil diffusion pumping system.

The procedure for obtaining the data was as follows. The relative intensity I_o was measured with the cell evacuated. The pressure in the cell was then increased until the transmitted intensity had dropped to about half of I_o, when the pressure and the intensity I were noted. The cell was then evacuated to check the value of I_o in case the intensity of the light source had drifted. This procedure was repeated at each wavelength setting. The use of several cells of various lengths enabled a reasonably small range of pressures to be used. Some of the measurements were repeated using a nitric oxide filled ionization chamber as the detector.

While using the wide band sodium salicylate detector it was important to make corrections for the scattered light which was present in the beam from the monochromator, but had a wavelength different from that of the beam. The intensity and wavelength distribution of the scattered light was investigated by placing a variety of windows in the path of the beam.

By placing a lithium fluoride window in the path of the beam, and setting the wavelength of the beam to a value just below 1050 Å, which is the transmission limit of lithium fluoride, only that portion of the scattered

light which had a wavelength greater than 1050 Å was able to reach the detector. Leaving the wavelength setting unaltered, and placing a calcium fluoride window in the path of the beam, the total intensity of the scattered light with wavelengths longer than 1220 Å was found to be about the same as that of the previous measurement, after a correction had been made for the different transparencies of the two windows. A sapphire window produced a similar result, showing that most of the scattered light had a wavelength greater than 1420 Å.

To test the dependence of the scattered light intensity on the wavelength setting of the monochromator, the intensity of the radiation transmitted by a sapphire window was recorded as the wavelength setting was scanned from 1050 Å to 1350 Å. The intensity was found to be reasonably constant in this region. A correction was made for the scattered light intensity simply by subtracting a constant bias from the photomultiplier signal. The bias was checked at frequent intervals by setting the wavelength to a value less than 1050 Å, and adjusting the detector signal to zero. The adequacy of the correction was indicated by the agreement between cross-sections obtained by this method, and those obtained using a gas filled ionization chamber as the detector.

II.2.3 Total absorption cross-sections for molecular oxygen in the region 1050 Å to 1250 Å.

The cross-section for absorption by molecular oxygen in the region 1050 Å to 1250 Å is shown in Fig.14. Watanabe (Watanabe 1958) has reviewed earlier measurements of this cross-section, and a more recent measurement has been made by Metzger and Cook. (Metzger and Cook 1964b). The present results are in general agreement with those of the previous workers. The absorption spectrum in this region has a complex band structure which is diffuse because of pre-dissociation. (Price and Collins 1935). Many of the bands have not been identified. There are seven absorption windows between the bands where the absorption cross-section is very low ($\sigma < 5.10^{-20}$ cm.^{2}). There may be a weak dissociation continuum in this region, but it must have a cross-section smaller than 10^{-20} cm.^{2}.

The most important of the absorption windows is the one which coincides almost exactly with the wavelength of the hydrogen Lyman-α line. Since molecular oxygen is the principal atmospheric absorber at these wavelengths, the intense solar Lyman-α line is able to penetrate to an altitude of about 80 km., and may be important in the formation of the D-region of the ionosphere. An accurate value of the absorption cross-section of molecular oxygen at the wavelength of Lyman-α is also necessary for the

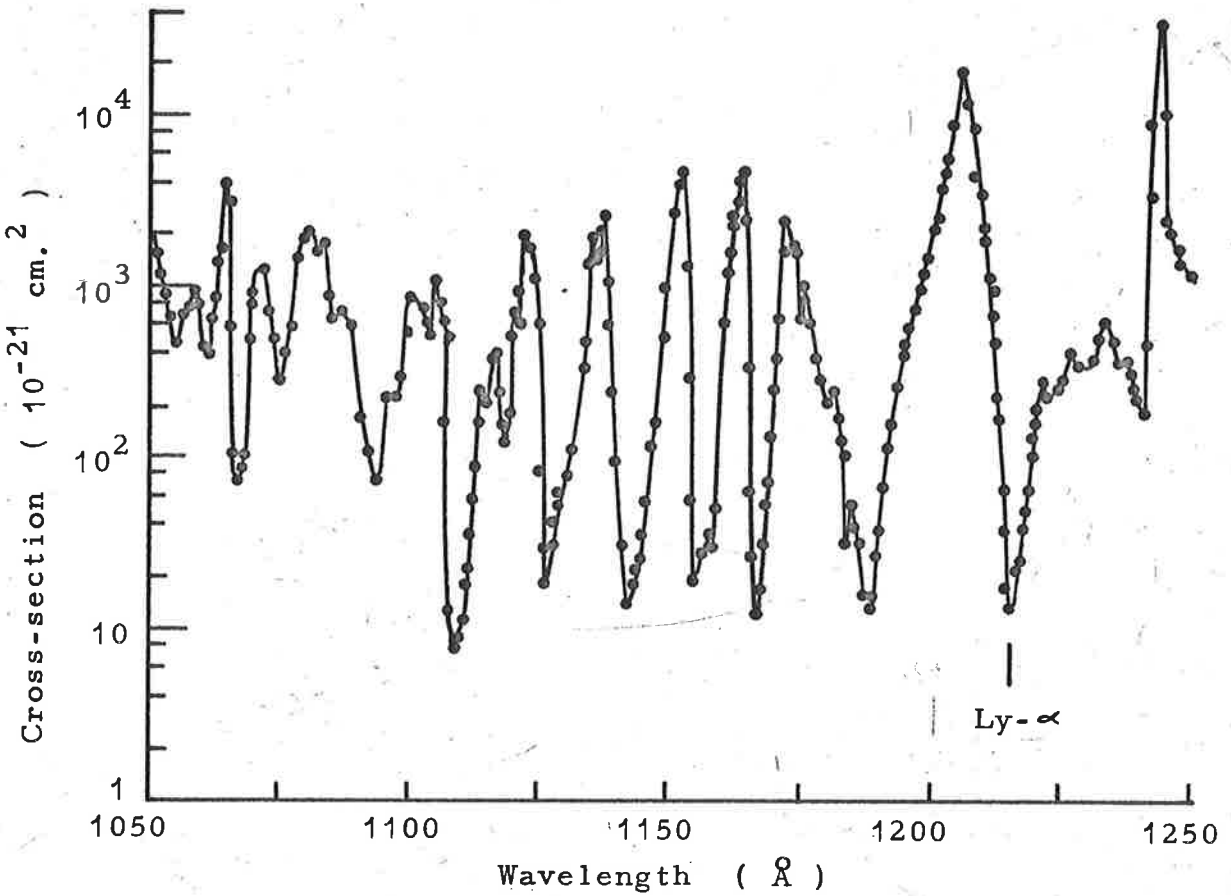

Fig.14. Total absorption cross-section of molecular oxygen.

determination by absorption methods of molecular oxygen densities in the 70-90 km. region of the atmosphere. (Carver and Mitchell 1966).

For these reasons the absorption cross-section in the region of 1216 Å was studied in greater detail. The shape of the absorption window shown in Fig.15 is in good agreement with that given by previous workers. (Ditchburn et al 1954; PoLee 1955; and Watanabe 1958). The cross-section at the wavelength of Lyman-α was found to vary linearly with pressure in the range from 2 mm. Hg. to 50 cm. Hg., as shown in Fig.16. This is in agreement with the measurements of other workers. (Preston 1940; Watanabe et al 1953b; and Watanabe 1958) Ditchburn et al (Ditchburn et al 1954) and PoLee, (PoLee 1955) who used photographic methods, found no pressure dependence at this wavelength. The pressure dependence of the cross-section is probably due to the pressure broadening (Herzberg 1950) of the nearby absorption bands. The cross-section for the absorption of Lyman-α radiation at zero pressure was estimated by extrapolation to be $(1.12 \pm 0.05)_x 10^{-20}$ cm.^{2}. This is in good agreement with other values determined by photoelectric methods, but is higher than values obtained by photographic methods.

II.3 Photoionization Yield Measurements

Since the photoionization yield of the rare gases

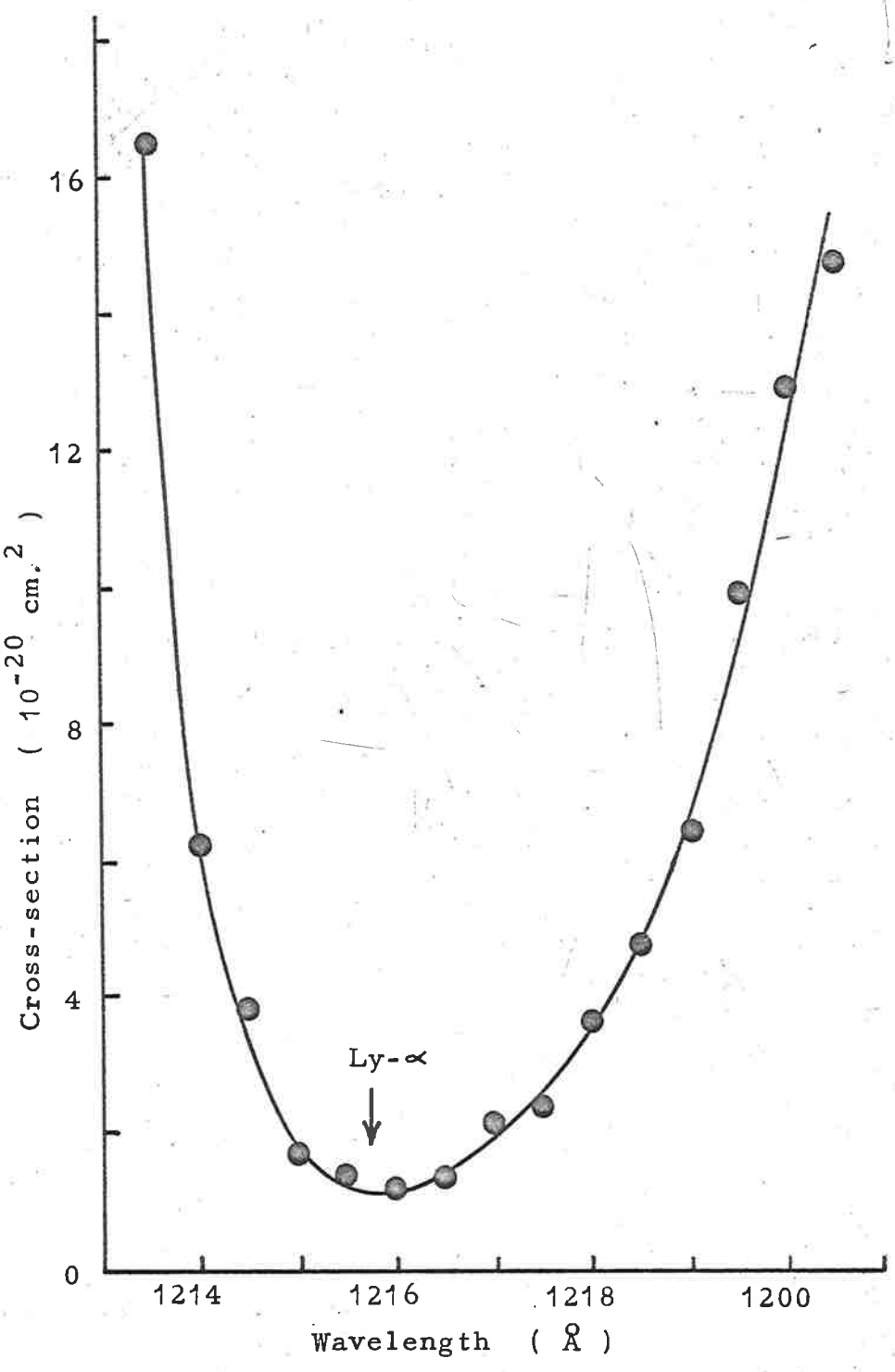

Fig.15. Total absorption cross-section of O_2 near the wavelength of Ly-∝

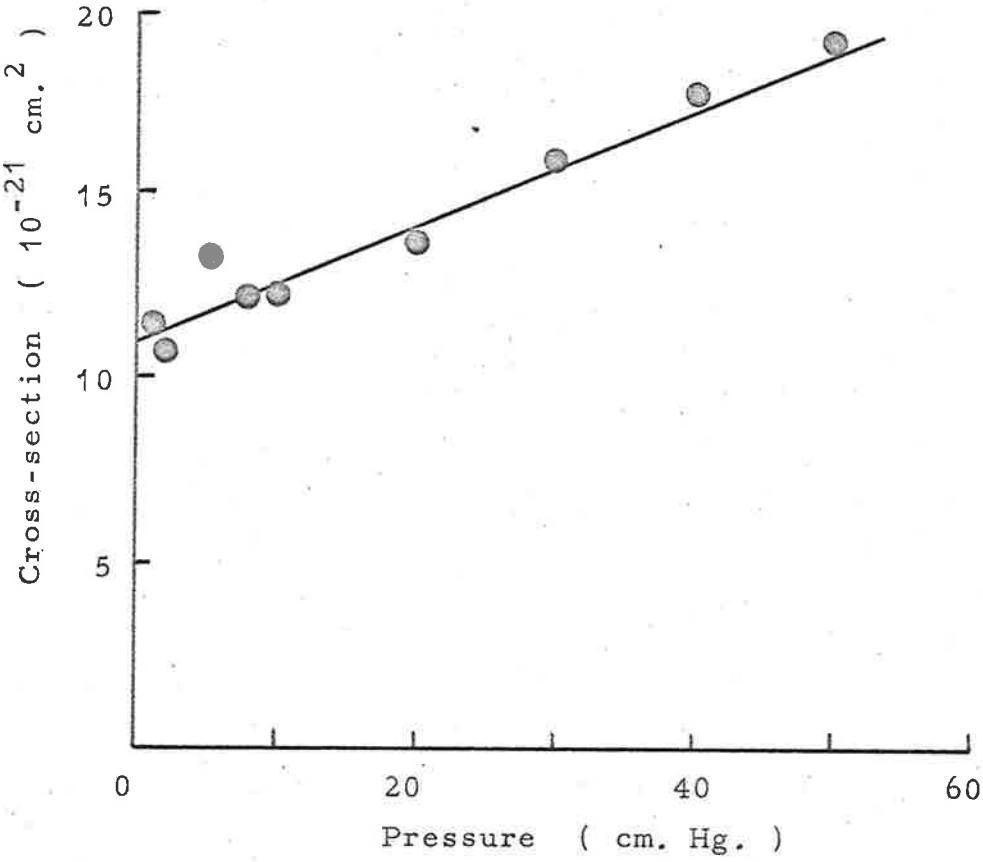

Fig.16. Variation with pressure of the total absorption cross-section of O_2 at the wavelength of Ly-α

is equal to unity, (Samson, 1964d; Watsunaga et al 1965) the photoionization cross-section is equal to the total absorption cross-section. The photoionization cross-sections of these gases may therefore be measured by the absorption method described above. This applies even in the regions of autoionization of the rare gases, and probably applies to other atomic gases.

Molecular gases usually have a photoionization yield which is less than unity, and in order to determine the photoionization cross-section both the total absorption cross-section, and the yield must be measured at each wavelength. There are two general methods for determining photoionization yields.

II.3.1 The single ion chamber method

Watanabe et al (Watanabe et al 1953a) determined the photoionization yield of nitric oxide with an apparatus of the type shown in Fig.17. They determined the rate at which photons were absorbed in the cell by measuring both the absolute intensity of the beam entering the cell, and the total absorption cross-section of the gas. The total absorption cross-section was measured in the manner already described, using the detector at the end of the cell.

They measured the ion production rate with the parallel plate ion chamber which was contained in the absorption cell. A voltage applied to one plate repelled

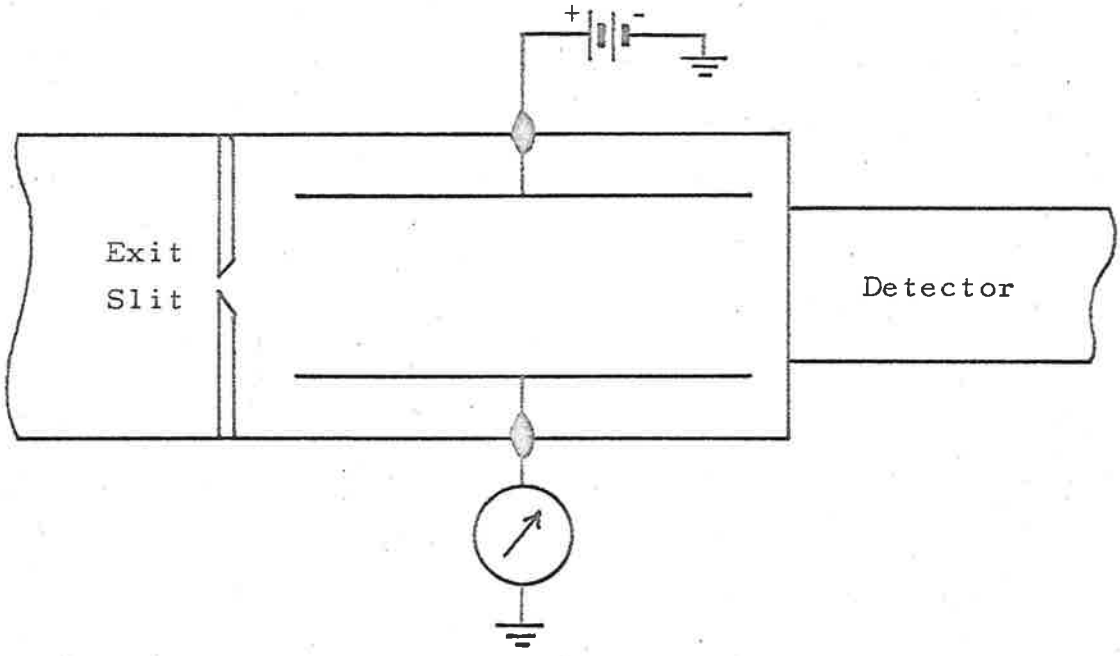

Fig.17. Single ion chamber for measuring photoionization yields.

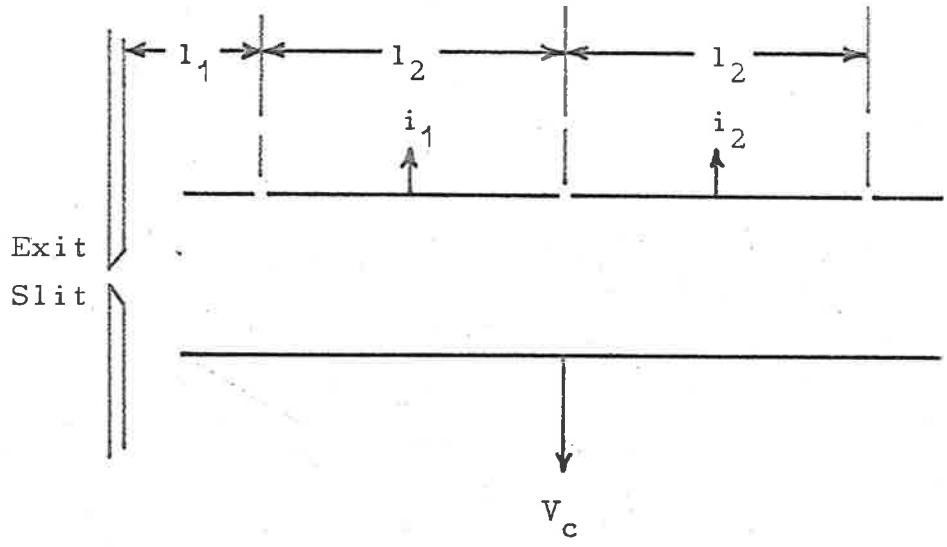

Fig.18. Double ion chamber for measuring photoionization yields.

the ions towards the other plate where they were collected with a sensitive electrometer. The ratio of the ion production rate to the photon absorption rate gave them the value of the photoionization yield.

II.3.2 The double ion chamber method

Another method for measuring photoionization yields has been developed by Wainfan et al (Wainfan et al 1955). This method involves the use of the double ion chamber shown in Fig.18, and has the advantage that all the measurements necessary to determine the total absorption cross-section and the photoionization yield may be made simultaneously.

Expressions for the ion currents i_1 and i_2 collected from the two ion chambers may be written down in terms of the total absorption co-efficient k of the gas, the absolute beam intensity I_o which enters the cell, the photoionization yield Y, and the path lengths x_1 and x_2 through l_1 and l_2 centimetres of the gas respectively:

$$i_1 = YI_o(e^{-kx_1} - e^{-k(x_1 + x_2)}) \qquad (19)$$

$$i_2 = YI_o(e^{-k(x_1 + x_2)} - e^{-k(x_1 + 2x_2)}) \qquad (20)$$

Dividing equation (19) by equation (20) gives:

$$\frac{i_1}{i_2} = e^{kx_2} \qquad (21)$$

Thus the total absorption coefficient is determined by

measurements of the two ion currents, and the path length through the gas. The yield is found by inserting the values of the absorption coefficient and the absolute beam intensity I_o into equation (19) or (20).

II.3.3 Intensity measurements in the ultraviolet region

The only method available to early experimenters of determining absolute beam intensities (Packer and Lock 1951) was that of using a sensitive thermopile to transfer the calibration from a standard lamp to the ultraviolet region, where it was used to calibrate a secondary standard, such as a sodium salicylate detector. It had to be assumed that the thermopile was equally black to ultraviolet and visible radiation. Because of the relatively low sensitivity of the thermopile, the slits of the monochromator had to be made wider than is usual during an experiment in order to obtain a measurable signal from the thermopile. The signal to noise ratio was improved by the use of a chopped beam and synchronous amplifiers, but the measurements were very difficult. Johnston and Madden (Johnston and Madden 1965) have recently reviewed the use of thermopiles in the ultraviolet region.

Samson (Samson 1964d) used the double ion chamber technique, which was discussed in the previous section, with a rare gas to measure absolute beam intensities. Since the photoionization yield of the rare gases is equal

to unity, inserting the total absorption coefficient into equation (19) or (20) gives the beam intensity I_o. This method is limited to wavelengths shorter than 1010 Å, which is the ionisation threshold of xenon.

In the experiment to measure the total photoionisation cross-section of nitric oxide (Sec.II.3.4), an absolute calibration of the beam detector was made using the double ion chamber by assuming the value of 81% given by Watanabe and Matsunaga (Watanabe and Matsunaga 1961) for the photoionization yield of nitric oxide at the hydrogen Lyman-α wavelength.

II.3.4 Procedure for measuring the total photoionization cross-section of nitric oxide

The experimental arrangement which was used to measure the total photoionisation cross-section of nitric oxide is shown in Fig.19. The plates of the ion chamber were constructed of stainless steel, and insulated from earth with teflon. The electrode structure was mounted in a copper vacuum chamber which could be evacuated to a pressure of less than 10^{-6} mm. Hg. with a two inch pumping system. The half metre Seya-Namioka monochromator was used with slit widths of 60μ corresponding to a resolution of 2 Å.

The collecting plates of the ion chamber can be seen in Fig.20. A guard electrode at either end of the

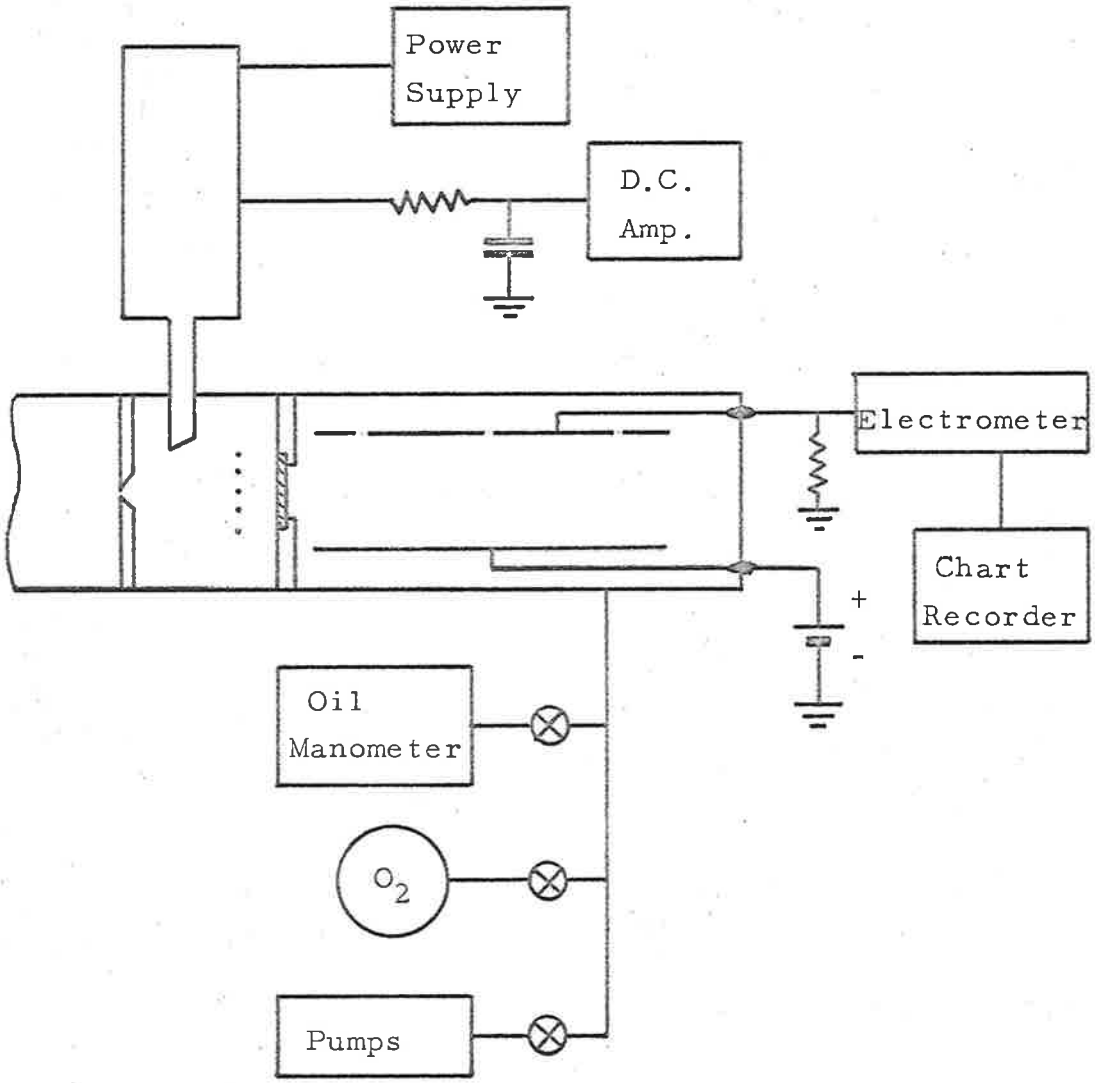

Fig.19. Experimental arrangement for measuring the total photoionization cross-section of nitric oxide.

Fig.20. Plates of the double ion chamber used for measuring the total photoionization cross-section of nitric oxide.

collecting region ensured that the ions were collected from well defined areas. The ion current saturation characteristic of the ion chamber is shown in Fig.21. A collecting potential of 60 volts was sufficient to cause saturation, but not so large as to cause secondary effects.

A resistance of 10^{11} ohms at the input of the electrometer (Wayne-Kerr model M141) was sufficient to measure the ion current, which was of order 10^{-12} amps. While the current from one plate was being measured, the other plate and the guard electrode were connected to the guard terminal of the electrometer, which was maintained at the same potential as the input terminal of the electrometer. The voltage output from the electrometer was fed into a strip chart recorder, which indicated when the electrometer reading, which had a long time constant, had reached a constant value.

The intensity of the beam was measured by a calibrated beam sampling device placed at the exit slit of the monochromator. The sampling device, shown in Fig.22, was similar to the one used by Ditchburn (Ditchburn 1962). A wire grid coated with sodium salicylate placed in the path of the beam, intercepted a small, but constant, fraction of the beam. The fluorescence induced in the sodium salicylate was observed by a photomultiplier tube through a perspex light pipe. A filter circuit at the

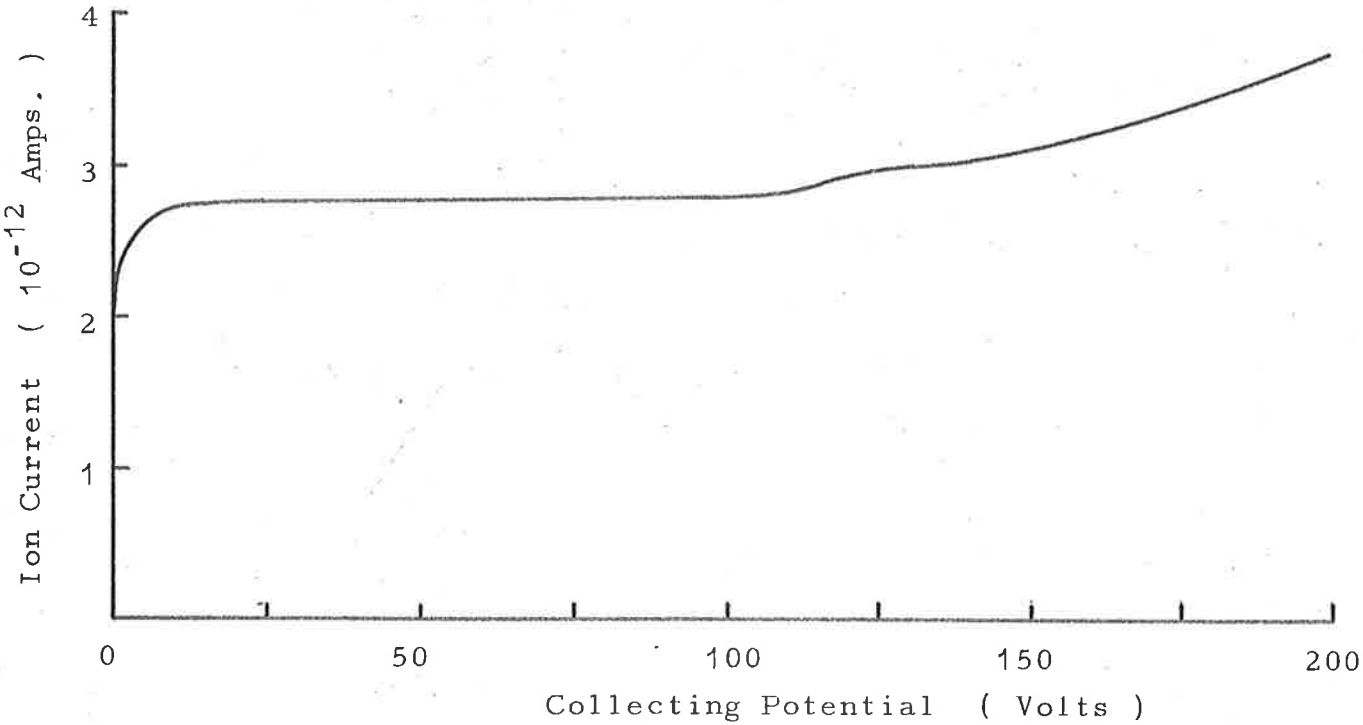

Fig.21. Saturation characteristic of the double ion chamber.

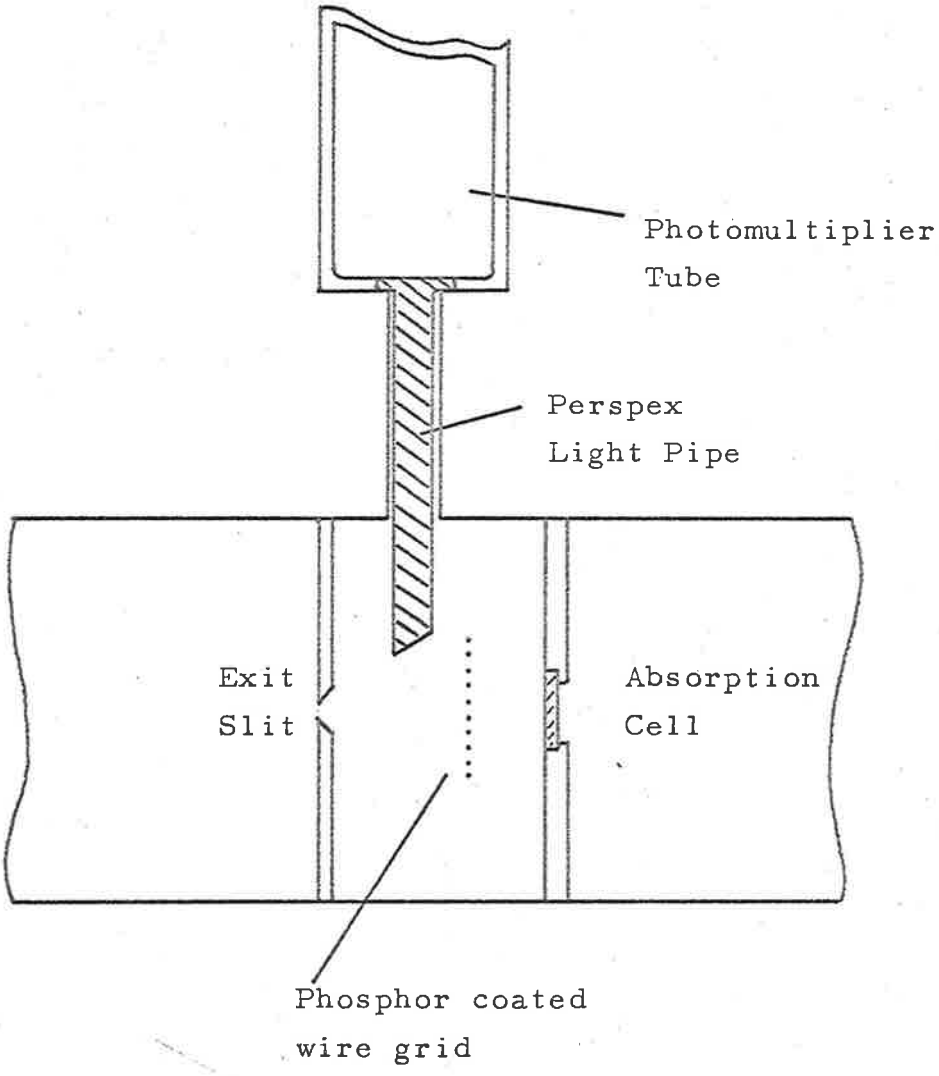

Fig.22. Beam sampling arrangement at the exit slit of the monochromator.

input of the d-c amplifier (Hewlett-Packard model 425A) which was used to amplify the signal from the photomultiplier tube, had a time constant equal to that of the electrometer, and averaged out high frequency fluctuations in the beam intensity.

The nitric oxide, which was supplied by Matheson, was purified by passing it through a U-tube filled with silica-gel, and cooled to -70°C with a mixture containing equal parts of carbon tetra-chloride and chloroform, which was frozen by stirring it with liquid air. The gas pressure, which was of order 1 mm. Hg., was measured with an oil manometer. The manometer had to be outgassed frequently, as the oil absorbed nitric oxide.

II.3.5 Nitric oxide total photoionization cross-section in the 1150 Å to 1350 Å region

The total absorption cross-section and the total photoionization cross-section of nitric oxide in the 1150 Å to 1350 Å region are shown in Fig.23. The band structure in the absorption cross-section does not appear to be appreciably autoionized as it does not appear in the photo-ionization cross-section. The total photoionization cross-section is in good agreement with that of Watanabe, (Watanabe 1954) as indeed it should be since the photo-ionization yield was normalised to that of Watanabe at the wavelength of Lyman-α.

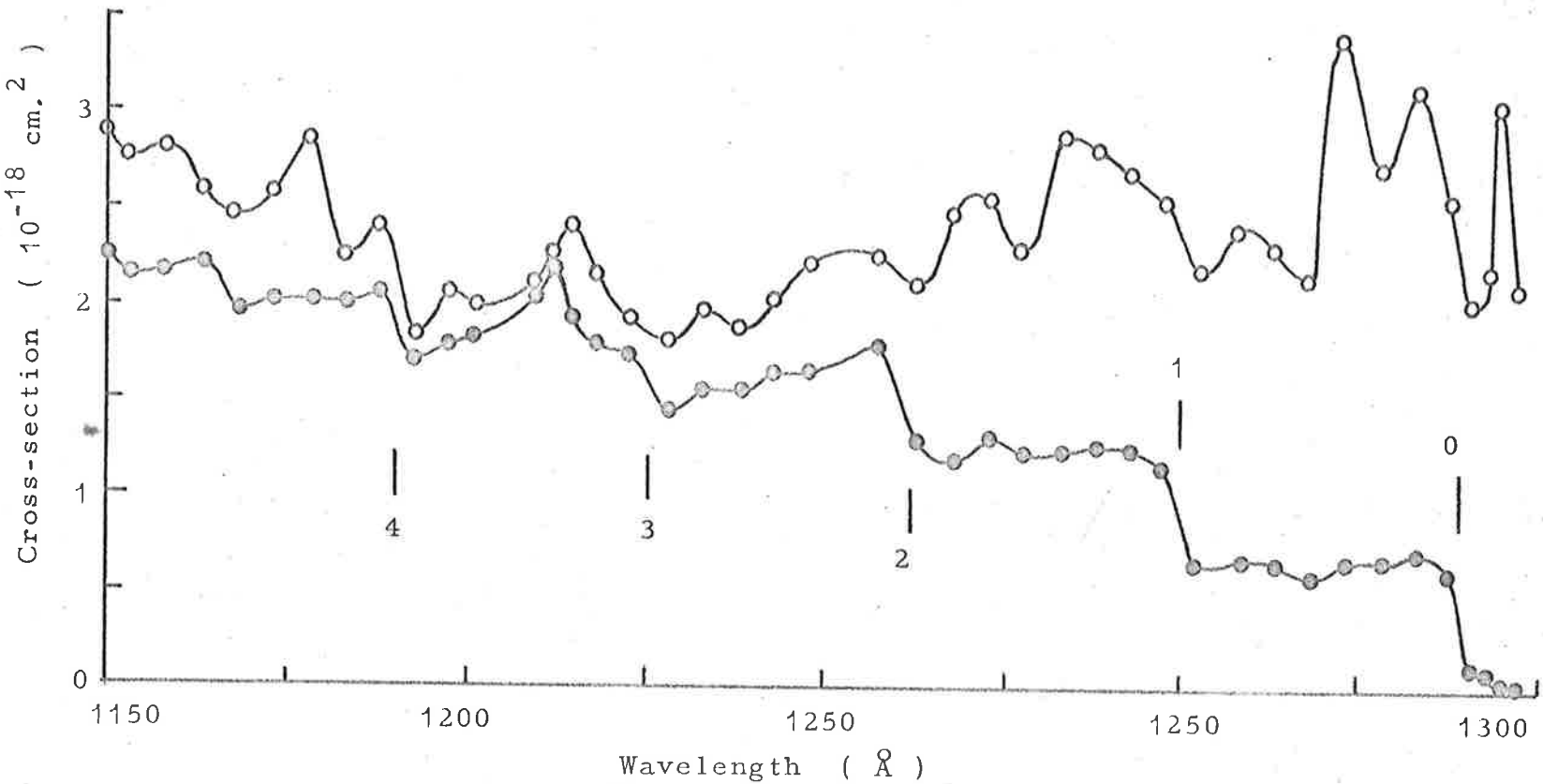

Fig.23. Total photoionization (●) and total absorption (o) cross-sections of nitric oxide.

The most interesting feature of the photoionisation cross-section is the steplike increase from threshold. Steps appear at 1339 Å, 1300 Å, 1262 Å, 1225 Å, and 1190 Å. The mean separation of these steps is 0.29 eV. Watanabe (Watanabe 1954) has suggested that these steps indicate the thresholds of the vibrational levels of the ground state of NO^+. The measured separation of the steps is in excellent agreement with the value of 0.29 eV for the separation of the 0-0 and 0-1 bands of the Miescher-Baer emission system of nitric oxide, (Miescher and Baer 1952) which has been associated with these levels. The shape of the present photoionisation cross-section is in better agreement with that of Watanabe (Watanabe 1954) than with that of Nicholson (Nicholson 1963).

The relative height of the five steps decreases fairly uniformly from the first to the last. Taking account of the Frank-Condon principle, this indicates that the first step corresponds to a vertical transition, since the height of a given step may be considered to be an indication of the cross-section for the transition to the particular vibrational level. (Morrison 1962). Because of this the first step may be confidently associated with the adiabatic ionization potential of the molecule (see Sec.I.4.3). The ionization potential was associated with the steepest part of the first step, and the value obtained

was 9.26 ± 0.02 eV. This compares well with the value of 9.25 ± 0.02 eV given by Watanabe, (Watanabe 1957) and 9.250 ± 0.005 given by Nicholson (Nicholson 1963).

CHAPTER III

THE PHOTOELECTRON SPECTROMETER

III.1 Introduction

In Chapter I it was pointed out that a knowledge of the partial cross-sections for particular photoionization processes is essential for a further understanding of the processes of photoionization. It was indicated that the most promising method of obtaining partial cross-sections was a study of the energy distribution of the photoelectrons. A knowledge of the photon energy and the photoelectron energy uniquely determines the energy of the state of the ion relative to the ground state of the molecule. Although the partial photoionization cross-sections of Schoen (Schoen 1964) shown in Fig.8 do not contain very much detail, they indicate the possibility of a more detailed study of partial photoionization cross-sections.

Apart from determining which of a number of known energy states the ion is in, a photoelectron spectrometer provides a new method of determining the energies of the ionic states, as has been shown by Al-Joboury and Turner. (Al-Joboury and Turner 1963). Another possible application of a photoelectron spectrometer is its use as an ultraviolet spectrometer. If the spectrometer is filled with a gas in which monoenergetic photoelectrons are produced by a

monochromatic beam of ultraviolet radiation, then the energy spectrum of the photoelectrons produced by a non-monochromatic beam is the same as the spectrum of the beam. This application is discussed further in Appendix I.

III.2 Requirements of the Spectrometer

The essential features of a photoelectron spectrometer are an ionisation region where a beam of radiation may pass through a sample of the gas under study, a means of collecting the photoelectrons from the ionization region and of measuring their energies, and a means of detecting the electrons. In the present experiment it was planned to study each ionising process over a range of wavelengths extending from threshold towards higher energy. Thus a spectrometer was required which was capable of measuring electron energies ranging from near zero to some tens of electron volts. It was also desirable that the spectrometer should have a resolution of better than one tenth of an electron volt, which is the order of separation of the vibrational levels of many molecules. Finally, it was essential that the energy scale of the spectrometer be determined at least sufficiently well to identify the peaks in the photoelectron spectra, and preferably sufficiently accurately to make independent determinations of the energies of the molecular states.

III.2.1 Choice of spectrometer

Some order of magnitude calculations of the numbers of electrons which may be detected under typical conditions, using the various methods of analysis and detection of low energy electrons, are helpful in making a choice between the possible spectrometer designs.

Experimental limitations which are common to all types of spectrometer are the gas pressure which may be used, and the intensity of the beam of ultraviolet radiation which may be obtained in the laboratory. The gas pressure in the ionization region is limited by the fact that the mean free path for the electrons in the gas must be sufficient to allow the electrons to travel to the detector without having collisions with other gas molecules. This places an upper limit of about 10^{-2}mm. Hg. on the gas pressure. The maximum beam intensity which may be obtained from the vacuum ultraviolet monochromators used in the present experiment is typically of order 10^{9} photons per second. Taking as a typical set of conditions a gas pressure of 10^{-2}mm. Hg., a beam intensity of 10^{9} photons per second, and a photoionization coefficient of 500 cm.$^{-1}$, the number of photoelectrons produced per centimetre path along the beam is of order 10^{7} electrons per second.

The number of photoelectrons collected from the ionization region by a given detector is also affected by

the distribution of the directions in which the photoelectrons are emitted. The direction of emission is defined by the angles θ and ϕ as shown in Fig.24. Sommerfeld (Sommerfeld 1930) has shown that for electric dipole transitions, the probability of an electron being emitted in a direction (θ, ϕ) is independent of ϕ, but depends on $\sin^2\theta$, (see Sec.IV.1.1). The spectrometer should, therefore, be designed to accept electrons travelling in a direction perpendicular to the beam direction.

Of the methods available for analysing low energy electrons, the parallel plate electrostatic analyser is capable of the best resolution. However, an analyser of this type necessarily accepts electrons from only a small solid angle, and few electrons enter the analyser. An analyser of moderate resolution operating under the conditions outlined above accepts photoelectrons at the rate of only 100 per second, and moreover, this number of electrons is spread over the whole spectrum. The problem of detecting such a small number of electrons makes the use of this type of analyser very difficult.

The retarding potential analyser has the advantage that its aperture is not limited, since it may consist of two wire grids of large area. The electrons must be collimated so that only those travelling in a direction normal to the plane of the grids reach the analyser, since

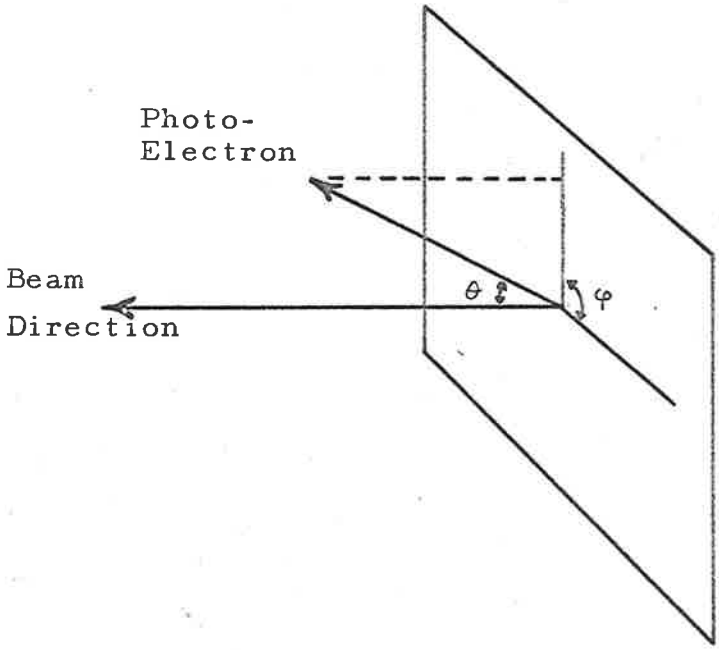

Fig.24. Diagram defining the angles θ and φ which describe the direction of emission of a photoelectron.

otherwise only a component of the electron energy is measured. Several forms of retarding potential analyser may be considered. An analyser of spherical geometry, with a point source of radiation at the centre, requires no collimation, and under typical conditions, with an effective point source consisting of a one centimetre cube, collects about 10^7 electrons per second. An analyser of cylindrical geometry has the advantage that electrons are collected from a region which may extend indefinitely along the beam, but the electrons must be collimated. A cylindrical analyser of length 20 cm., in which the electrons are collimated so that the spread in the measured energy component is 5%, collects about 10^7 electrons per second under the same conditions. A plane parallel retarding potential analyser with a length of 5 cm., and with collimation with respect to both θ and ϕ allowing a 5% spread in the measured energy component, collects electrons at a rate of order 10^5 per second.

Each of the analysers must be considered together with an appropriate form of detector. Low energy electrons may be detected and counted simply by collecting them on an anode, and measuring the electron current with a sensitive electrometer. In order that the measurement should not be too difficult, the current must be greater than 10^{-13} amps., i.e. more than 10^6 electrons must be

collected per second. Other methods of detection are possible if the electrons are accelerated to an energy sufficient to produce secondary effects. In the electron multiplier tube, for example, secondary emission from dynode surfaces produces sufficient amplification to allow individual electrons to be counted. (Lassettre et al 1964). However, these detectors require a reasonably good vacuum ($< 10^{-4}$ mm.Hg.), and have a limited aperture. Methods of detection in which individual electrons are counted have a high sensitivity, and are suitable for use with the electrostatic analyser or the plane parallel retarding potential analyser which were discussed above. The electrostatic analyser presents the possibility of measuring the angular distribution of the photoelectrons, but the very small number of electrons which may be detected makes this a difficult approach to the experiment. The cylindrical retarding potential analyser with anode detection was chosen because of its simplicity. The current of 10^{-12} amps. expected with 5° collimation is easily detected. Although an energy spread of 5% is too large to properly resolve vibrational structure in the spectra, the advantages of better collimation are outweighed by the disadvantages of a smaller electron current in this type of apparatus. Retarding potential analysers of cylindrical geometry have been used previously for electron impact studies, (Lozier

1930) and as photoelectron spectrometers. (Vilesov et al 1961; Al-Joboury and Turner 1963; and Schoen 1964).

III.3 Construction of the Apparatus

A diagram of the photoelectron spectrometer is shown in Fig.25. The spectrometer consisted of three concentric electrodes - the collimator, the analysing grid, and the anode.

III.3.1 The collimator

The inner electrode shown in Fig.26 performed two tasks. Firstly it produced a field free region in the centre, through which the ultraviolet beam passed, and from which the photoelectrons were collected. The electrode structure continued past the electron collection region at each end to eliminate electric field penetration into the ionization region. Since the photoelectrons were produced in a field free region, the measurement of their energy did not depend on the position in which they were formed. Secondly the inner electrode acted as a collimator, being transparent only to those electrons which travelled in a direction within 12° of the direction of a radius normal to the axis of the spectrometer. This angle of 12° defined the 5% energy resolution. Collimation with respect to θ was achieved with a series of equally spaced annuli. These had inner and outer diameters of 1.5 inches and 3 inches respectively, and were spaced at intervals of 3/16 of an

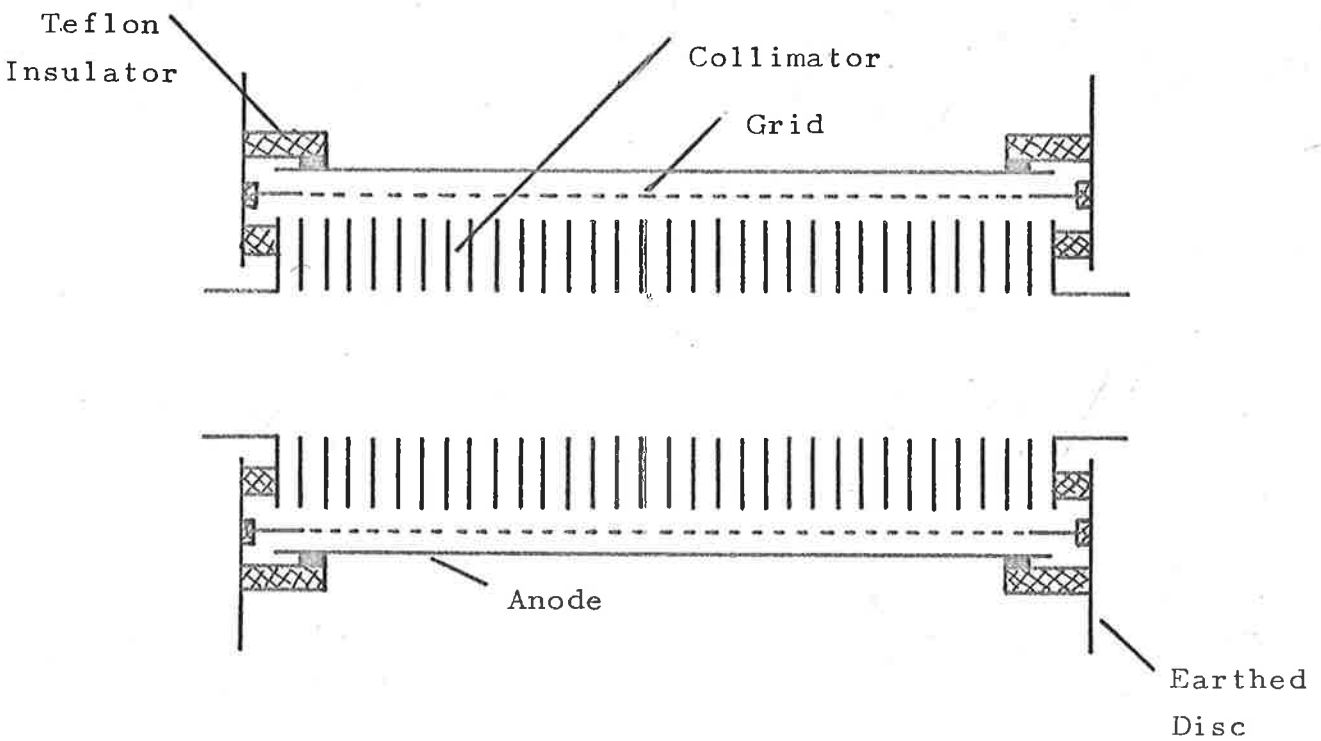

Fig.25. Diagram of the photoelectron spectrometer.

Fig. 26. Collimating electrode of the photoelectron spectrometer.

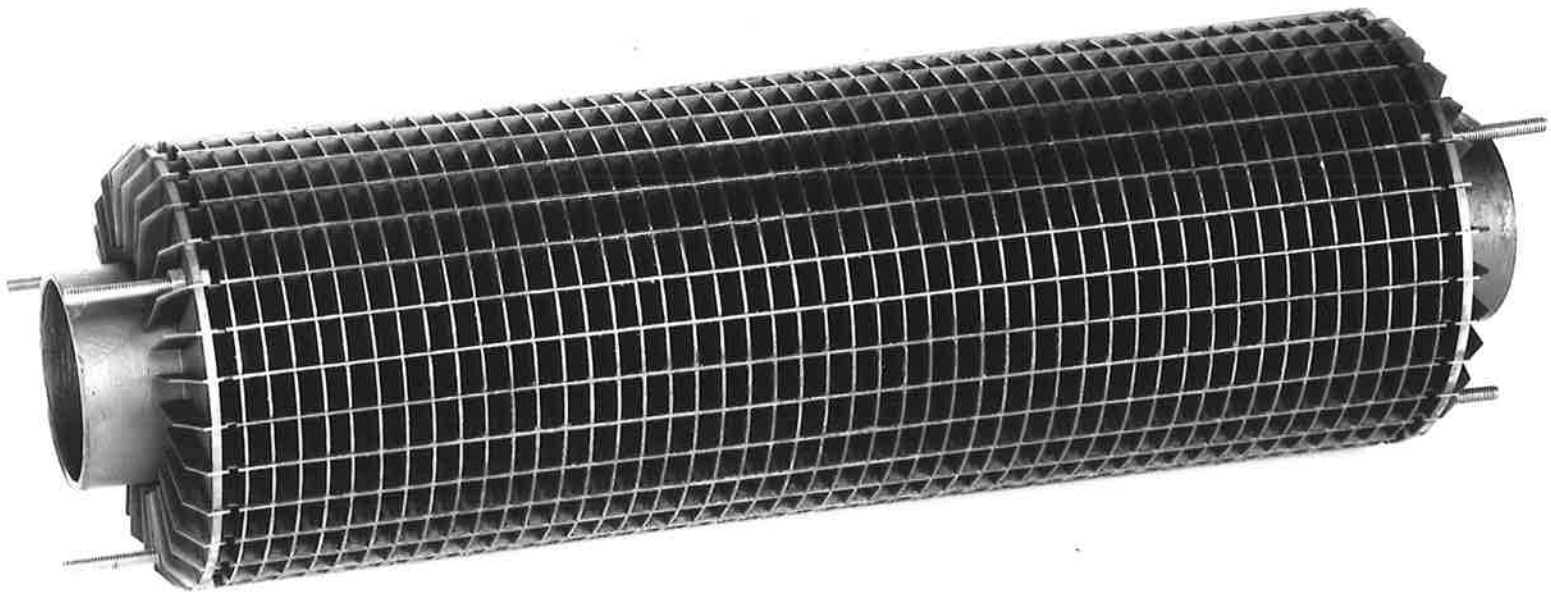

inch. Collimation with respect to ϕ was necessary because the beam from the monochromator almost filled the space within the collimator, and an electron produced at the edge of the beam, and travelling in a tangential direction, made a large angle with the retarding field. Collimation in this sense was achieved by including strips in the electrode which lay in planes which included radii of the spectrometer at 12° intervals. These longitudinal strips may be seen in Fig.26. The collimating electrode was constructed of copper, and coated with graphite (Aquadag) to reduce electron reflection and secondary emission, as explained in the Sec.III.5.1.

III.3.2 The analysing grid and anode

The analysing grid consisted of a cylinder of stainless steel wire mesh having 80 wires per inch. The grid was 3.5 inches in diameter, and 8.5 inches in length. Ideally the grid represents a cylindrical equipotential surface, which is transparent to electrons, but in fact the potential in the space between any pair of grid wires is different from the potential of the wires when there is a potential gradient either side of the grid, as shown in Fig.27. This potential variation may be reduced by placing the grid wires closer together, but a compromise has to be reached between the resolution of the grid and its transparency to electrons. An expression is derived in

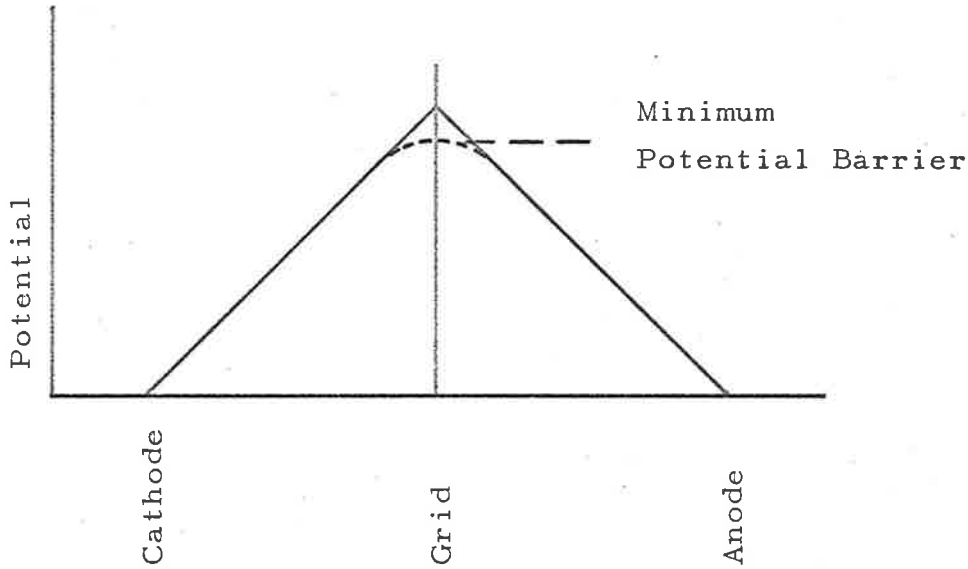

Fig.27. Potential barrier in a retarding potential analyser.

—— plane drawn through a grid wire.

---- plane drawn between a pair of grid wires.

Appendix II which gives the potential variation over the surface of a grid consisting of parallel wires in terms of the spacing of the wires, and the potential gradients on either side of the grid. The wire mesh which was used had a transparency of about 60%.

The anode was a cylinder of mild steel 4 inches in diameter, and 8.5 inches in length. Apart from acting as the anode, this cylinder provided shielding against magnetic fields; the magnetic field strength inside the anode was less than 40 milligauss.

III.3.3 Construction of the spectrometer

The completed spectrometer is shown in Fig.28. The three concentric electrodes were suspended from an earthed disc at either end of the spectrometer, as shown in Fig.25. The collimator and grid were insulated from the earthed discs with Teflon washers, and the minimum leakage path to earth from the anode was over a Teflon surface one inch in length. As well as being structural components of the spectrometer, the two earthed discs ensured that electrons not produced within the collimator could not reach the anode. The spectrometer was shielded by the metal walls of the vacuum chamber.

Because low gas pressures were used, only a small fraction of the beam was absorbed within the spectrometer. The remainder of the beam passed into the beam trap shown

Fig. 28. Photoelectron spectrometer and beam trap mounted on the end plate of the vacuum chamber.

in Fig.28, which was maintained at a positive potential of 22.5 volts to ensure that the electrons could not escape. The beam trap was coated on the inside with Aquadag to reduce secondary electron emission.

III.3.4 The vacuum chamber

The vacuum chamber (Fig.29) was constructed of copper tubing 6 inches in diameter. The spectrometer and beam trap were supported from the end plate of the vacuum chamber by four stainless steel rods, as shown in Fig.28. A sodium salicylate coated wire grid was supported from the end plate nearest to the monochromator, and was used to monitor the beam intensity in the manner described in Sec.II.3.4. Electrical connections to the electrodes were made through glass-covar seals in the end plate of the vacuum chamber. The vacuum chamber was windowless, and the ultraviolet beam entered through a wedge shaped channel, which constricted the flow of gas sufficiently to maintain a spectrometer operating pressure of 10^{-2} mm.Hg. while the pressure in the monochromator main chamber was less than 10^{-4} mm.Hg.

A two inch oil diffusion pumping system was used to evacuate the vacuum chamber to a pressure of less than 10^{-6} mm.Hg. A liquid air cooled trap was included to remove condensable impurities from the oxygen and nitrogen during experiments with these gases. The gas entered the chamber

Fig. 29. The spectrometer vacuum chamber and light source mounted on the 1-metre monochromator. The large tube in the background is part of the differential pumping system. The solid coaxial line can be seen in the foreground.

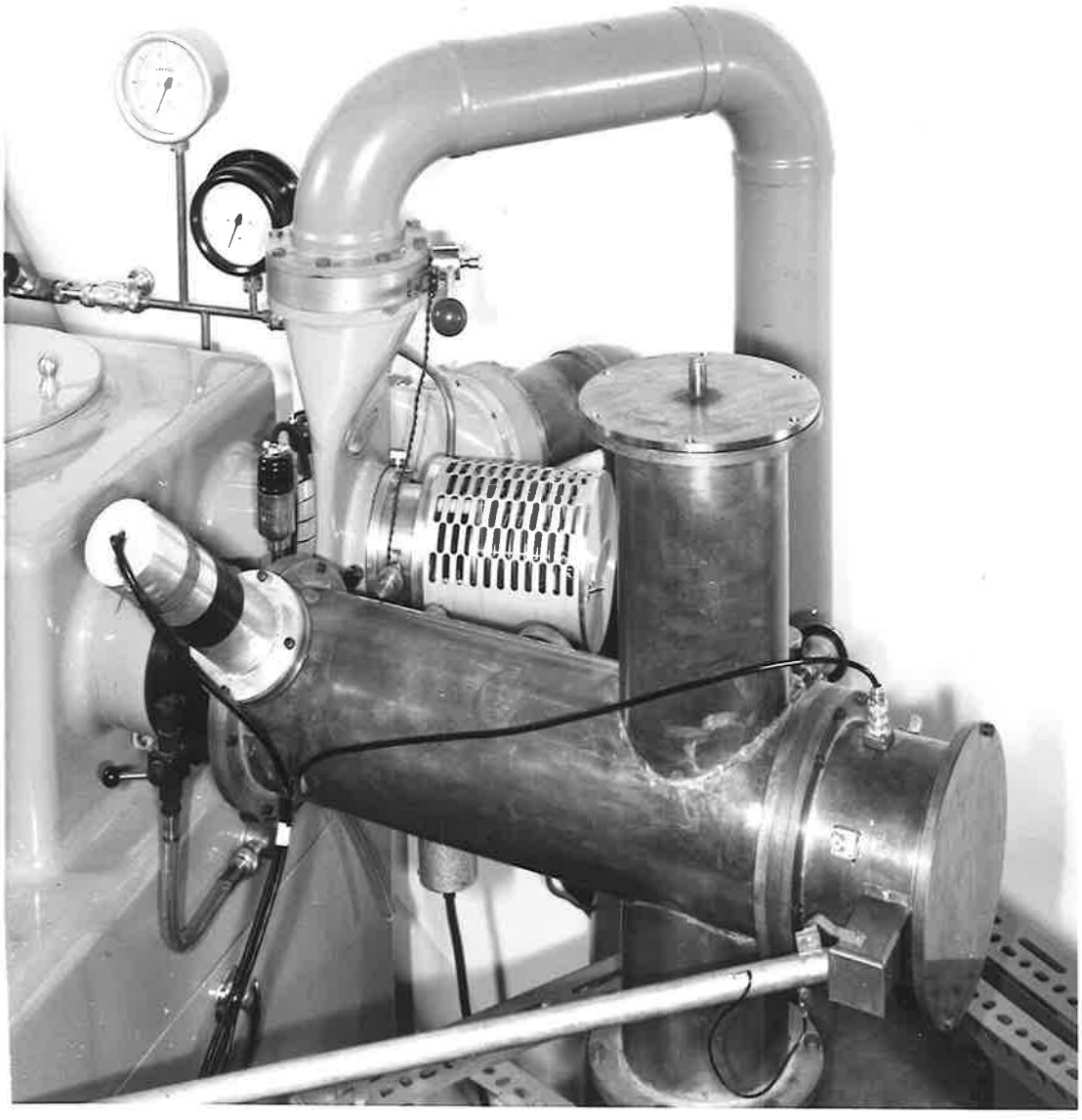

through a needle valve, which was adjusted to maintain a constant pressure in the chamber, and facilities were provided for attaching an ionization vacuum gauge, and a Pirani gauge to the chamber. The ionization gauge was used to measure the residual gas pressure when the chamber was evacuated, and the Pirani gauge was used to monitor the gas pressure during an experiment.

III.3.5 The monochromator

In the initial experiments with the photoelectron spectrometer a half-metre Seya-Namioka monochromator (McPherson model 235) was used. The light source was a capillary discharge through helium (Sec.II.1) at a pressure of 50 mm.Hg. The lamp was isolated from the monochromator by a single stage of differential pumping, provided by a mechanical booster pump (Speedivac IR5) and a backing pump (Speedivac 1SC450).

The partial cross-sections presented in Chapter IV were obtained from the results of experiments in which a one-metre near normal incidence monochromator (McPherson model 225) was used, with a 1200 line per mm. Bausch and Lomb replica grating, blazed for 1000 Å. An exit slit width of 1000μ gave a resolution of 9 Å. In this case the light source was isolated from the monochromator by a two stage differential pumping system, in which the first stage

was pumped by a mechanical booster pump* and a backing pump, while the second stage was pumped by an oil booster pump** and a backing pump. The differential pumping assembly allowed a maximum entrance slit width of 100μ, and with a slit of this width a pressure of better than 10^{-4} mm.Hg. could be maintained in the main chamber of the monochromator with the light source running. A general view of the experimental arrangement with the one-metre monochromator is shown in Fig.30.

III.4 Operation of the Spectrometer

III.4.1 Electrode voltages

The circuits for supplying potentials to the electrodes are shown in Fig.31. The anode was connected to the input terminal of an electrometer, and was restricted to earth potential. A collecting potential was applied between the analysing grid and the anode, to ensure that all the electrons which penetrated the grid were collected on the anode. Fig.32 is a plot of the electron current against the collecting potential for a constant (zero) retarding potential, which shows that the current was constant for collecting potentials greater than 5 volts.

---

* Godfrey KB/V400/28.

** Dynavac OB1500.

Fig. 30. General view of the apparatus used to record photoelectron energy spectra.

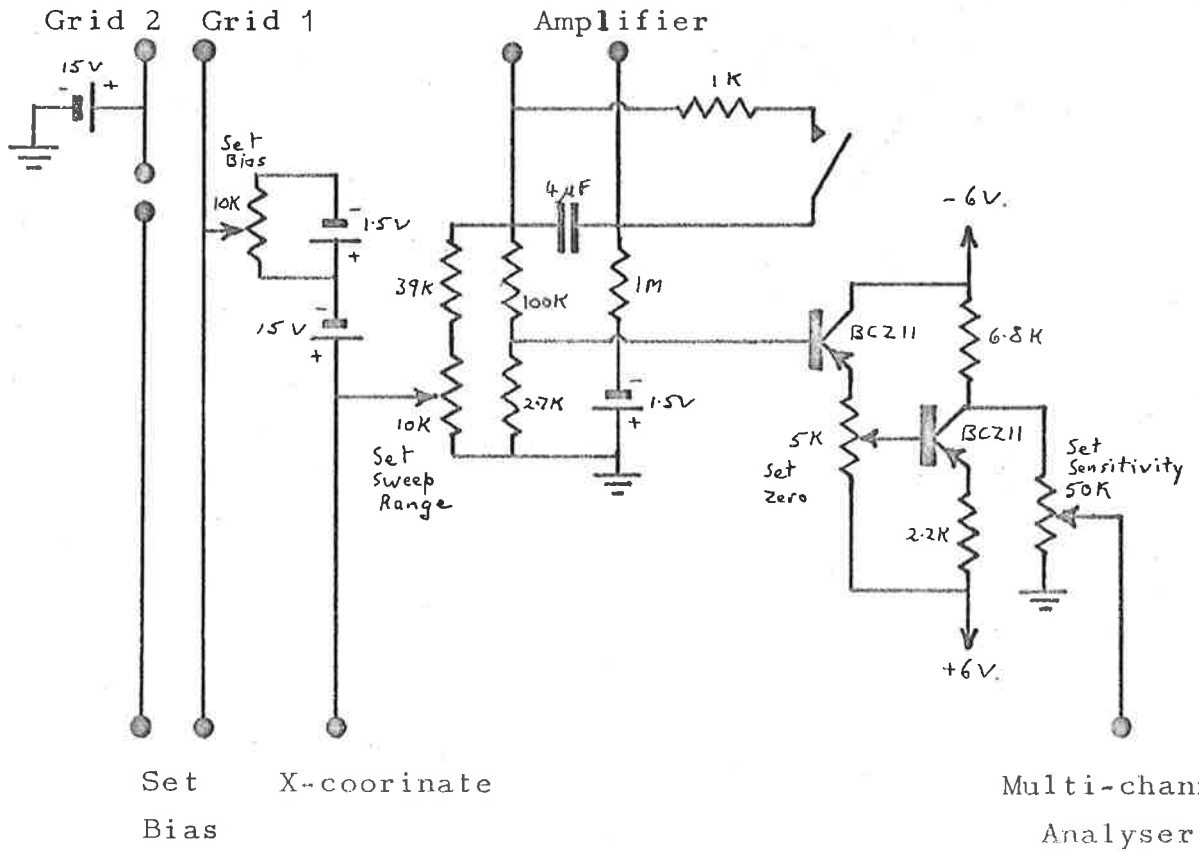

Fig.31. Circuit for supplying potentials to the spectrometer.

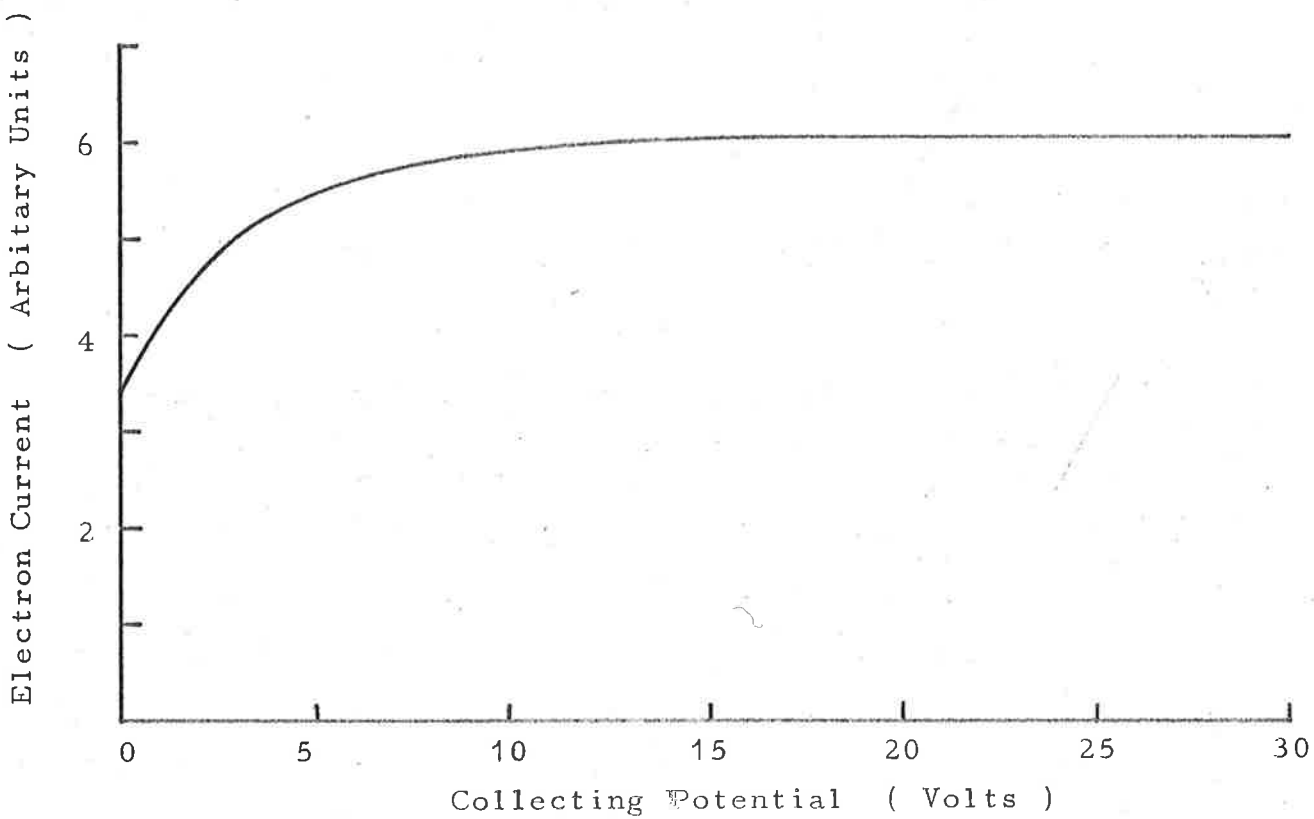

Fig.32. Saturation characteristic of the photoelectron spectrometer.

During the experiments the grid was held at a negative potential of 15 volts with respect to earth potential.

Since there was a relatively large capacity (200 pF) between the anode and the grid, the electrometer was very sensitive to transient voltages on the grid. For this reason the battery supplying the potential to the grid was placed in a shielded chamber at the end of the vacuum chamber, and no other connections were made to the grid. This chamber also contained the battery supplying the potential to the beam trap, and the input resistor for the electrometer.

The retarding potential was applied by changing the potential of the collimator relative to that of the grid, and the spectrum of electron energies was scanned by sweeping the retarding potential linearly with time. The linear sweep was generated by using an operational amplifier (Philbrick USA-3) to integrate a constant potential. After four minutes the potential was shorted for one minute with a cam operated micro-switch, and then allowed to start again. Because of a small amount of capacitive coupling between the collimator and the anode, a transient appeared on the anode when the retarding potential sweep was started. The effect of this transient on the spectrum was eliminated by applying a bias to the collimator potential so that each sweep started from a negative potential of one volt.

This allowed the circuit to recover from the transient before the scan through the spectrum was started. The bias was adjusted before each experiment by measuring directly the potential difference between the grid and the collimator.

III.4.2 Recording of the spectra

The electron current from the anode produced a small voltage across the high resistance (10^{10} ohms) at the input of the electrometer (Wayne-Kerr model M141). Flexible coaxial cables were found to be unsatisfactory for making the connection between the anode and the electrometer because of the potentials generated in the cable when it moved. The connection was made with a solid coaxial line consisting of a $\frac{5}{8}$ inch diameter brass tube with a $\frac{1}{8}$ inch diameter brass rod supported along its axis with Teflon spacers, which eliminated vibration from the line.

The curve obtained by recording the electron current as a function of the retarding potential is the integral of the electron energy spectrum, since all electrons with energies greater than the retarding potential are detected. In principle the curve consists of a series of steps - one step for each discrete energy present in the spectrum. In the curves which have been obtained, the steps are not well defined because of the limited resolution

of the apparatus, and because of the fine structure in the spectra. An integral spectrum from molecular oxygen is shown in Fig.33.

The electron energy spectrum was obtained by differentiating the electron current with respect to the retarding potential. Since the retarding potential was swept linearly with time, the differential with respect to the retarding potential was equal to the differential with respect to time, and the electron energy spectra were recorded directly by differentiating the output voltage of the electrometer. The circuit for recording the spectra is shown in Fig.34. The differentiating circuit consisted of a paper condenser, and the input resistance of a d.c. amplifier (Hewlett-Packard model 425A). An X-Y coordinate plotter (Mosely model 2D-2) was used to record the spectra; the retarding potential was applied to the X-axis, and the output of the differentiating circuit to the Y-axis. A photoelectron energy spectrum from oxygen at an incident beam wavelength of 584 Å is shown in Fig.35.

III.4.3 Digital noise averaging

The electron energy spectra recorded directly on the X-Y coordinate plotter were found to be of poor quality because of the large amount of noise on the trace. Most of the noise probably originated in the input circuit of the electrometer, which was very sensitive to electrical

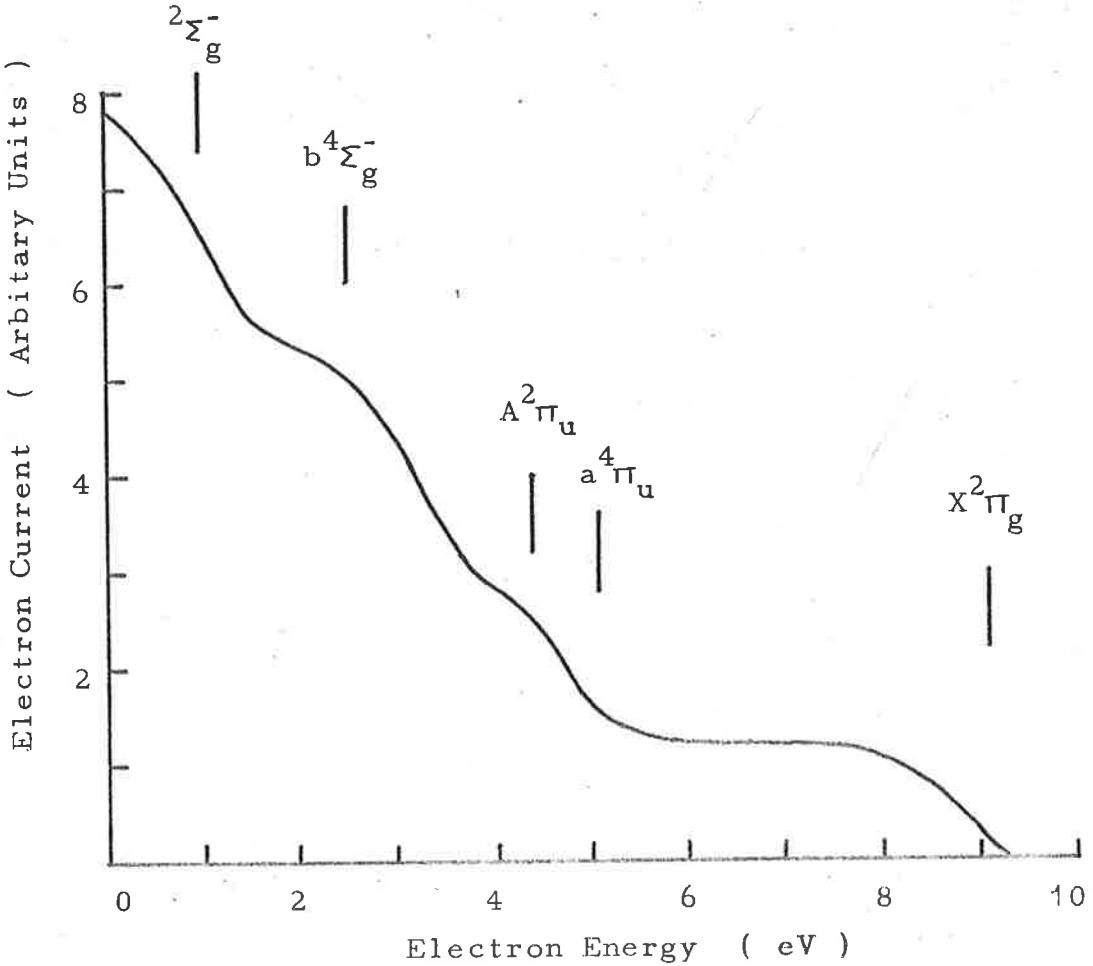

Fig.33. Integral photoelectron spectrum from O_2 with an incident beam wavelength of 584 Å.

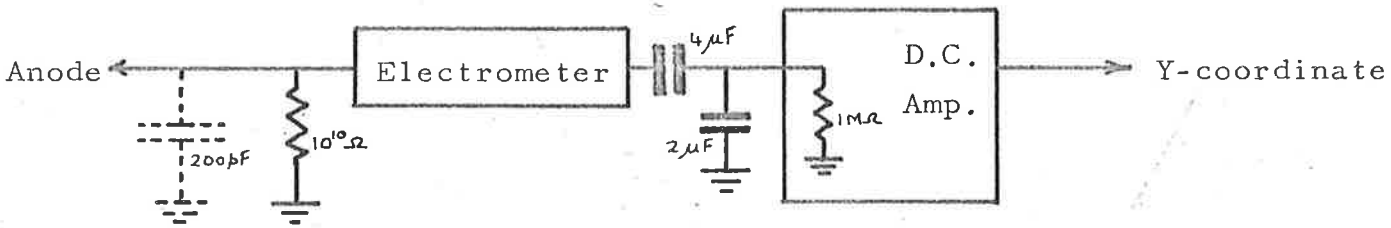

Fig.34. Circuit for recording electron energy spectra.

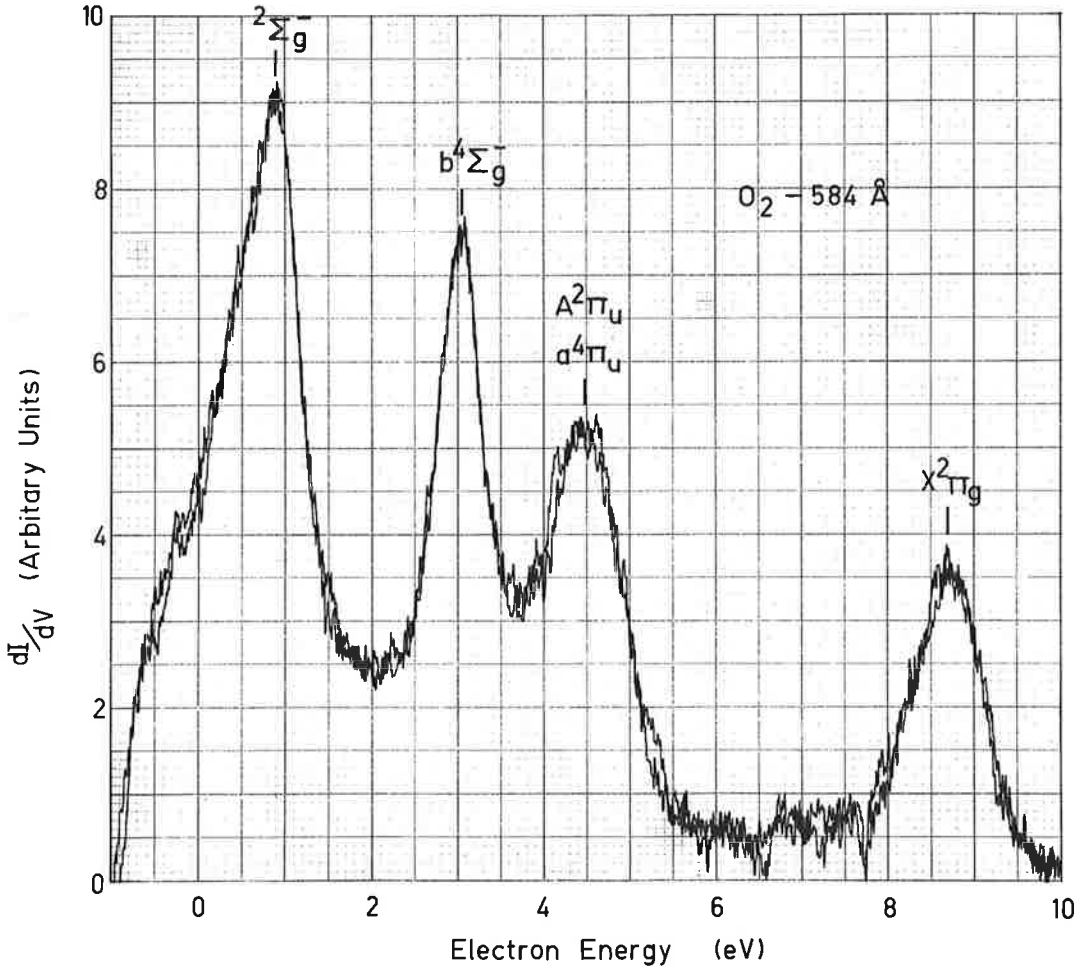

Fig.35. Photoelectron spectrum from O_2 at a resolution of 0.4 eV with an incident wavelength of 584 Å.

interference and mechanical vibration. A large amount of electrical noise was generated at the spark gap of the power supply for the monochromator lamp. The effect of this noise was minimised by careful shielding of the input circuit, and by choosing the best time constants in the electrical circuits. These time constants are discussed in the next section. Some mechanical vibration was always present because of the mechanical vacuum pumps. The effect of this vibration was minimised by using the solid coaxial line to the electrometer, and by making all parts of the input circuit as rigid as possible.

For some spectra, where the noise on the trace was relatively small, sufficient averaging of the noise was achieved by super-posing several traces of the spectrum. Spectra which could not be satisfactorily smoothed by this method were smoothed by converting the spectra to digital form, and numerically adding as many scans of the spectrum as were required to produce a smooth curve. This digital averaging of the noise provided a powerful method of producing satisfactory spectra under adverse conditions which existed, for example, in regions where the intensity of the light source was low.

Analogue to digital conversion of the spectra was achieved with the circuit shown in Fig.36. The voltage output from the differentiating circuit was sampled ten

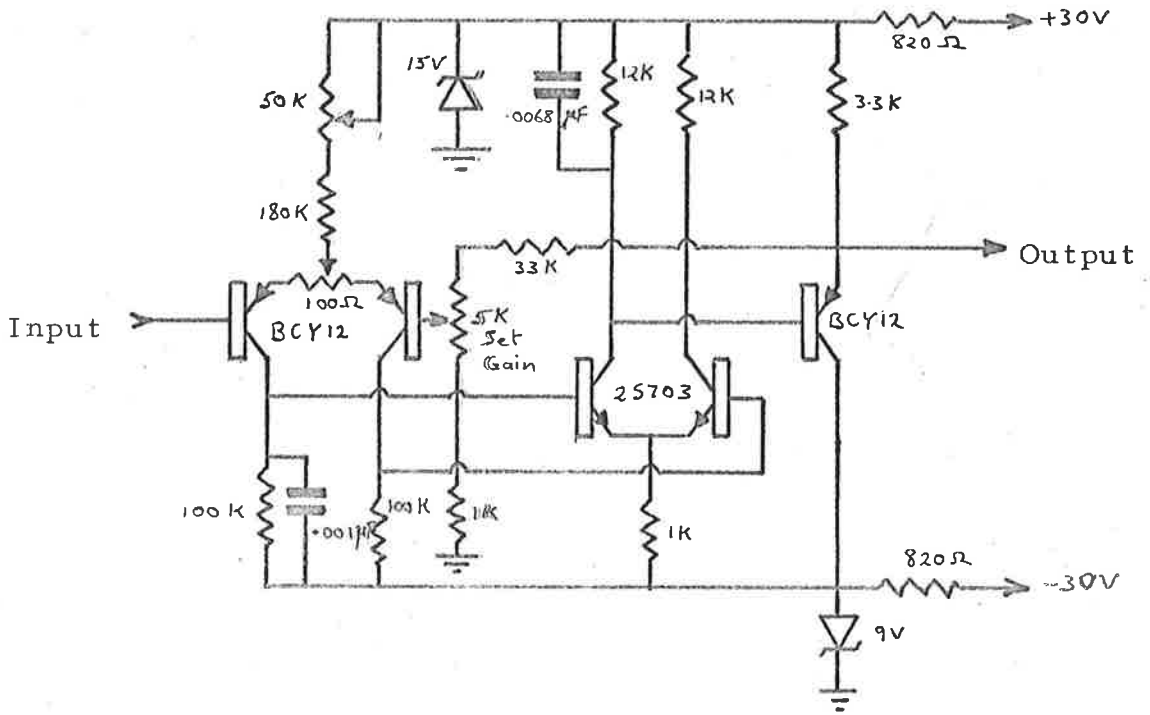

Fig.36. Analogue to digital converter
(a) D.C. amplifier

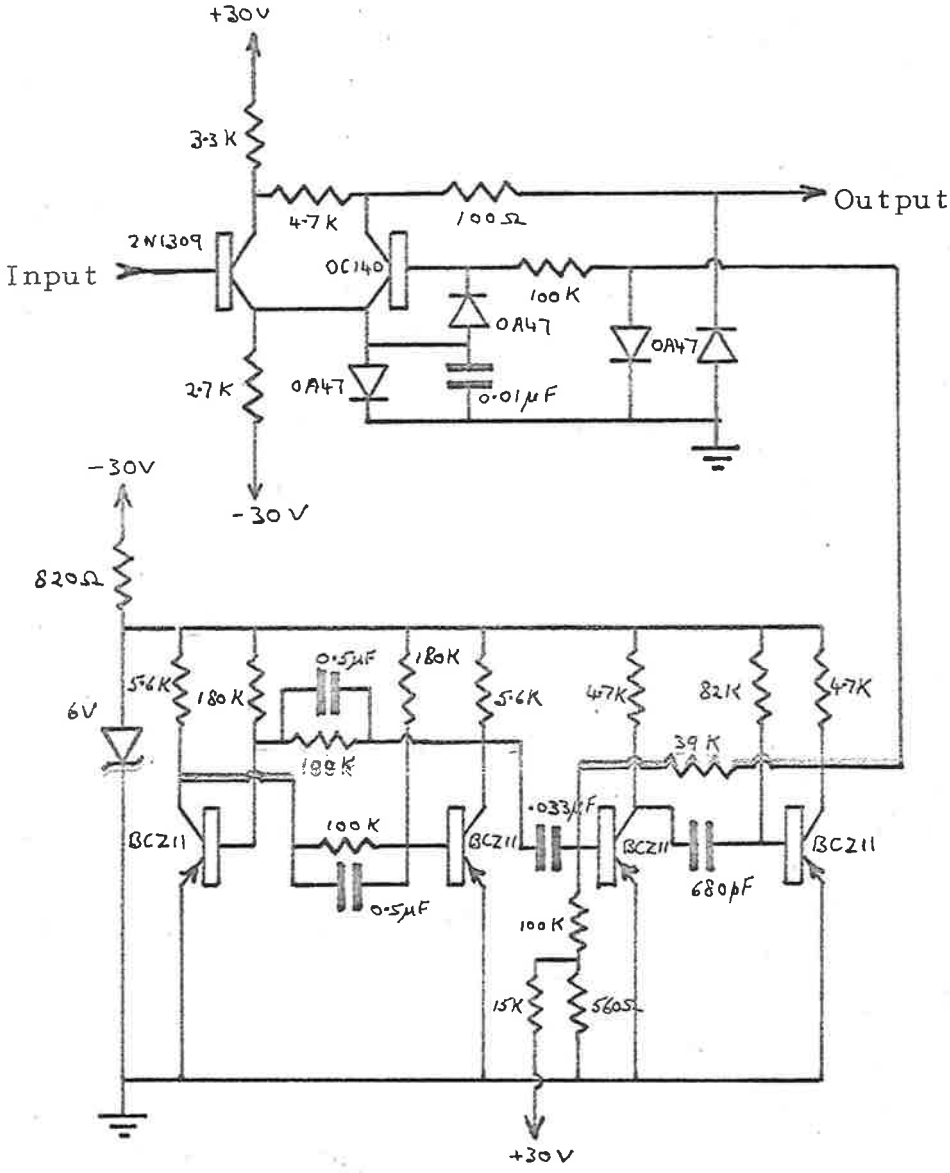

Fig.36. Analogue to digital converter
(b) Linear sampling gate

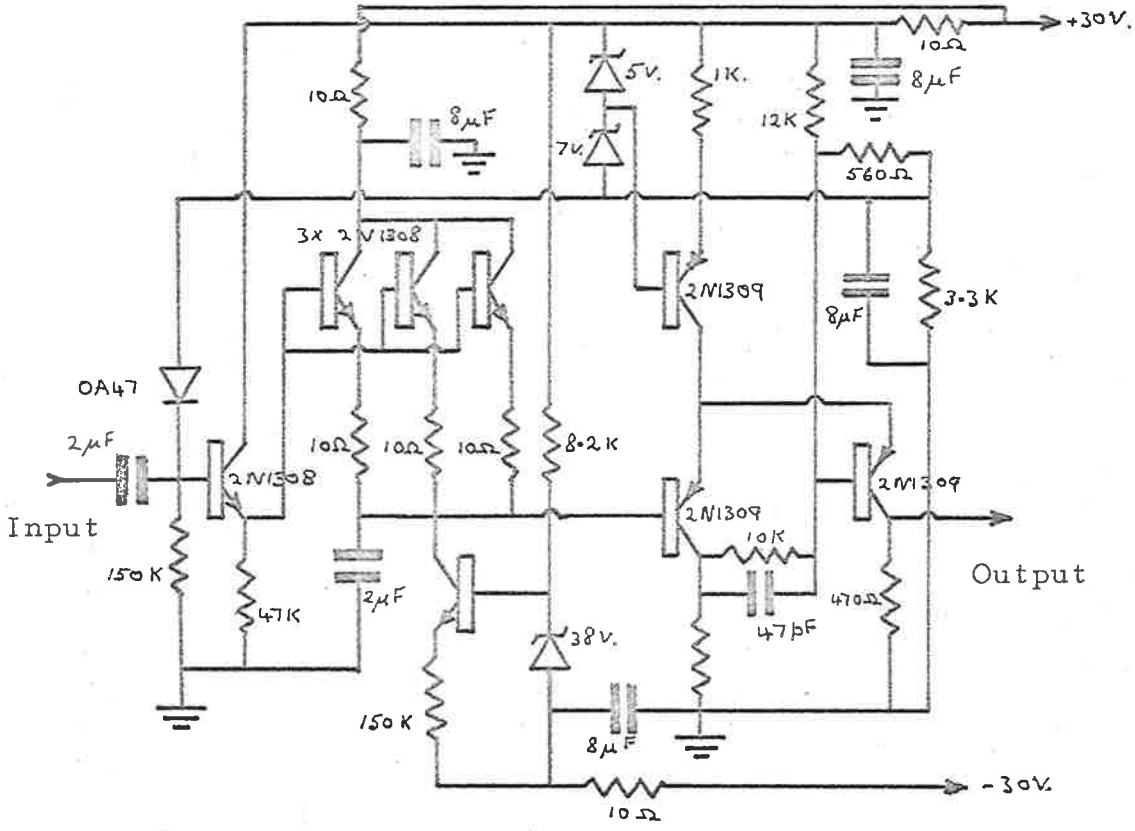

Fig.36. Analogue to digital converter.
(c) Pulse duration modulator.
(Waugh 1964)

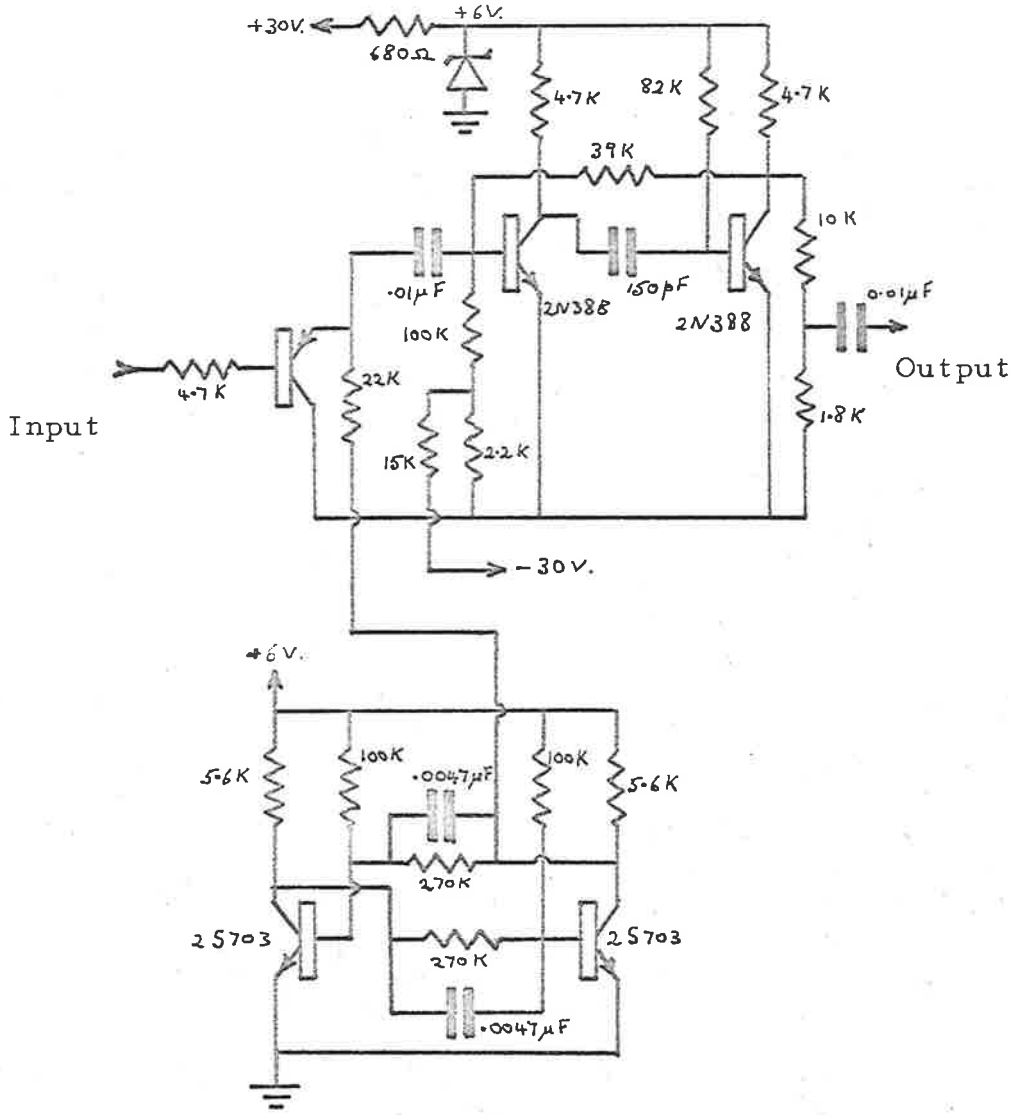

Fig.36. Analogue to digital converter.
(d) Oscillator and gate.

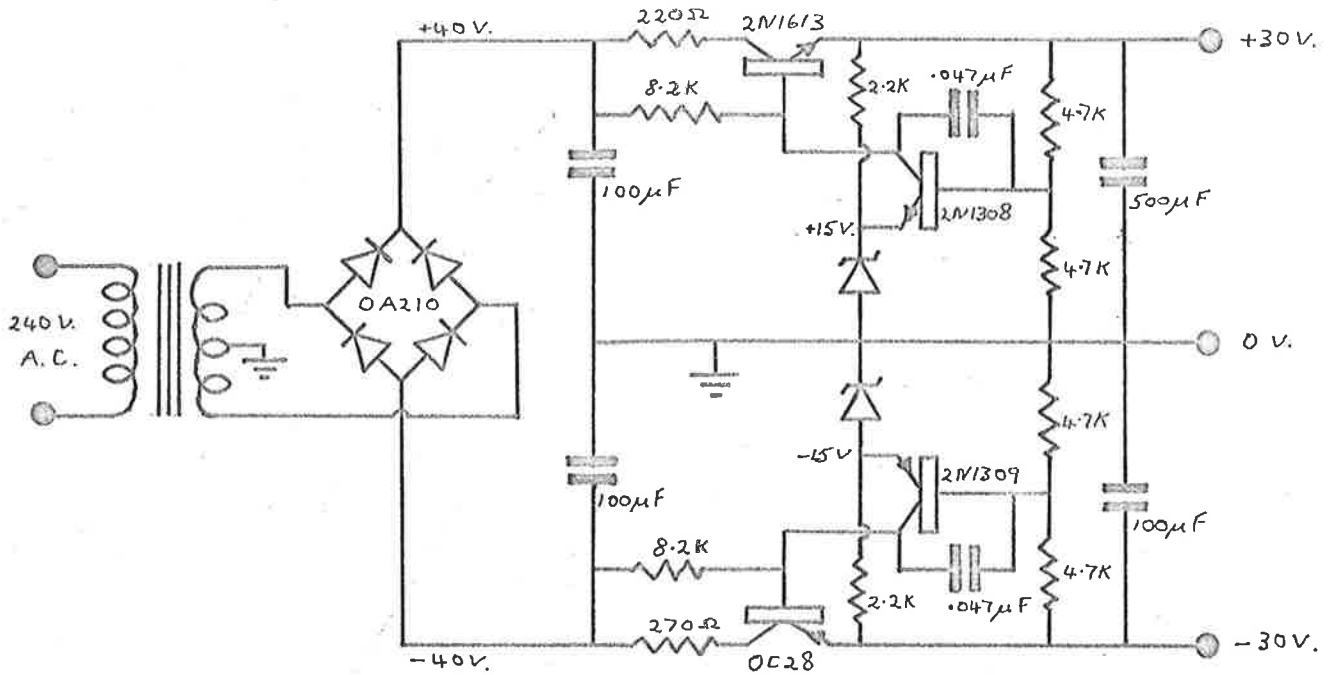

Fig.36. Analogue to digital converter.
(e) Regulated power supply.

times per second, and a pulse duration modulator (Waugh 1964) was used to gate an oscillator. The gain of the amplifier at the input of the analogue to digital converter was adjusted for each spectrum, so that best use was made of the range of input voltages for which the converter was found to be linear. The pulses from the analogue to digital converter were fed into a 400 channel pulse height analyser (R.I.D.L. model 34-12B). Each pulse was stored in the channel whose number was proportional to the retarding potential at the time of arrival of the pulse.* The overall linearity of the system was checked by supplying the analyser with pulses at a constant frequency, while the channels were addressed with the retarding potential. This procedure produced a flat spectrum, indicating that, as required, the retarding potential increased quite linearly with time. (c.f. Sec.III.4.2). Only two hundred of the channels were used to store each spectrum, because the time required for the analyser to store a pulse in a channel of number higher than two hundred did not allow a sufficiently high count rate. However, the spacing between the two hundred channels was much smaller than the resolution of the experiment. Each spectrum was recorded

---

*This facility of addressing channels in which the channel number is proportional to an analogue voltage is provided as a standard feature of the R.I.D.L. model 34-12B.

by allowing the retarding potential to recycle until the stored spectrum became smooth, and did not change in shape as further scans were added. The final spectrum was returned to analogue form and recorded on the X-Y coordinate plotter. Individual scans of the spectrum were also recorded on the X-Y plotter, so that spectra with large transients could be discarded.

The retarding potential was measured under the condition that no current was being drawn from the circuits supplying the potential, using the circuit shown in Fig.37, which was connected directly between the collimator and the grid only when a measurement was being made. Zero retarding potential was identified on each spectrum.

III.4.4 Time constants of the apparatus

The important time constants of the apparatus were the time constant at the input of the electrometer, the time constant of the differentiating circuit, and the rate of scan of the retarding potential. Of these time constants only the time constant of the electrometer could not be easily changed over a wide range. The factors which determined this time constant were dominated by the capacitance between the spectrometer anode and earth (~200 pF), and the input resistance to earth (~10^{10} ohms), which gave a time constant of not less than two seconds. The value of 10^{10} ohms for the input resistance was the

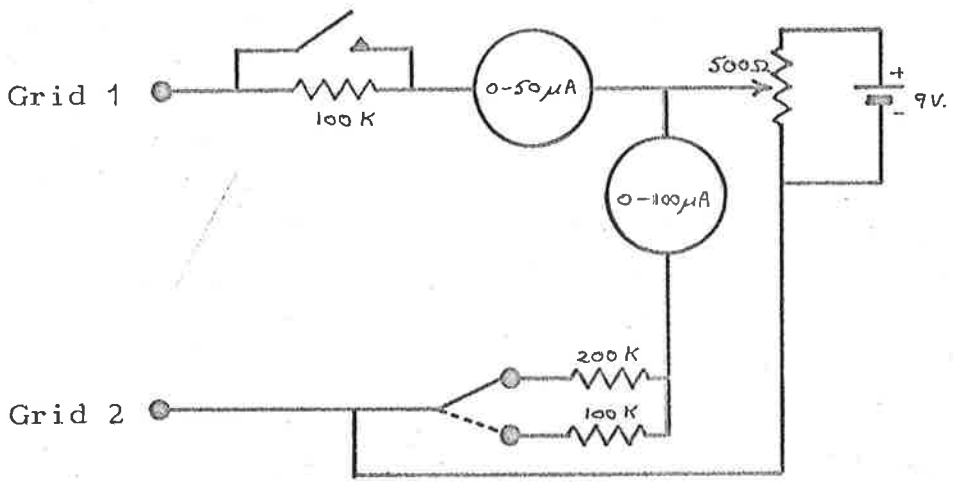

Fig.37. Circuit for calibrating the energy scale of the smoothed spectra.

minimum value necessary to produce a sufficient potential at the input of the electrometer.

The time constant of the differentiating circuit was adjusted to a value at least as large as the time constant of the electrometer input circuit, so that the differentiating circuit tended to smooth out the noise in the electrometer output. In most of the experiments the differentiating time constant was four seconds. The circuit consisted of a 4μF paper condenser, and the one megohm input resistance of the d.c. amplifier. For each spectrum the gain of both the electrometer and the d.c. amplifier were adjusted to give the largest possible signal in each part of the circuit. The noise was further reduced by adding another time constant of two seconds at the input of the d.c. amplifier, as shown in Fig.34. This was necessary because of electrical interference from the spark gap of the lamp power supply.

The rate of scan of the retarding potential was adjusted so that the effect of the time constants of the electrical circuits did not contribute greatly to the resolution of the apparatus. The scan rate was set as large as possible, so that a large signal was obtained from the differentiating circuit. A rate of scan of 30 mV per second was found to be the maximum rate which did not appreciably increase the width of the peaks in the spectrum.

The photoelectron spectra recorded with the apparatus had a resolution corresponding to a full width at half maximum 0.4 eV under the best conditions.

III.5 Performance of the Spectrometer

Before the electron spectra could be interpreted in terms of partial cross-sections corresponding to transitions to a particular state of the ion, several characteristics of the spectra had to be studied. These were the detailed shape of the individual peaks of the spectrum, the resolution of the spectrometer, and the calibration of the energy scale. The spectrometer was checked using argon, and a monochromatic beam of radiation. This provided almost monoenergetic photoelectrons, since only the doublet ground state $^2S_{\frac{1}{2},3/2}$ of the argon ion was accessible with the photon energies which were used in the experiment.

III.5.1 The monoenergetic electron spectrum

In the initial experiments with the spectrometer the photoelectron spectra from argon which were recorded were of the form shown in Fig.38. This spectrum contained a single peak at the energy equal to the excess of the photon energy over the ionisation potential of argon, and also a large area at low energy. Several possible origins of the low energy portion of the spectrum were investigated. Spectra obtained over a range of gas pressures (Fig.38) were

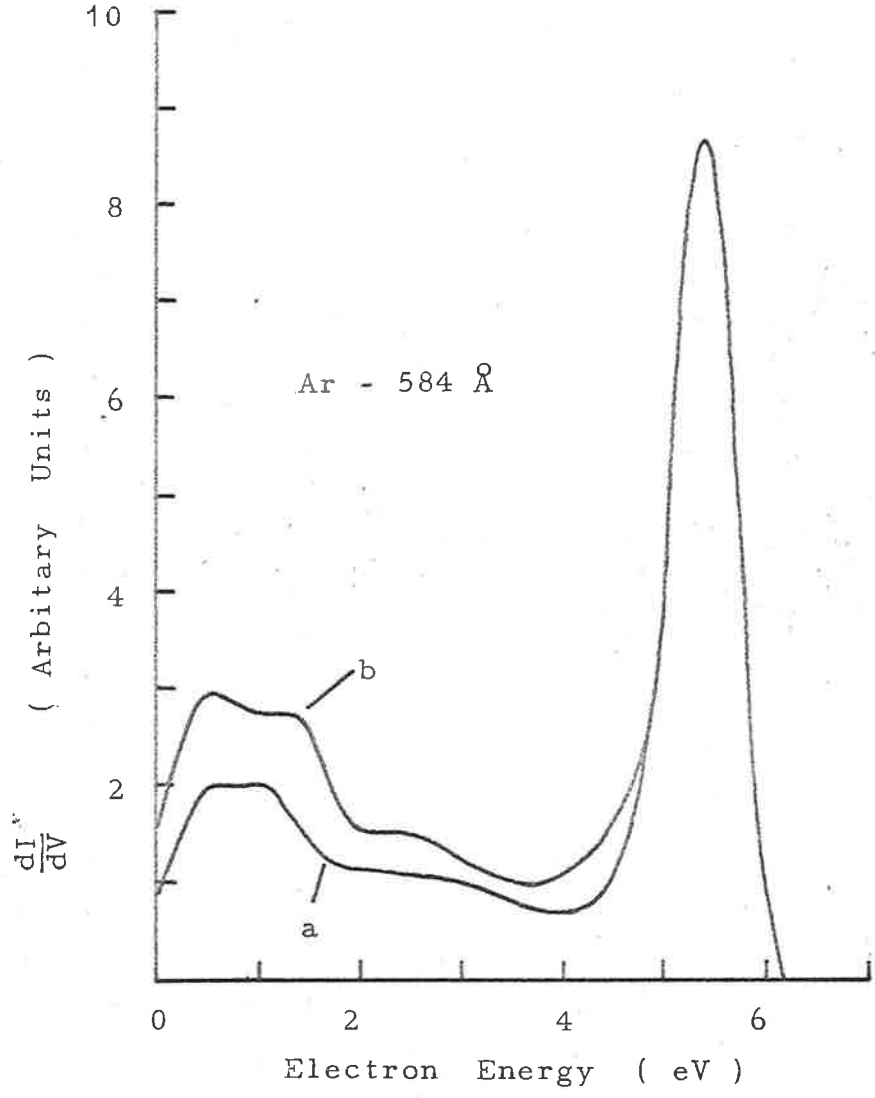

Fig.38. Photoelectron energy spectra from argon at different pressures.
(a) 1.5×10^{-3} mm. Hg.
(b) 10×10^{-3} mm. Hg.

all similar in shape, showing that the low energy component of the spectrum was not due to electron collisions with gas atoms. Scattering of this nature was not expected to be important, since the mean free path of electrons in argon at the pressures used was of order 20 cm., (Healey and Reed 1941) while the distance which the electrons had to travel to the analysing grid was not greater than 6 cm. The effect of magnetic fields on the spectra was also investigated, but no difference was found between spectra obtained with a steel anode, which provided magnetic shielding, and those obtained with a copper anode. The remaining possible origin of the low energy part of the spectrum was reflection at the surface of the collimating electrode. When a coating of colloidal graphite (Aquadag) was placed on the collimator, the greatly improved spectrum shown in Fig.39 was obtained. Aquadag has the property of reducing electron reflection and of producing a more uniform contact potential over a surface (Hasted 1964).

For the purpose of analysis the spectrum was divided into two parts. The first was a symmetrical peak, marked A_1 in Fig.39, and the second was the remaining low energy part, marked A_2 in Fig.39, which was due to electron reflection and secondary emission from the electrode surfaces. It was assumed that the peak shape depended only on the peak energy, and the ratio of the areas A_1

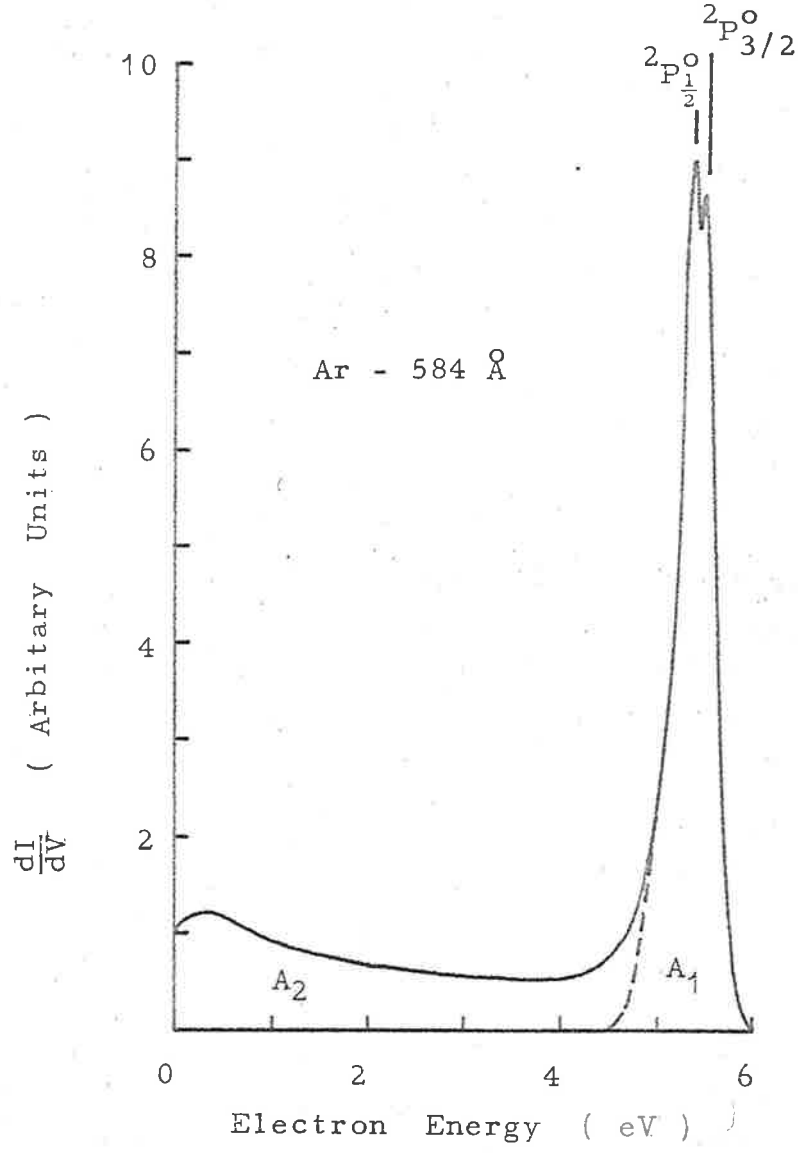

Fig.39. Photoelectron energy spectrum from argon with an incident beam wavelength of 584 Å.

and A_2 was measured over a range of peak energies in order to unfold more complicated spectra. (See Sec.IV.1.2). The results are shown in Fig.40. The shape of the argon spectrum was compared with that of the molecular hydrogen spectrum (Fig.41) which contained a single band with a width of 1.7 eV. The ratios A_2/A_1 obtained from hydrogen spectra at two different wavelengths, which are shown in Fig.40, are in good agreement with the points obtained from argon spectra, showing that the spectrum shape does not depend critically on the peak width.

The effectiveness of the electron collimation was checked by recording a spectrum from argon with the collimating electrode removed, and replaced by a second grid. A spectrum which was recorded in this manner is shown in Fig.42. The shape of this spectrum is determined by the angular distribution of the emitted photoelectrons, which has been shown (Bethe and Salpeter 1956) to be independent of ϕ for an unpolarized incident beam, and to depend on θ according to the expression:

$$f(\theta) = A + B \sin^2\theta \qquad (22)$$

where A and B are constants which depend on the quantum number ℓ of the electron. The peak shape is given by the function:

$$\frac{dN}{dE} = \frac{dN}{d\theta} \cdot \frac{d\theta}{dE} \qquad (23)$$

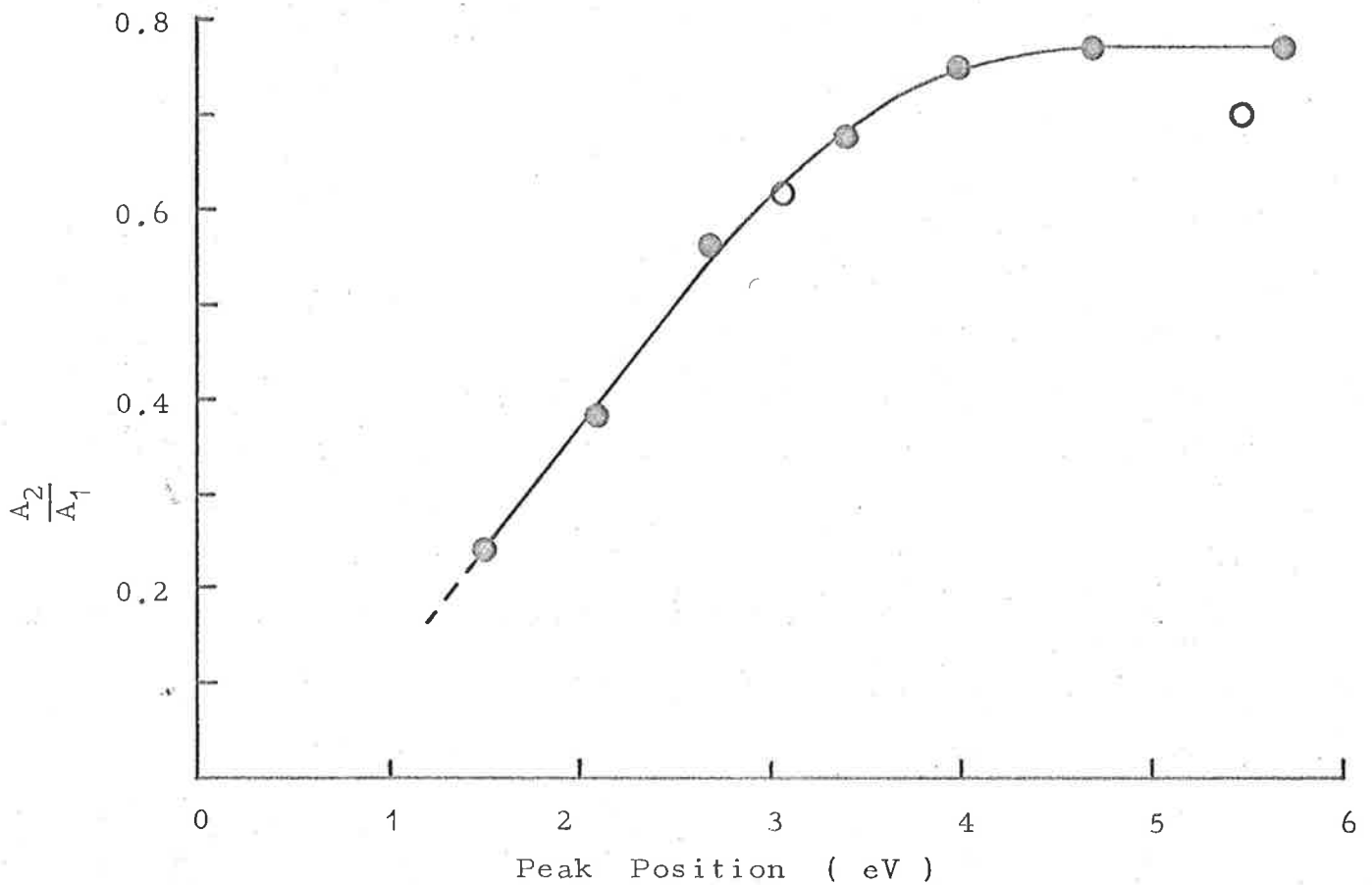

Fig.40. ● Argon peak shape as a function of peak position.
○ Hydrogen peak shape.

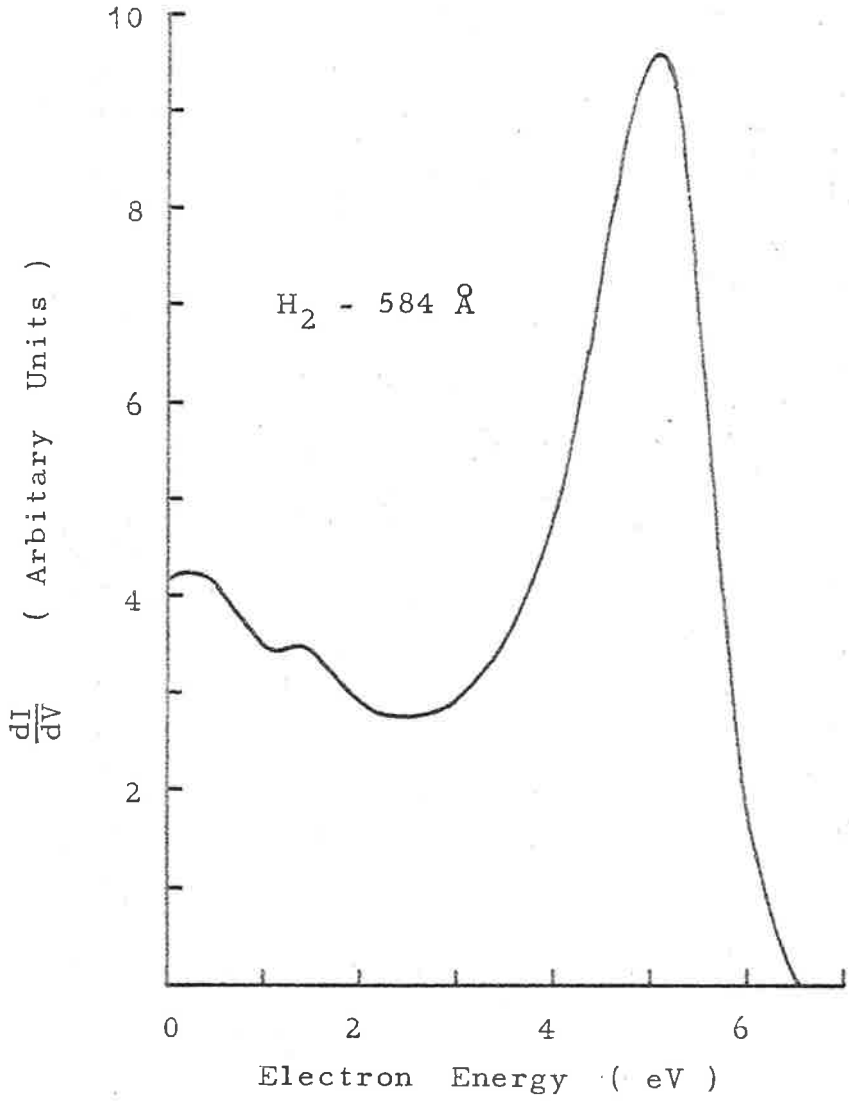

Fig.41. Photoelectron energy spectrum from hydrogen with an incident beam wavelength of 584 Å.

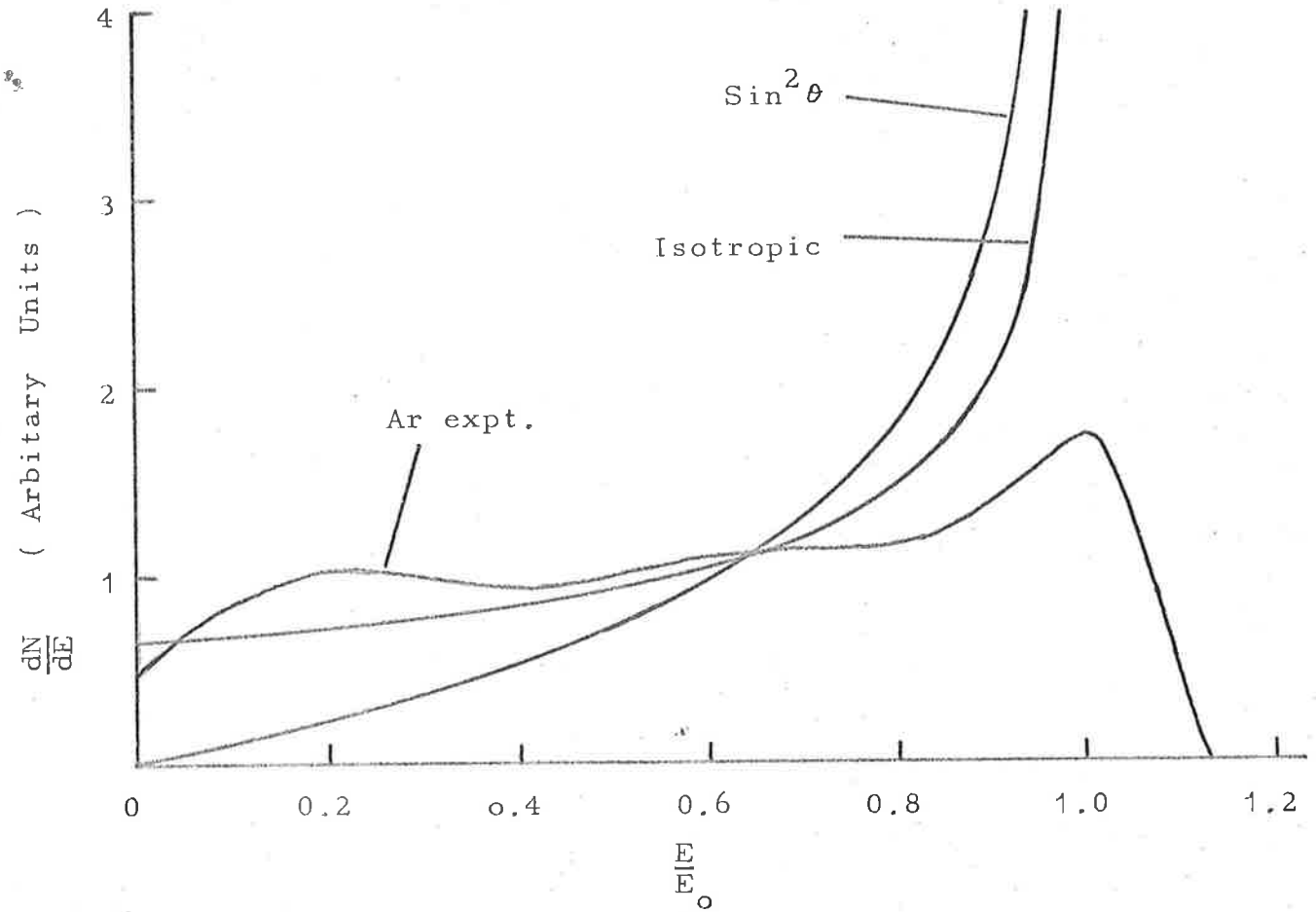

Fig.42. Theoretical uncollimated peak shapes for isotropic and $\sin^2\theta$ angular distributions compared with the experimental curve from argon.

where

$$E = E_o \sin^2\theta \qquad (24)$$

and therefore

$$\frac{dE}{d\theta} = 2E_o\left(\frac{E}{E_o}\right)^{\frac{1}{2}}\left(1 - \frac{E}{E_o}\right)^{\frac{1}{2}} \qquad (25)$$

The angular dependence of N can be written in the form:

$$\frac{dN}{d\theta} = \frac{dN}{d\Omega} \cdot \frac{d\Omega}{d\theta} = f(\theta) \sin\theta \qquad (26)$$

whence

$$\frac{dN}{dE} = \left(1 - \frac{E}{E_o}\right)^{-\frac{1}{2}} f(\theta) \qquad (27)$$

The peak shape must lie between the two extremes corresponding to A = 0, which gives a pure $\sin^2\theta$ distribution, and B = 0, which gives an isotropic distribution. These two peak shapes are compared in Fig.42 with the uncollimated peak shape obtained from argon, which corresponds to the removal of a p-electron. The three curves shown in Fig.42 are normalised so that they contain the same area. The experimental curve appears to correspond to an isotropic distribution.

III.5.2 Factors effecting the resolution

The resolution of the spectrometer was defined as the full width at half maximum of the peak produced by a monoenergetic electron source. The width of the argon peak was used as a measure of the resolution, and was found to be 0.4 eV under the best operating conditions, with 584 Å radiation incident on the gas, giving a peak energy

of 5 eV. This resolution was just sufficient, as shown in Fig.39, to distinguish the doublet terms of the ground state of the argon ion which have a separation of 0.18 eV.

Several factors contributed to the peak width. The range of angles accepted by the collimator represented a 5% spread in the apparent energy of the electrons, corresponding to a width of 0.25 eV at a peak energy of 5 eV. The contribution to the peak width from the time constants in the electronic circuits was small. A time constant of two seconds at the input of the electrometer gave an energy spread of 0.06 eV at a scan rate of 30 mV per second, and the differentiation time constant of one second corresponded to an energy spread of 0.03 eV. The variation of potential over the surface of the grid was 0.04 eV (see Appendix II). The exit slit of the monochromator was 300μ wide, giving a resolution of 2.5 Å, or an energy spread of 584 Å of 0.10 eV. To these factors must be added the natural width of 0.18 eV due to the separation of the unresolved doublet. Treating these factors as independent Gaussian distributions, and combining them quadratically, one obtains a total peak width of 0.46 eV, which compares well with the measured peak width.

Other factors which had an unknown effect on the resolution of the spectrometer were contact potentials in the electrodes, small distortions of the analysing grid from

cylindrical form, and an electrostatic lens effect at the outer surface of the collimating electrode. Although the photoelectrons were produced in a region of uniform potential, they may have been effected by an electrostatic lens effect, due to field penetration into the relatively coarse structure of the collimator. The significance of this effect was checked by wrapping a fine wire mesh around the collimator. Although there was a slight improvement in the peak width, the improvement did not compensate for the loss of transparency of the electrode system, and the extra grid was not used in later experiments.

The partial photoionization cross-sections were obtained from spectra obtained under conditions where the resolution was not as good as that quoted above. Some of the resolution was sacrificed in order to improve the signal to noise ratio in the spectra. The monochromator exit slit width was increased to 1000μ, giving an energy spread in the beam of 0.33 eV, and the electrometer time constant and the differentiation time constant were both increased to 4 seconds. This gave a total calculated peak width of 0.63 eV, compared with the measured peak width of 0.6 eV.

III.5.3 Calibration of the energy scale

The energy scale of the spectrometer was calibrated using the position of the argon peak as a standard. The

$^2S_{\frac{1}{2}}$ and $^2S_{3/2}$ levels of the argon ion were taken to be 15.76 eV and 15.93 eV respectively above the ground state of the argon atom. (Moore 1949). In spectra where the two levels could not be distinguished, the position of the peak was taken to be the average of the two levels. The wavelength scale of the monochromator was calibrated using as standards the helium and neon emission lines present in the lamp spectrum. In Fig.43 the peak position is plotted against the true peak energy over a range of photon energies. The points all lie very close to a straight line which does not pass through the origin, indicating that the apparent energy scale is displaced from the true one by 0.3 eV. The calibration had an accuracy of better than 0.1 eV.

The energy scale continued to be linear at least down to a peak energy of 0.25 eV. This was important because it allowed confidence to be placed in the partial cross-sections which were measured near the threshold energy of a transition.

III.5.4 Electron collecting efficiency.

Two possible sources of error in the spectra were variations of the electron collecting efficiency with the electron energy, and with the gas pressure. The electron collecting efficiency was measured as a function of electron energy using argon as a source of monoenergetic photoelectrons

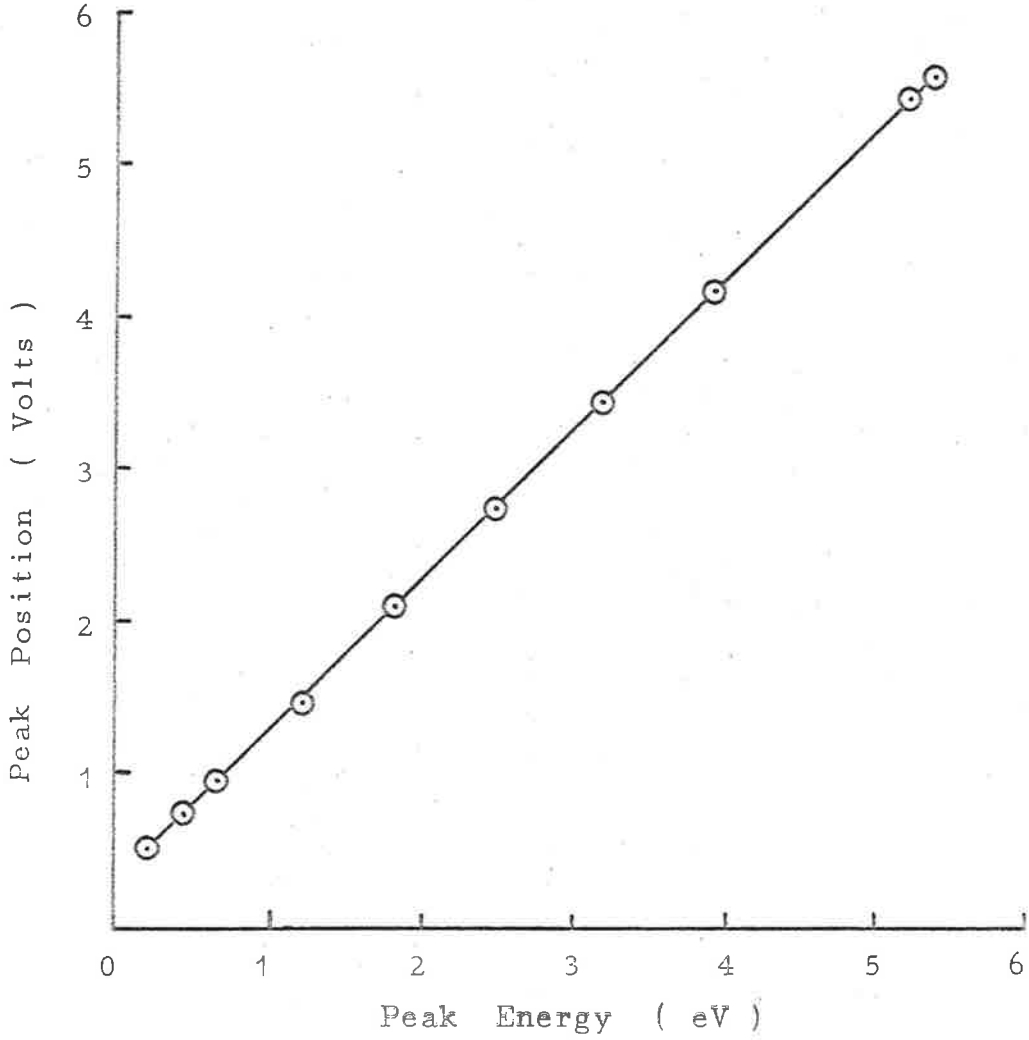

Fig.43. Calibration of the energy scale obtained from argon photoelectron spectra at various wavelengths.

whose energy could be adjusted by changing the wavelength of the incident beam. The spectrometer was used to measure the photoionisation yield of argon, and since this has been shown to be constant, (Samson 1964d) apparent changes in the yield reflected changes in the electron collecting efficiency of the spectrometer.

In Fig.44 x_1 is the path length through the gas between the beam sampling grid and the spectrometer, and x_2 is the path length through the spectrometer; I_0, I_1 and I_2 are the relative beam intensities at the points indicated on the diagram. Then:

$$I_1 = I_0 e^{-kx_1} \text{ and } I_2 = I_0 e^{-k(x_1 + x_2)}. \qquad (28)$$

The electron collecting efficiency is proportional to:

$$\frac{i_t}{I_1 - I_2} = \frac{i_t}{I_0 e^{-kx_1}(1 - e^{-kx_2})} \qquad (29)$$

where i_t is the total electron current collected at the anode with zero retarding potential. The relative beam intensity I_0 was measured with the beam sampling device, and the pressure was maintained at a constant value while the electron collecting efficiency was measured over a range of beam energies. The results are shown in Fig.45, and they indicate that only small variations in the collecting efficiency occurred, and that no correction factor was necessary.

The effects of electron scattering were investigated

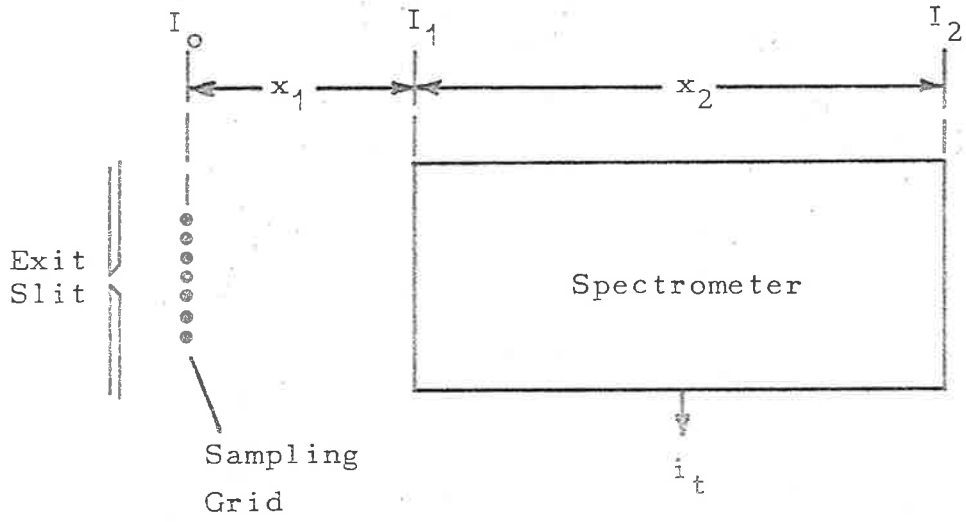

Fig.44. Measurement of the electron collecting efficiency of the spectrometer.

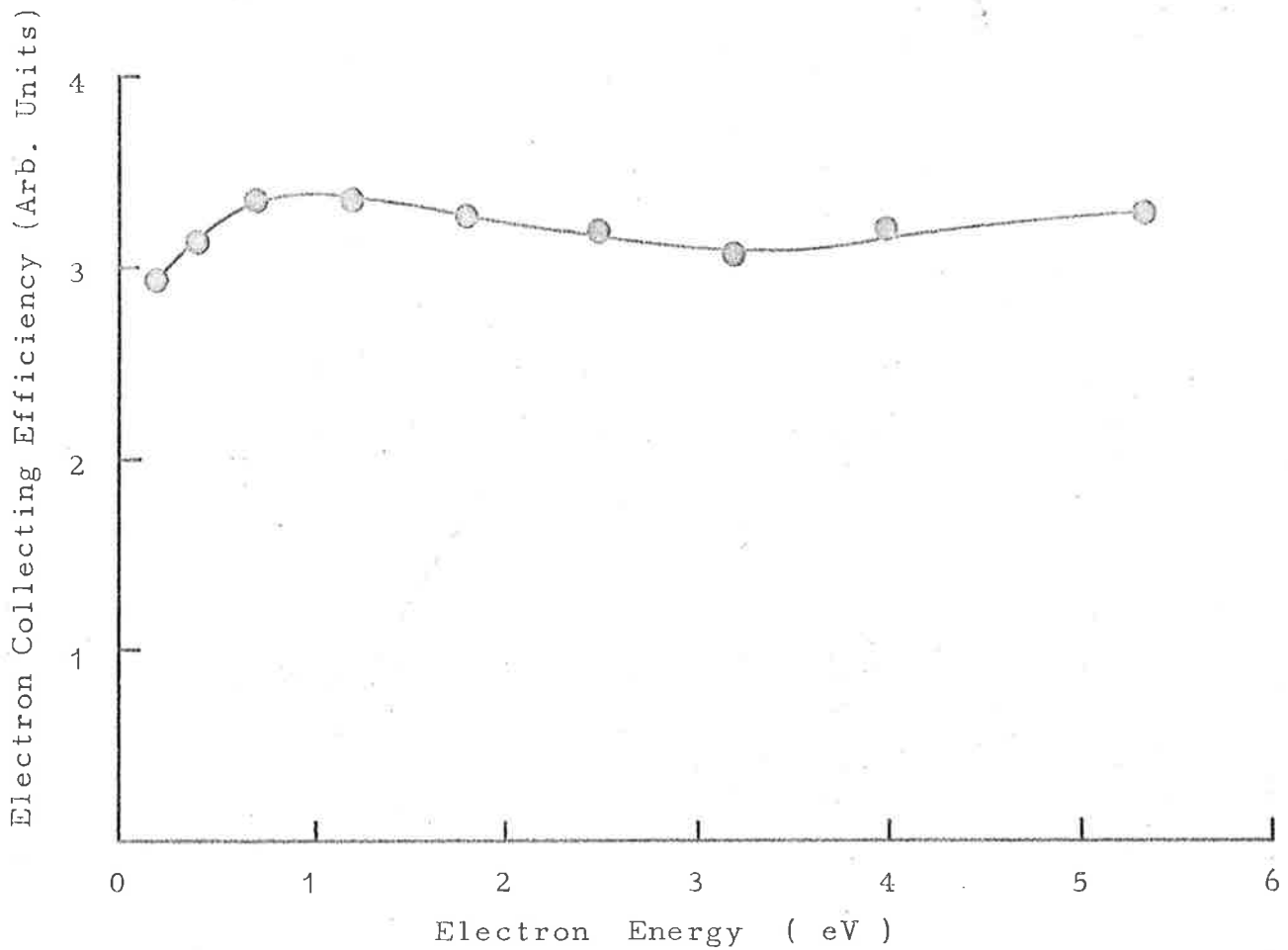

Fig.45. Electron collecting efficiency of the spectrometer as a function of the peak energy.

by measuring the electron collecting efficiency as a function of pressure for each gas which was used during the experiments. The beam intensity I_e was kept at a constant value while the collecting efficiency was measured at a number of pressures. The gas pressure was measured with a Pirani gauge which was calibrated for air. Curves of electron collecting efficiency for each gas are shown in Fig.46. The collecting efficiency in all the gases decreased for pressures greater than 3×10^{-3} mm. Hg., but some compromise between the collecting efficiency and the signal to noise ratio was necessary, since in most cases the electron current was too small to measure with pressures of less than 3×10^{-3} mm.Hg. Most of the spectra were obtained with pressures between 4 and 5×10^{-3} mm. Hg. In order to ensure that electron scattering was not having any effect on the shape of the spectra, spectra were recorded over a range of pressures for each gas. No difference could be detected between the shape of spectra obtained at a pressure of 5×10^{-3} mm.Hg. and those obtained at lower pressures.

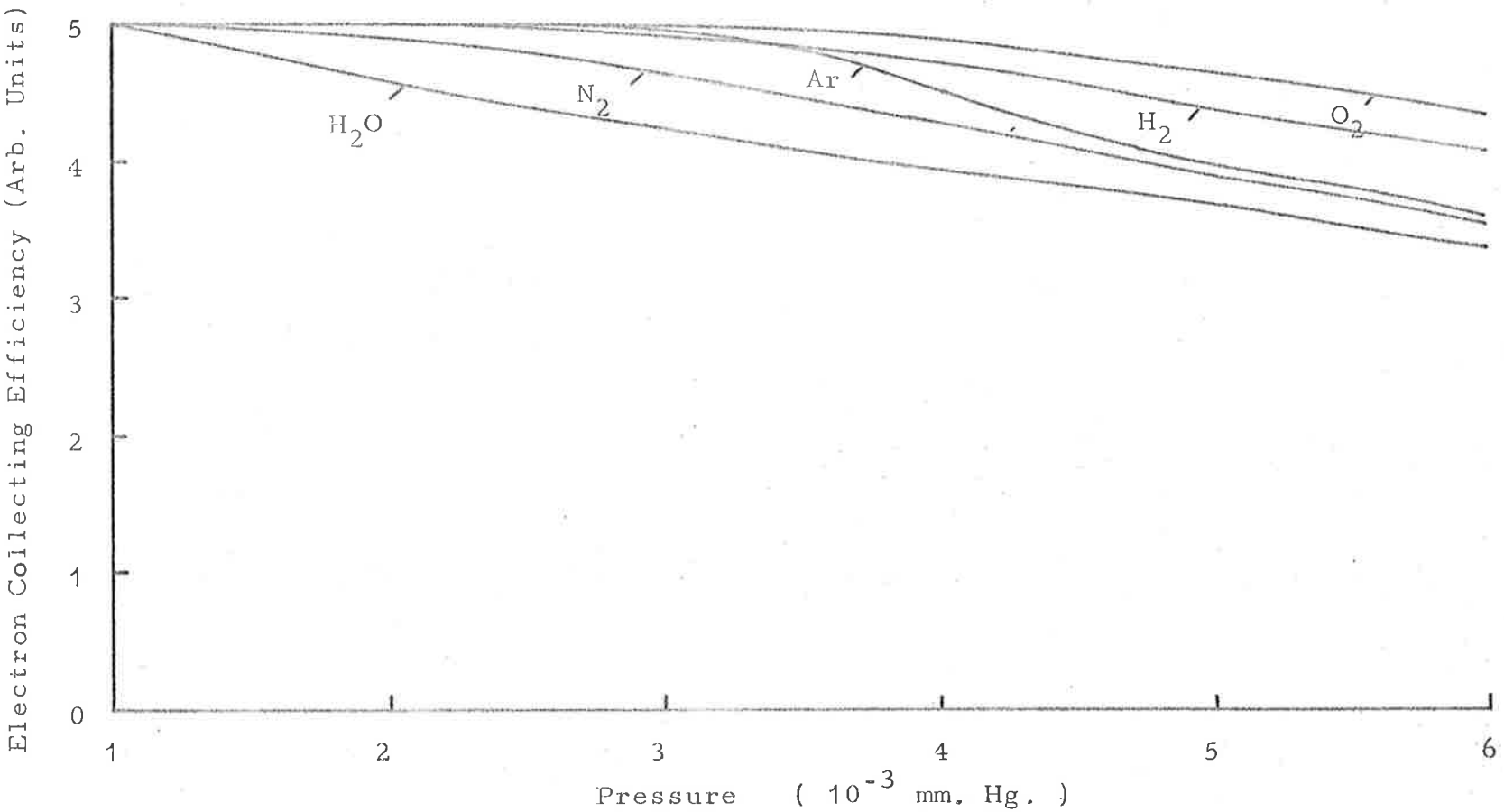

Fig.46. Electron collecting efficiency as a function of pressure measured by a Pirani gauge calibrated for air.

CHAPTER IV.

PARTIAL PHOTOIONIZATION CROSS-SECTIONS

IV.1 Molecular Oxygen

In the previous chapter it was shown that the photoelectron spectrometer which was described enabled photoelectron energy spectra with reasonably well understood characteristics to be recorded. The spectra which are obtained from molecular gases contain, in general, several peaks, which can be identified with the energy states of the molecular ion. These spectra have been analysed to yield partial photoionization cross-sections for the production of ions in particular states, and the variation with wavelength of the partial cross-sections was studied by recording photoelectron energy spectra at many different wavelengths.

IV.1.1 Oxygen photoelectron energy spectra

Using the Hopfield continuum of helium as a light source, photoelectron energy spectra from molecular oxygen were recorded for wavelengths at 5 Å intervals in the range from 775 Å to 615 Å, and also at 584 Å. The longest wavelength (775 Å) corresponded to the threshold for the production of ions in the first excited state. Several spectra were also recorded in the wavelength range 775 Å to 900 Å. These spectra were recorded under conditions corresponding to a peak width of 0.6 eV in the argon spectrum.

(Sec.III.5.2) The oxygen was nitrogen free 'medical grade' gas, which was further purified with two cold traps, one cooled to a temperature of $-70^{\circ}C$ with the mixture described in Sec.II.3.4, and the other cooled with liquid air, which removed condensible impurities from the gas. The spectrometer operating pressure measured by a Pirani gauge was 5×10^{-3} mm.Hg. The spectrum at 584 Å shown in Fig.47 is typical of the spectra recorded during the experiments. A corresponding spectrum given by Al-Joboury et al (Al-Joboury et al 1965) is shown in Fig.48. Their spectrum was obtained without collimation of the electrons, and a comparison of these spectra shows clearly the importance of collimation when the spectrum is intended to yield information about the partial photoionization cross-sections, since the peaks are more distinctly separated in Fig.47.

IV.1.2 Identification of the peaks

Each peak in the spectra was identified with one of the states of the singly charged molecular ion. The state was identified in each case by comparing the energy given by the peak position and the photon energy with the known energy states of the ion. Most of the peaks in the spectra had a width greater than the instrumental resolution, and the peaks were interpreted as bands having unresolved vibrational structure. Al-Joboury et al (Al-Joboury et

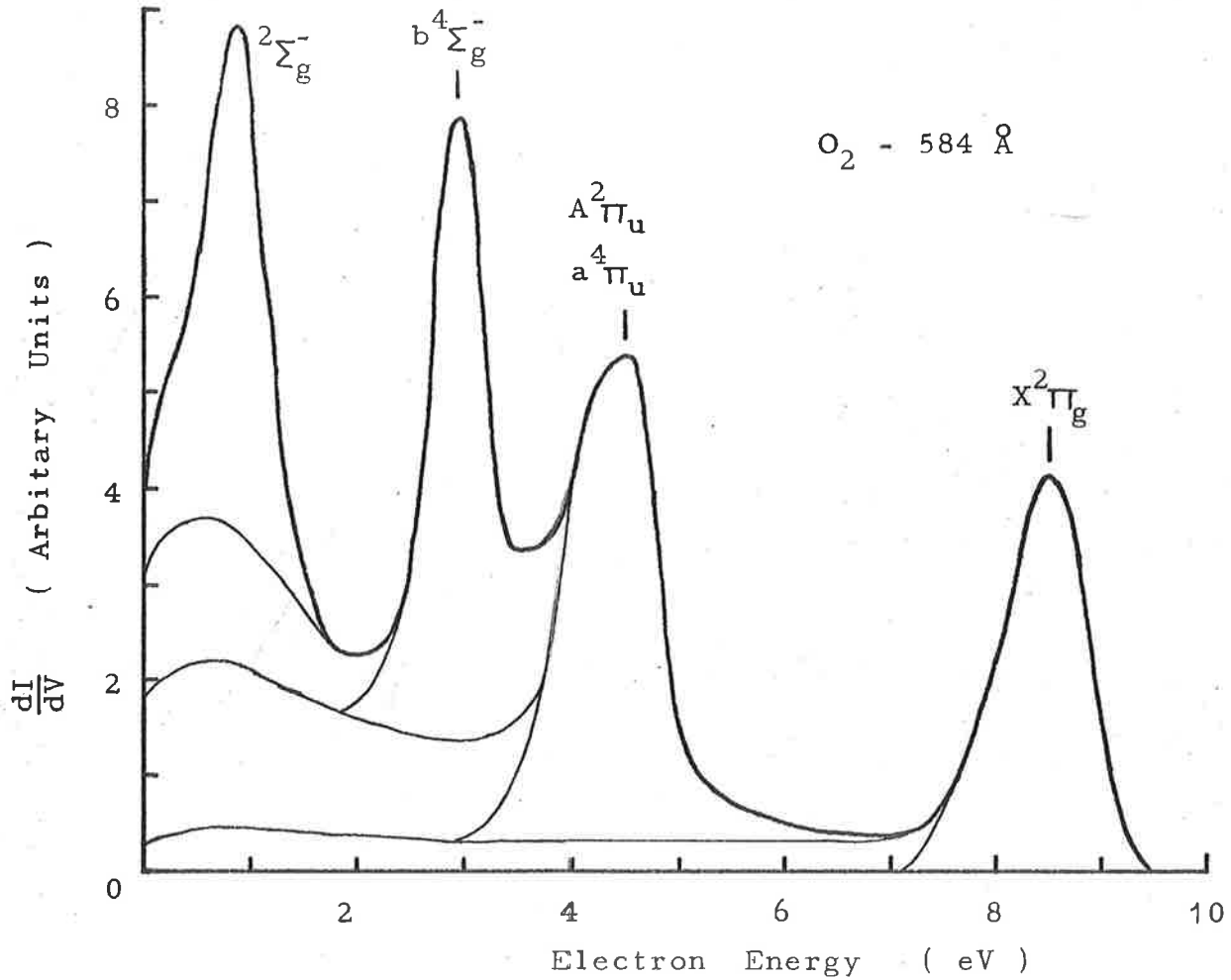

Fig.47. Photoelectron spectrum from O_2 with an incident beam wavelength of 584 Å , illustrating the unfolding procedure.

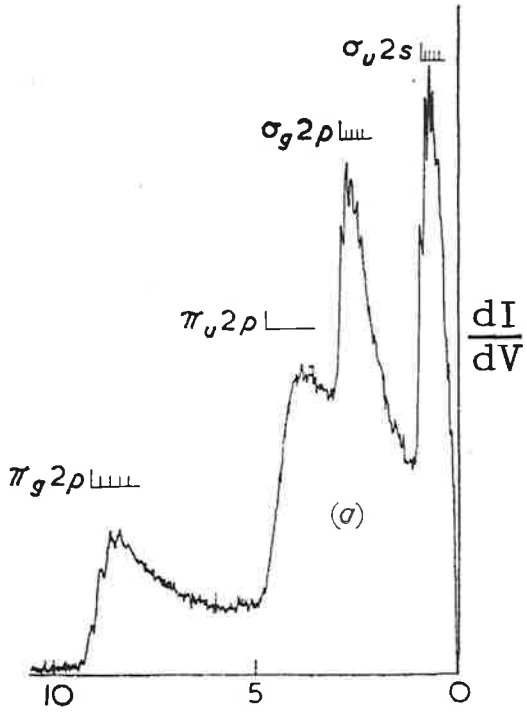

Fig.48. Electron energy spectrum from O_2 at 584 Å.
(Al-Joboury et al 1965)

al 1965) had an energy resolution sufficiently good to partly resolve the vibrational structure in the bands. The vibrational structure was not resolved in the present experiments, because the resolution had to be reduced in order to obtain a satisfactory signal to noise ratio with the low intensity dispersed light source. The intense undispersed helium light source used by Al-Joboury et al was more suitable for making accurate determinations of the energies of the states of the ion. Frank-Condon considerations (Sec.I.4.2) suggest that the position of the maximum of a peak may not correspond to the lowest vibrational level of the state, and a measurement of only the peak position would not give the adiabatic value for the energy level of the ion.

Some of the photoelectrons may have resulted from processes of dissociative photoionization, which occur when the ion is left with an amount of vibrational energy greater than the dissociation energy of the electronic state of the ion. The ion then dissociates within a time of the same order of magnitude as the period of vibration. The state of the molecular ion corresponds to a point on the potential energy curve (Fig.4) for the electronic state of the ion which is higher than the dissociation energy. This process appears only as a distribution on the low energy side of the peaks in the photoelectron spectra, and could not be

distinguished in the present experiment. However, measurements with a mass-spectrometer (Weissler et al 1959) have shown that dissociative photoionisation accounts for less than 10% of the ions produced, and the error caused by ignoring these processes was small.

The energy levels of molecular oxygen which were accessible with the range of wavelengths used in the experiments were the $X^2\Pi_g$ (12.075 eV), $a^4\Pi_u$ (16.106 eV), $A^2\Pi_u$ (16.824 eV), $b^4\Sigma_g^-$ (18.173 eV), and $^2\Sigma_g^-$ (20.308 eV) levels. (Watanabe 1957, Namioka and Tanaka 1962, Tanaka and Takamine 1942, Gilmore 1965).

A comparison of the spectra shown in Figs.47 and 48 shows that the positions of the peaks are in good agreement. The highest energy peak in Fig.47 occurs at an energy of 8.6 eV, which agrees well with that of Al-Joboury et al, and corresponds to the third vibrational level of the $X^2\Pi_g$ state of O_2^+. The second peak has a maximum at 4.35 eV, and must contain a contribution from the $a^4\Pi_u$ state which has a threshold corresponding to an energy of 5.10 eV in this spectrum, but it may also contain an unresolved contribution from the $A^2\Pi_u$ state which has a threshold corresponding to 4.39 eV. Al-Joboury et al identified the vibrational structure of this peak with the $a^4\Pi_u$ level. The third and fourth peaks were identified with the $b^4\Sigma_g^-$ and $^2\Sigma_g^-$ levels respectively, in agreement with the

interpretation of Al-Joboury et al.

IV.1.3 Unfolding the spectra

In order to interpret the photoelectron energy spectra in terms of partial photoionization cross-sections, the area under the spectrum associated with each peak must be determined. This was done by assuming that the spectrum was equivalent to the sum of several monoenergetic spectra with the shape shown in Fig.39. The spectra were unfolded by the following procedure. The most energetic peak was completed to form a symmetrical shape, and the area (A_1) contained by the curve was measured with a planimeter. A symmetrical shape was chosen because, in general, the shape of the high energy side of the peak was well defined, but the low energy side was not. The argon spectra were analysed in a similar way. The shape of the spectrum corresponding to the peak was determined by the energy of the peak, and the area at low energy (A_2) which was associated with the peak was found by reference to the curve shown in Fig.40. The complete area associated with the peak was then drawn onto the spectrum, as shown in Fig.47. Each successive peak was treated in the same manner, and the self consistency of the unfolding was indicated by the shape of the area which remained for the last peak. This was required to have a shape consistent with its energy, as determined from Fig.40.

IV.1.4 The partial photoionization cross-sections of oxygen

The number of ions produced in each state was assumed to be directly proportional to the area of the spectrum which was associated with the corresponding peak, and the measurement of this area allowed the percentage of ions in a given electronic state, or the branching ratio, to be found. The branching ratios for oxygen are shown in Fig.49. Because the $a^4\Pi_u$ and $A^2\Pi_u$ levels were resolved in only a few spectra, the sum of the branching ratios for these states is shown in Fig.49.

No measurement of absolute cross-sections was attempted with this apparatus, and the results shown in Fig.49 were combined with published values of the total photoionization cross-section of molecular oxygen. This cross-section has been measured by several workers, (Wainfan et al 1955, Watanabe and Marmo 1956, Nicholson 1963, Samson and Cairns 1964, Cook and Metzger 1964a) but the most comprehensive results are those of Cook and Metzger, which are shown in Fig.7. The Hopfield absorption bands (Hopfield 1930) are very dense, and are diffuse because of autoionization. Some of the bands have been assigned to Rydberg series which converge to higher electronic states of the ion. The total photoionization cross-section of oxygen which is shown in Fig.50 has been averaged over 10 Å intervals to produce an effective

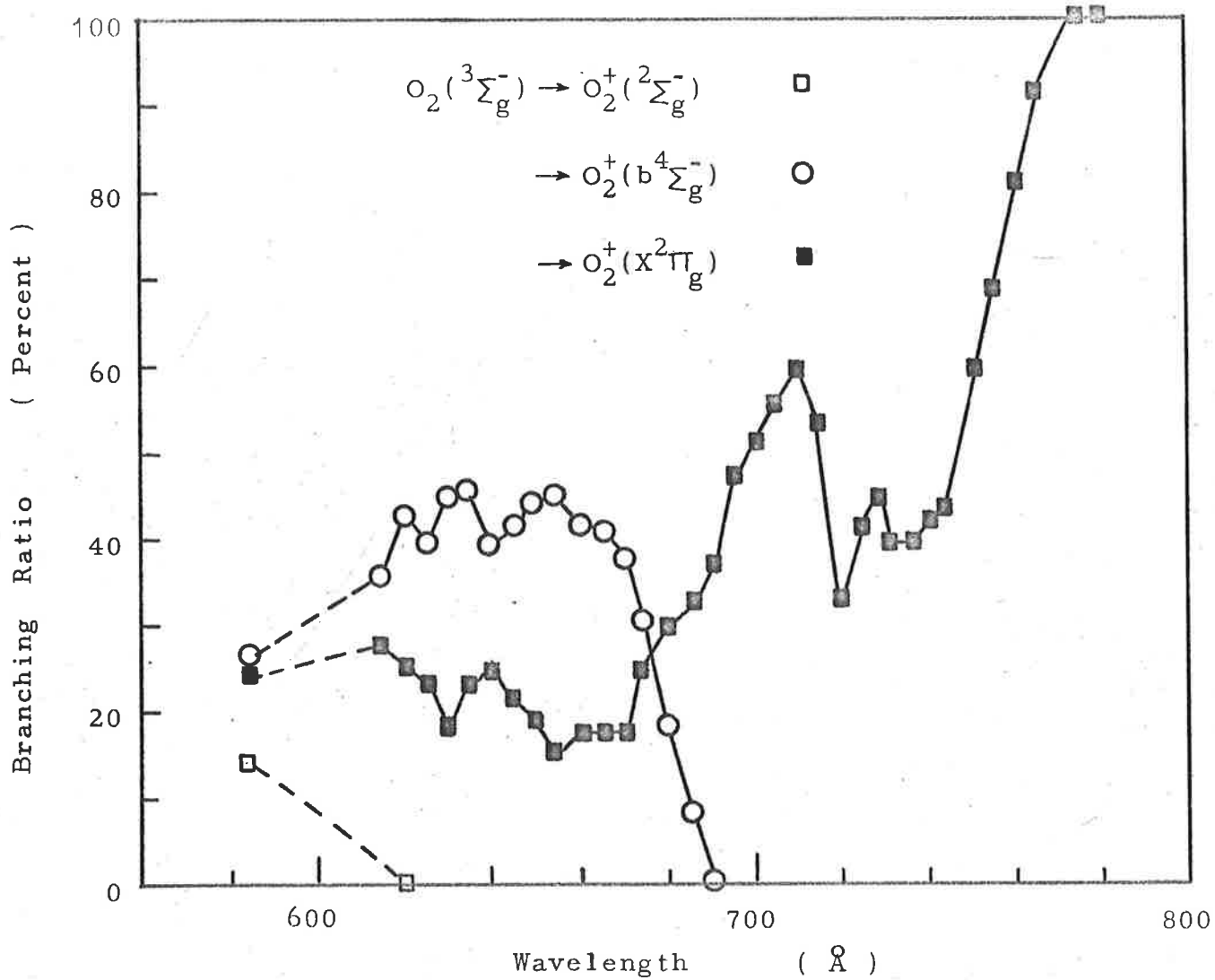

Fig.49 (a) Branching ratios for the various photoionizing processes in O_2.

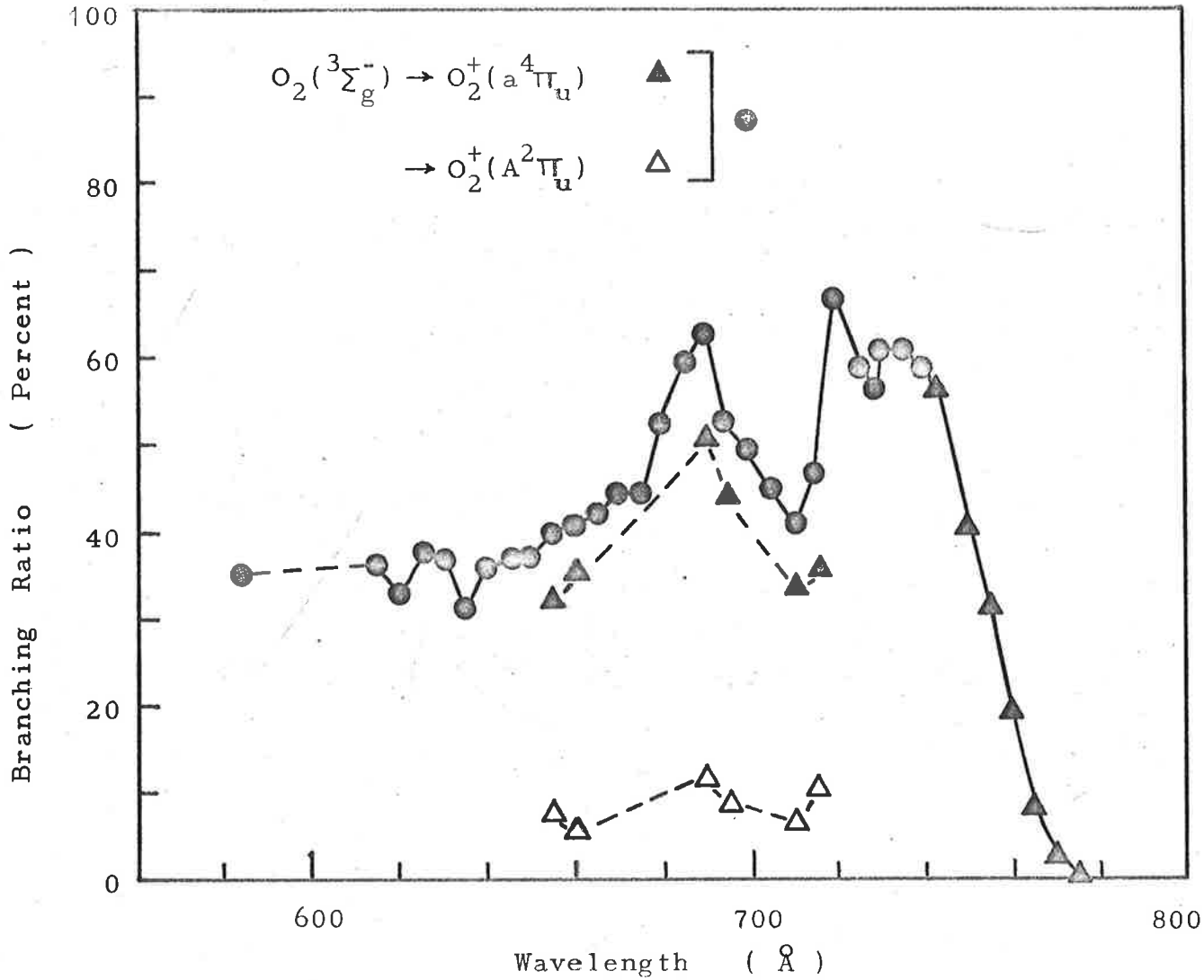

Fig.49(b) Branching ratios for the various photoionizing processes in O_2.

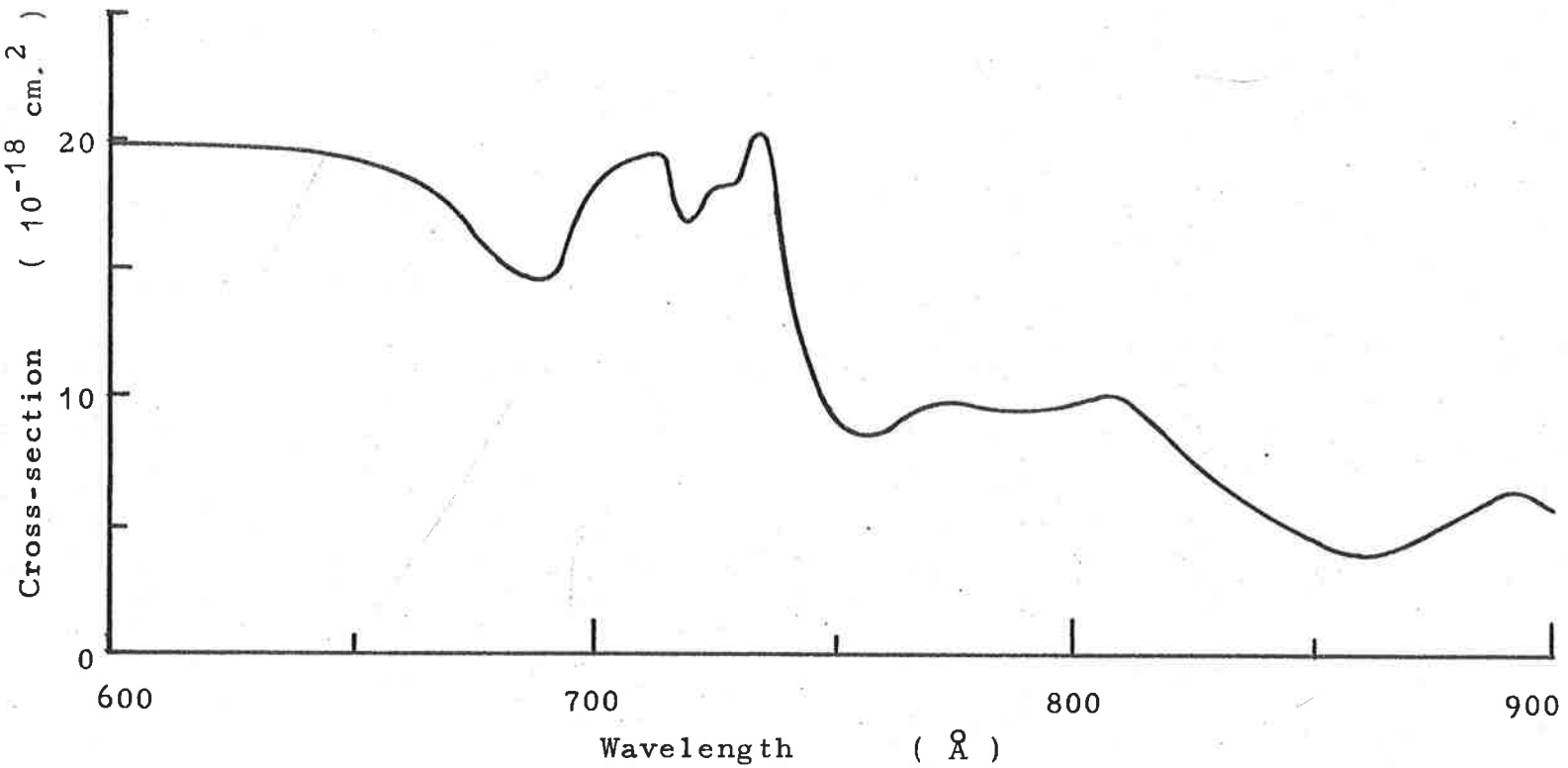

Fig.50. Total photoionization cross-section of molecular oxygen (Cook and Metzger 1964a) reduced to a resolution of 10 Å.

resolution equivalent to that of the present experiment.

The partial photoionization cross-sections of oxygen as a function of wavelength are shown in Fig.51. The $^2\Sigma_g^-$ peak appeared only in the spectrum obtained at 584 Å, since no spectra were obtained in the region from 584 Å to 615 Å because of the low intensity of the light source. Separate peaks corresponding to the $a^4\Pi_u$ and $A^2\Pi_u$ levels were distinguished in only six spectra, and in these the two peaks were considerably overlapped, as shown in Fig.52 (b) and (c), and their separate areas could not be determined accurately. However, in the cases for which estimates of the individual areas were made, the $a^4\Pi_u$ peak was about four times stronger than the $A^2\Pi_u$ peak. The spectra obtained at wavelengths longer than 680 Å contained an abnormally large area between the $X^2\Pi_g$ and $a^4\Pi_u$ peaks, and this was associated with the autoionised structure which appears in the total photoionization cross-section in this region. This area was included as part of the $X^2\Pi_g$ peak for the purpose of calculating the partial photoionisation cross-sections, and its significance will be discussed further in a later section.

The accuracy of the partial cross-sections was limited by the uncertainty involved in unfolding the spectra This uncertainty was due to the low energy region which was associated with each peak. There was also some

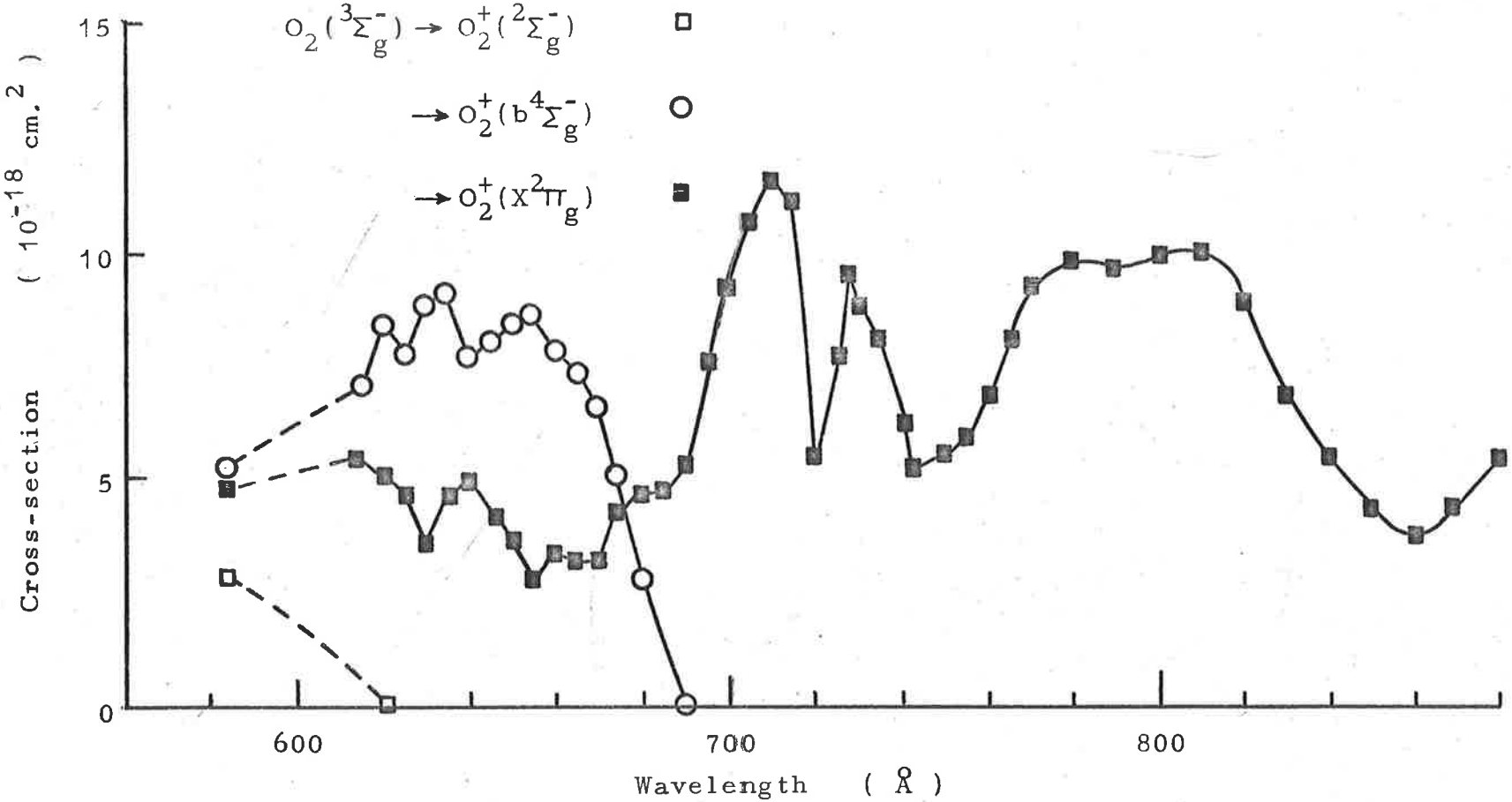

Fig.51 (a) Partial photoionization cross-sections of molecular oxygen.

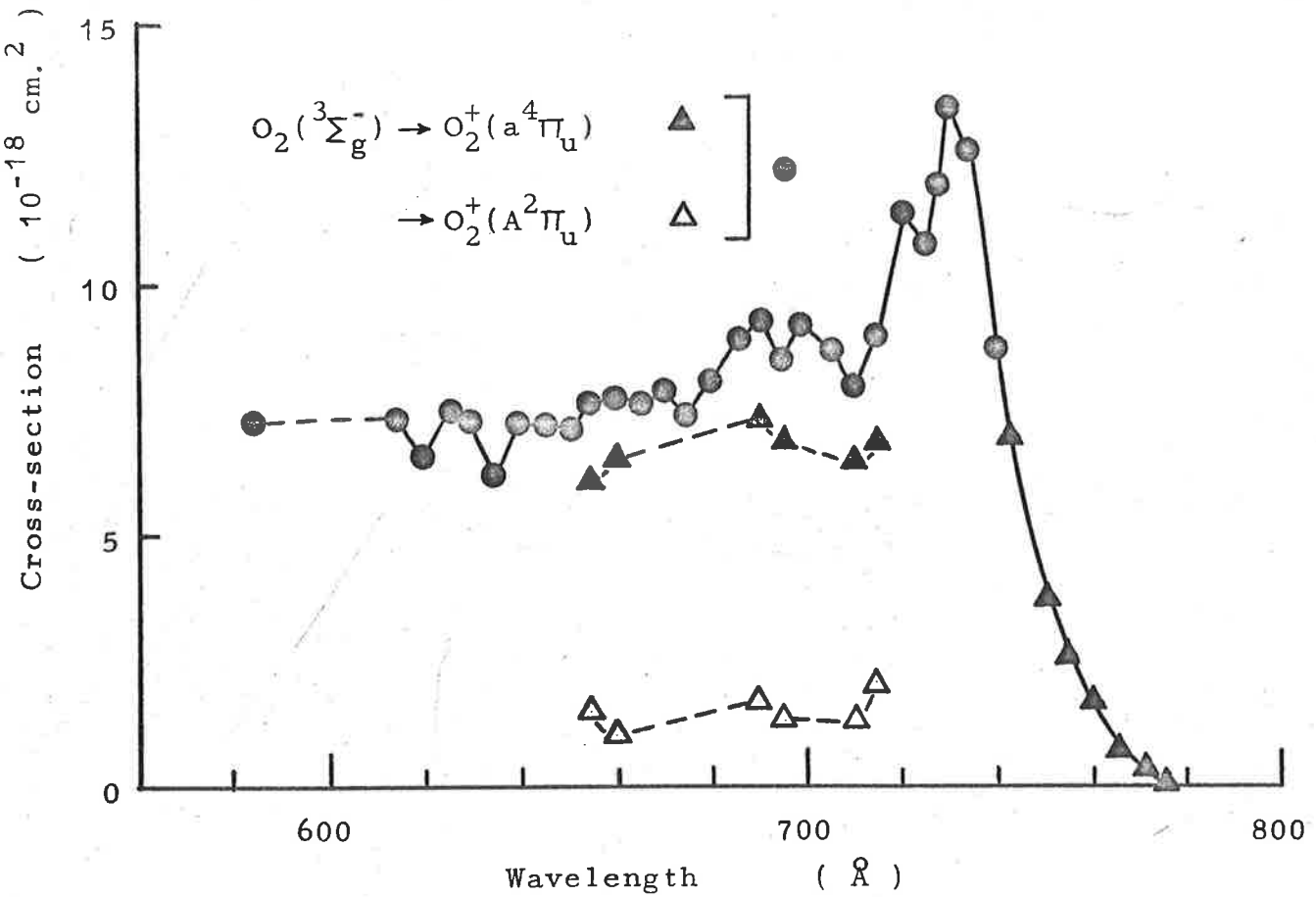

Fig.51 (b) Partial photoionization cross-sections of molecular oxygen.

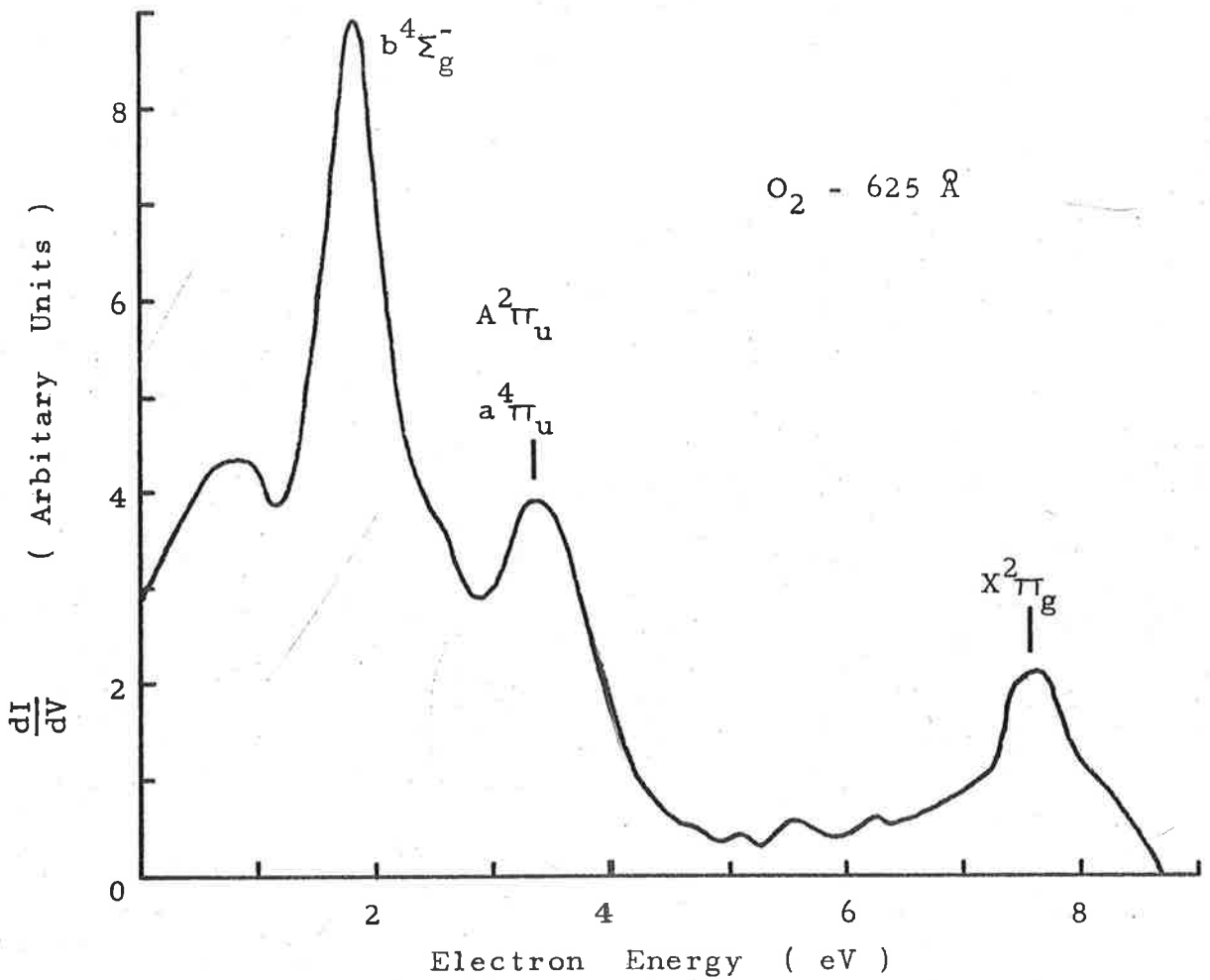

Fig.52 (a) Photoelectron energy spectrum from O_2 with an incident beam wavelength of 625 Å.

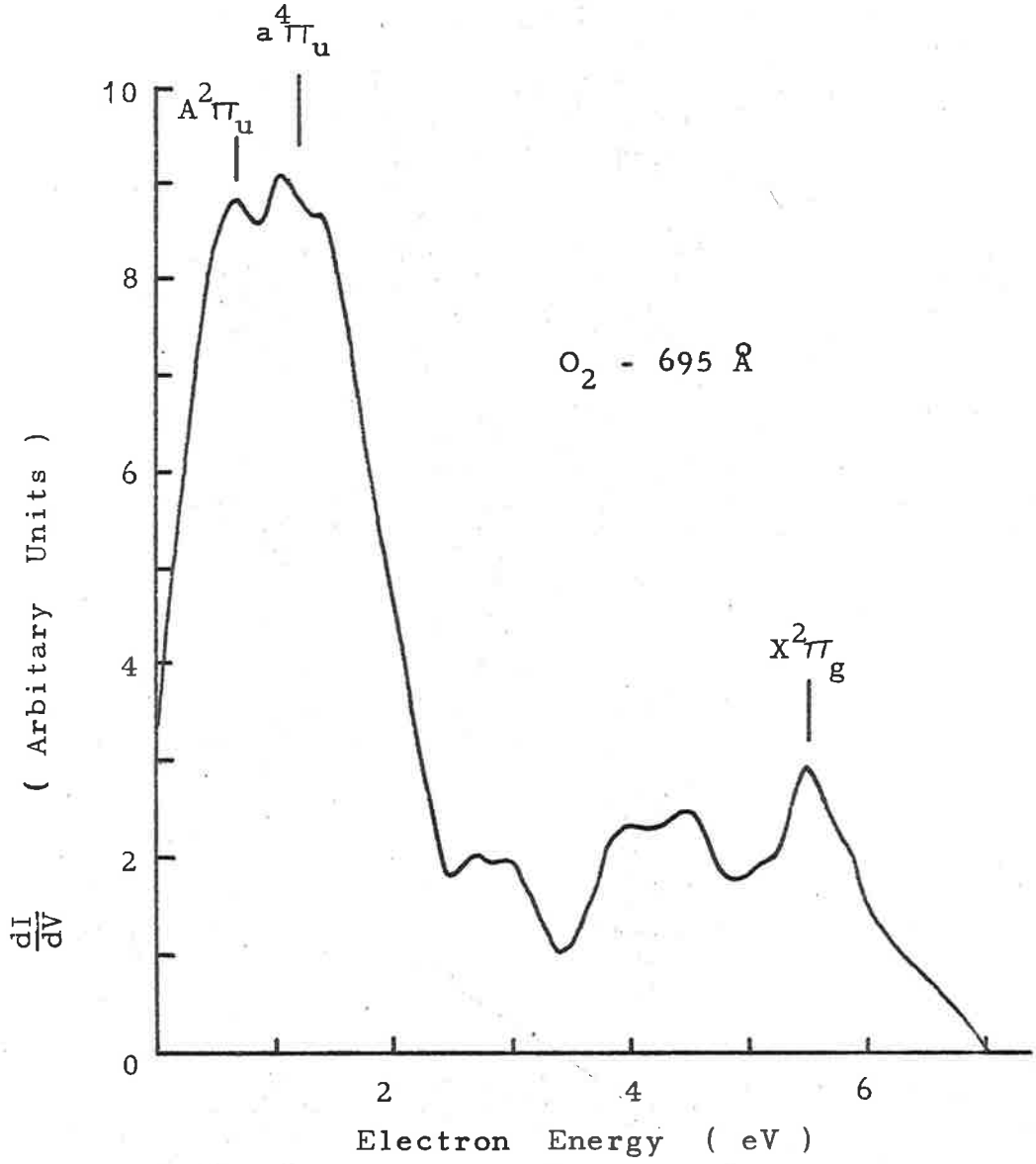

Fig.52 (b) Photoelectron spectrum from O_2 with an incident beam wavelength of 695 Å.

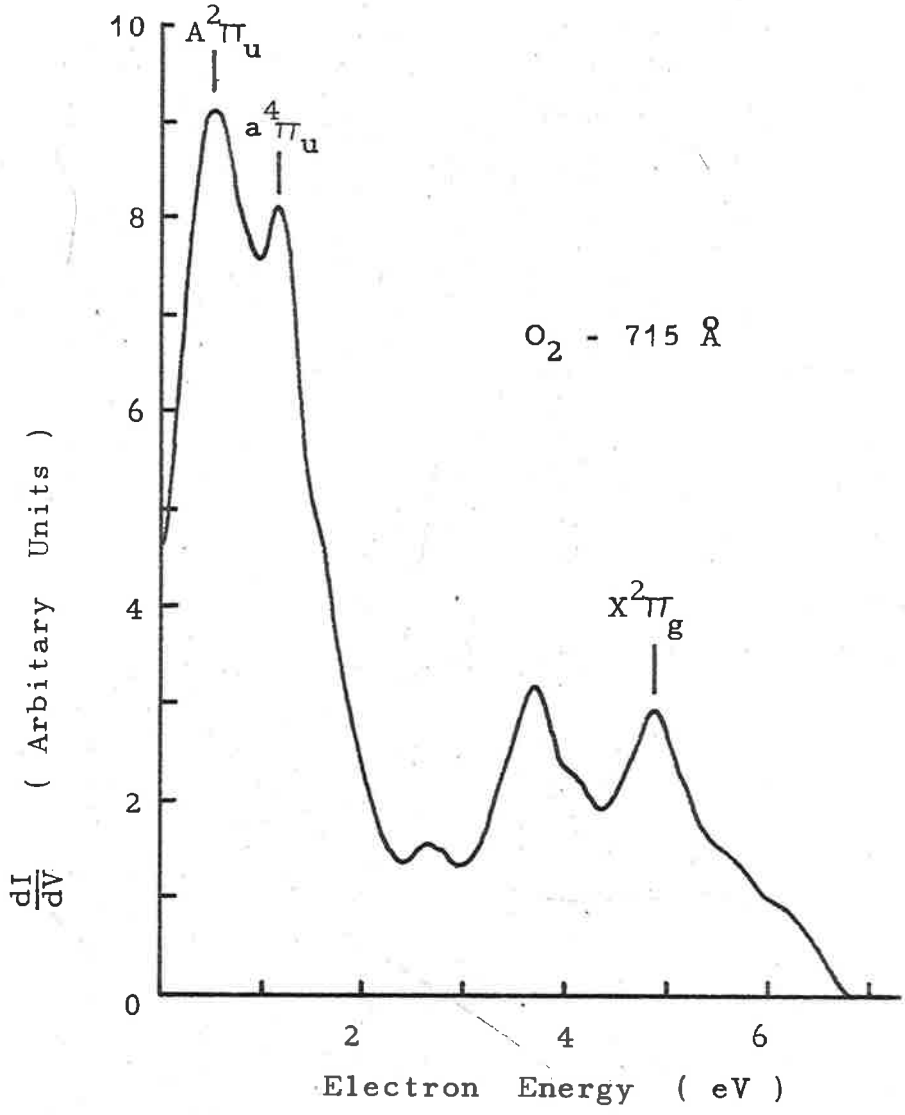

Fig.52(b) Photoelectron spectrum from O_2 with an incident beam wavelength of 715 Å.

uncertainty in measuring the area (A_1) under the peaks in some cases, because of the partial overlapping of the peaks. Better accuracy would be obtained with spectra of higher resolution. It was estimated that the area of a given peak was determined to an accuracy of 10%, but the absolute error accumulated during the unfolding process. The error in the lower energy peaks was reduced by demanding that the unfolding should be self consistent. The accuracy of the partial cross-sections varied greatly, depending on the separation, position, and size of the peak. The error was probably less than 20% in most cases, except near the threshold of each state, where the peak was small.

IV.1.5 Variation of the partial photoionization cross-sections with wavelength

The branching ratio for the formation of ions in the $X^2\Pi_g$ state (Fig.49) decreases rapidly from 100% at the $a^4\Pi_u$ threshold, and then rises to a maximum of 60% at 710 Å before dropping to a roughly constant value of 20% below 670 Å. The branching ratio for the $a^4\Pi_u$ and $A^2\Pi_u$ states rises sharply from the threshold, and goes through two maxima before becoming approximately constant at 35%. The $b^4\Sigma_g^-$ branching ratio has a single broad maximum at 640 Å. The maximum at 710 Å in the branching ratio for the $X^2\Pi_g$ state coincides in wavelength with the minimum in the

branching ratio for the $a^4\Pi_u$ and $A^2\Pi_u$ states, and also with the maximum in the total photoionization cross-section shown in Fig.50. The maximum in the total cross-section corresponds to a region where the band structure is strong, and which is bordered by regions of minimal structure. This indicates that the autoionizing processes in this region tend to produce ions in the $X^2\Pi_g$ state rather than the $a^4\Pi_u$ or $A^2\Pi_u$ states. The shape of the branching ratio curve for the $a^4\Pi_u$ and $A^2\Pi_u$ states has therefore been modified by autoionization from a single maximum similar to that of the branching ratio for the $b^4\Sigma_g^-$ state.

A comparison of the partial cross-sections shown in Fig.51 indicates competition between the various final states of the ion. The cross-section for the $X^2\Pi_g$ state rises towards longer wavelengths from the threshold of the $a^4\Pi_u$ state. The two peaks in the $X^2\Pi_g$ partial cross-section coincide in wavelength with those of the total photoionization cross-section, indicating that both of the peaks in the partial cross-section result from autoionizing processes. The general form of the individual photoionization continua is therefore similar to a step function which has been modified by competition between the final states and by autoionization.

The only results with which these may be compared are those of Schoen. (Schoen 1964). His integral

photoelectron energy spectrum at 554 Å is shown in Fig.53. Schoen used a retarding potential analyser of cylindrical geometry, but he did not collimate the electrons. The branching ratios given by Schoen are shown in Fig.8. Although his results do not show the detailed structure contained in the present results, they are in reasonable agreement when the detailed structure has been averaged out. Schoen's results give branching ratios for the $X^2\Pi_g$ and $b^4\Sigma_g^-$ states which are 8% lower and 7% higher respectively than the average value given by the present results.

The approximation made by Dalgarno et al (Dalgarno et al 1963) that the partial photoionization cross-sections are proportional to the statistical weight of the final state of the ion can obviously not be applied in detail, but it is interesting to compare the approximation with average values of the branching ratios. In the region below 690 Å the $X^2\Pi_g$, $a^4\Pi_u$ + $A^2\Pi_u$, and $b^4\Sigma_g^-$ branching ratios have average values in the ratio 2:3.25:2.9, compared to the ratio of statistical weights 3:9:2. The $a^4\Pi_u$ state has a branching ratio about four times larger than that of the $A^2\Pi_u$ state. In the region 690 Å to 775 Å the distribution is modified by autoionization, and the $X^2\Pi_g$ and $a^4\Pi_u$ + $A^2\Pi_u$ branching ratios have average values in the ratio 2:1.5 (2:6). The approximation made by Dalgarno is,

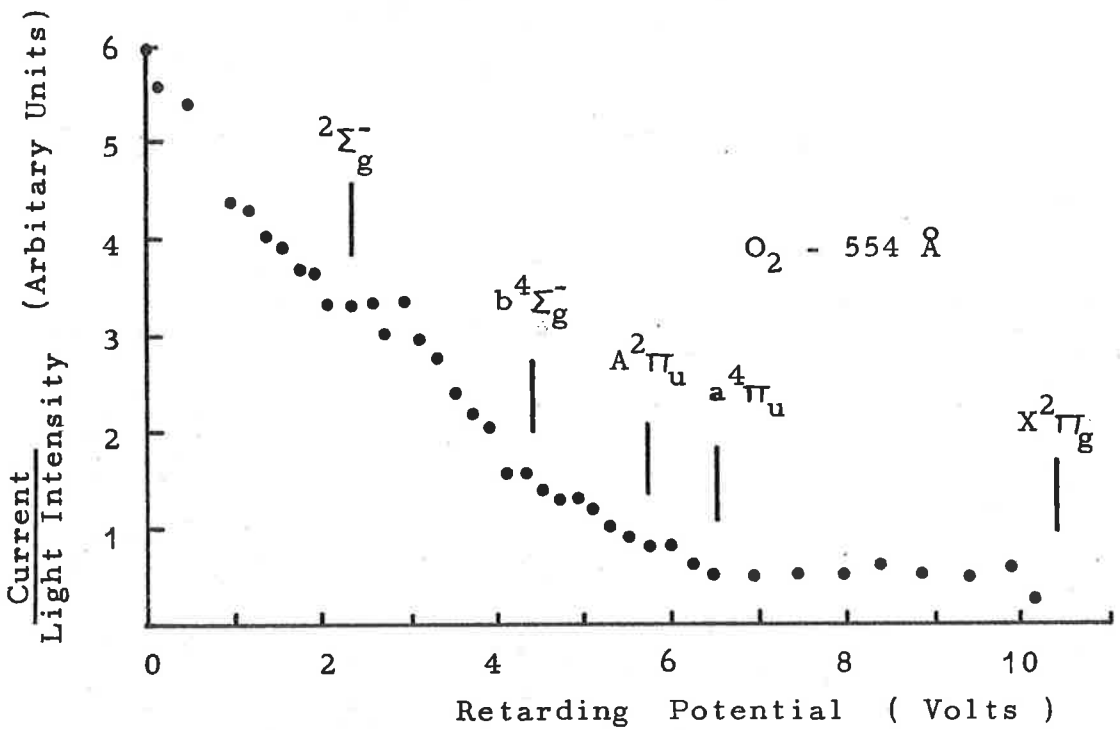

Fig.53. Photoelectron spectrum from O_2 at 554 Å.
(Schoen 1964)

therefore, an inaccurate one.

The partial photoionization cross-sections shown in Fig.51 provide valuable information about the oxygen molecule when combined with theoretical calculations on the structure of the molecule. Although wavefunctions which are sufficiently accurate to calculate the partial photoionisation cross-sections of molecular oxygen are not available, Tuckwell (unpublished private communication) is using the present experimental results to obtain semi-empirical wavefunctions. He evaluates the matrix elements for photoionization with simple central potential model wavefunctions, and fits the theoretical partial cross-section to the experimental ones by varying the parameters of the wavefunctions. Simple calculations using hydrogen atom type wavefunctions in which the effective nuclear charge is a parameter, and also calculations involving linear combinations of Hartree-Fock single electron wavefunctions are being performed.

IV.1.6 Autoionizing processes

At wavelengths longer than 775 Å only the ground state of the oxygen ion was accessible, and the photoelectron spectra at these wavelengths were expected to contain only a single peak. However, spectra recorded at wavelengths in the region 775 Å to 900 Å all contain a large peak at an energy of 0.5 eV, which does not move as the wavelength is

changed. Some of these spectra are shown in Fig.54. The low energy peak was not an instrumental effect, since no similar peak was observed in other gases. Spectra obtained with different oxygen pressures all contained the low energy peak. The presence of the low energy peak in the spectra must, therefore, indicate that many photoelectrons were being emitted with an energy of 0.5 eV. None of the photo-ionising processes which have been considered so far can account for the emission of these low energy electrons, which must indicate a process in which the excess energy is not all dissipated as kinetic energy of the photoelectron.

In Fig.55 the area of the low energy peak in the spectra shown in Fig.54 is plotted as an equivalent cross-section. Also plotted in Fig.55 is the area which appeared between the $a^4\Pi_u$ and $X^2\Pi_g$ peaks in the spectra recorded at wavelengths longer than 680 Å, but which was not associated with the shape corresponding to the $X^2\Pi_g$ peak. This curve has a minimum between 740 Å and 750 Å, and another at 720 Å, which correspond to the regions of minimal autoionized structure in the total photoionisation cross-section shown in Fig.7. The wavelength of 680 Å, which is the limit of the area plotted in Fig.55, is also the short wavelength limit of the autoionized structure in the total photoionization cross-section. This indicates that the process resulting in the emission of photoelectrons with energies

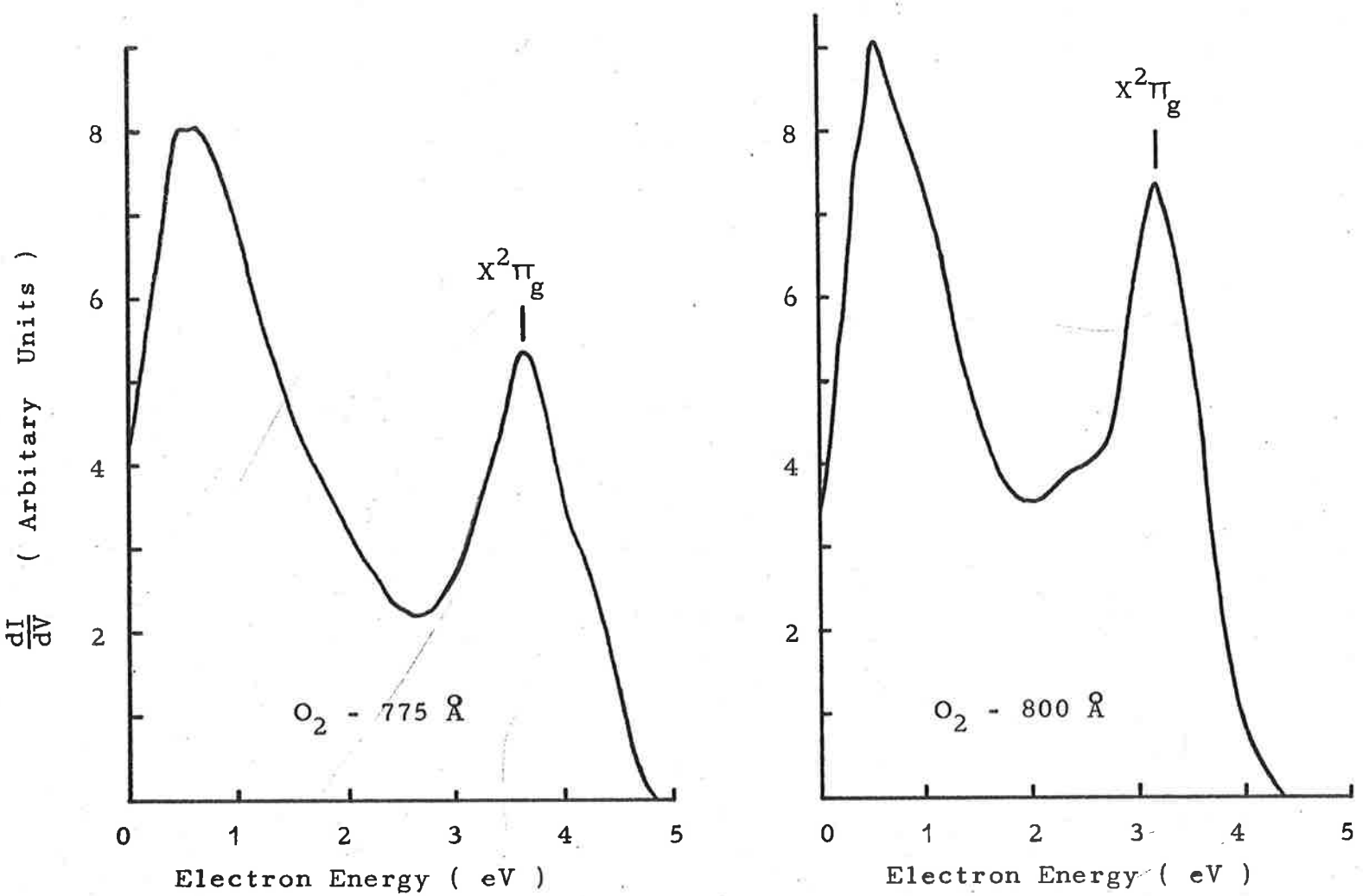

Fig.54. Photoelectron spectra from O_2 showing the unusual low energy peak.
(a) 775 Å (b) 800 Å

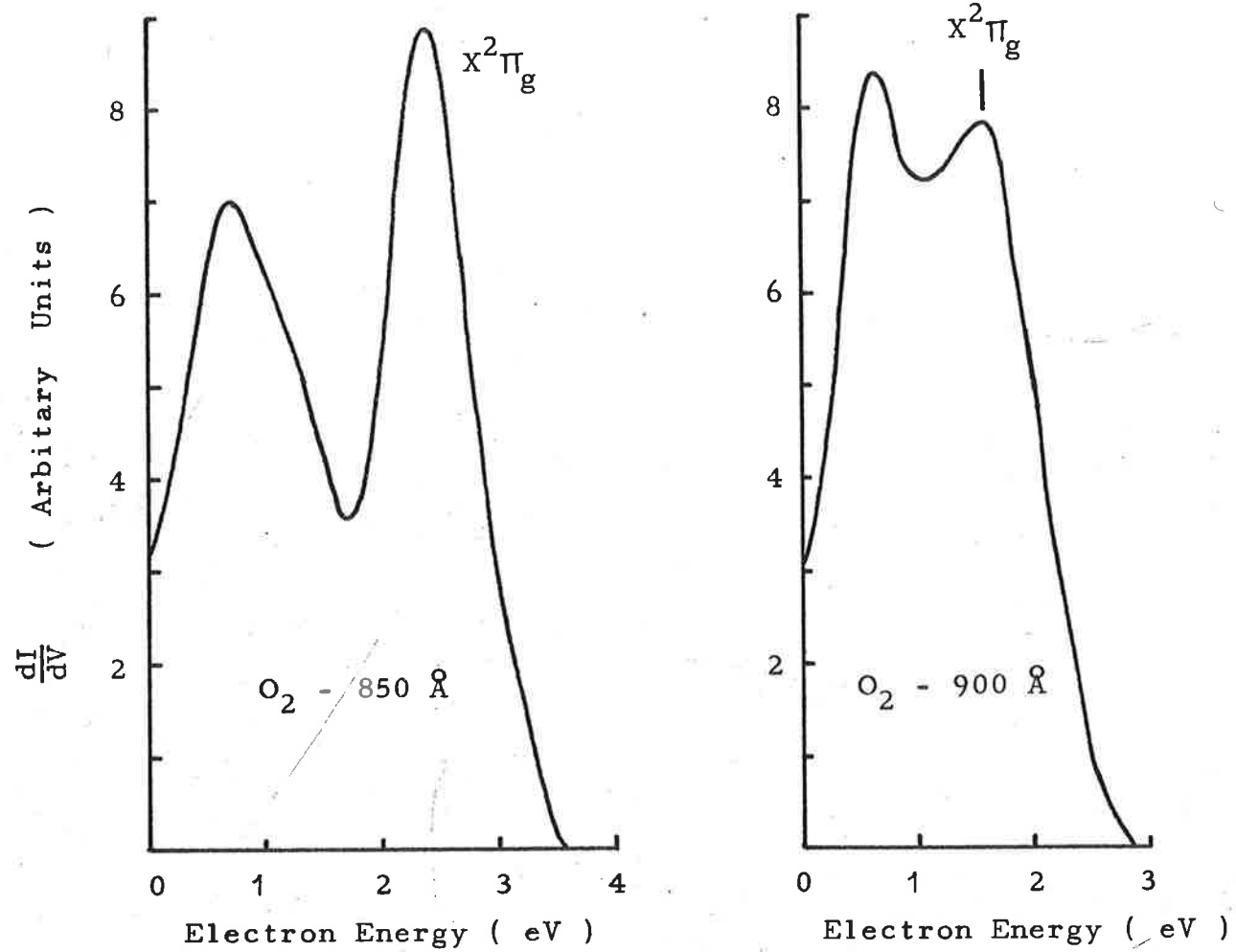

Fig.54. Photoelectron spectra from O_2 showing the unusual low energy peak.
(c) 850 Å (d) 900 Å

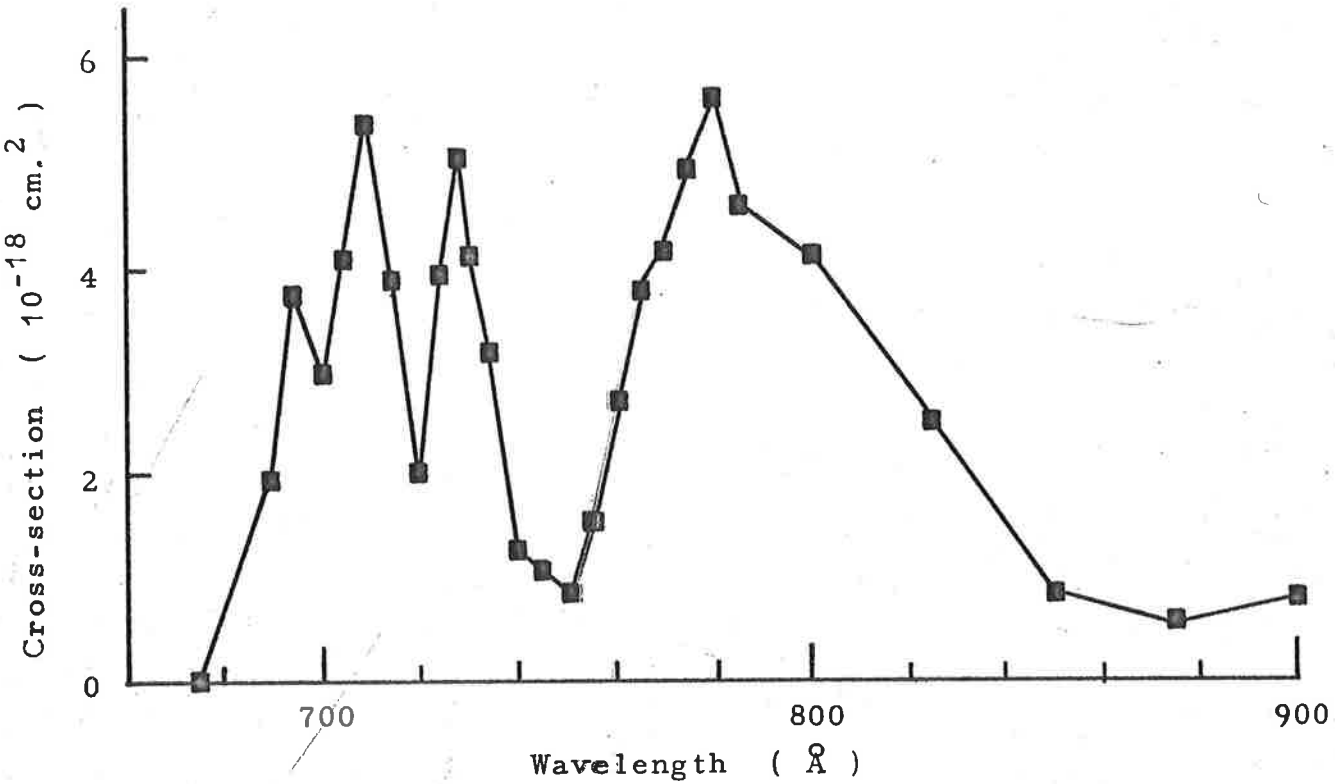

Fig.55. Cross-section for the production of O_2^+ in the ground state for which the photoelectrons do not belong to the main ground state peak.

not corresponding to the main peaks of the spectrum is associated with the autoionised structure in the total photoionisation cross-section.

The process of autoionization was discussed in Sec.I.3.2 in terms of the formation of a quasi-stable state of the neutral atom or molecule. A quasi-stable state is formed when a collective excitation of two or more electrons results from the absorption of a photon, and although the total energy of excitation is greater than the ionization potential of the molecule, none of the electrons has sufficient energy to escape. After a lifetime long compared to that of a normal continuum state, a rearrangement of the electron distribution occurs, in which all of the excitation energy is transferred to one of the electrons, which escapes, leaving the ion in one of its discrete energy states. These quasi-stable states are evident as lines in the photoionization cross-sections, which are broad and have an assymmetric shape. The line shape has been explained (Fano 1961) in terms of configuration interaction between the quasi-stable state and the continuum.

It is suggested that the low energy photoelectrons, which are emitted when radiation of wavelength longer than 775 Å is incident on molecular oxygen, are due to a fluorescent autoionising process, in which part of the energy of excitation is dissipated in the form of a photon.

When the molecule is excited to a quasi-stable state, the state must be sufficiently long lived for a fluorescent transition to a lower quasi-stable state to occur, and the transition to the ionization continuum is from this state. This process is illustrated in Fig.56. Many of the quasi-stable states of oxygen appear as band structure in the total photoionization cross-section shown in Fig.7. However, if only a single fluorescent transition occurs, then the lower quasi-stable state cannot be one of the states seen in the absorption spectrum, since a radiative transition between that state and the ground state of the molecule would be forbidden by the conservation of parity. (Herzberg 1950). If a cascade of fluorescent transitions with an even number of steps occurs, then the lowest quasi-stable state would be observable in the absorption spectrum. There are many of these states close to the ionization threshold of oxygen, and the band at 983 Å in Fig.7 indicates a state which is 0.54 eV above the ionization threshold. This may be the state indicated by the low energy peak in the spectra in the 775 Å to 900 Å region.

In some of the spectra which were recorded in the region 680 Å to 770 Å, the abnormally large area between the $X^2\Pi_g$ and $a^4\Pi_u$ peaks appeared to consist of several small peaks. (Fig.52). This indicates that a cascade of fluorescent transitions occurs, with some probability of a

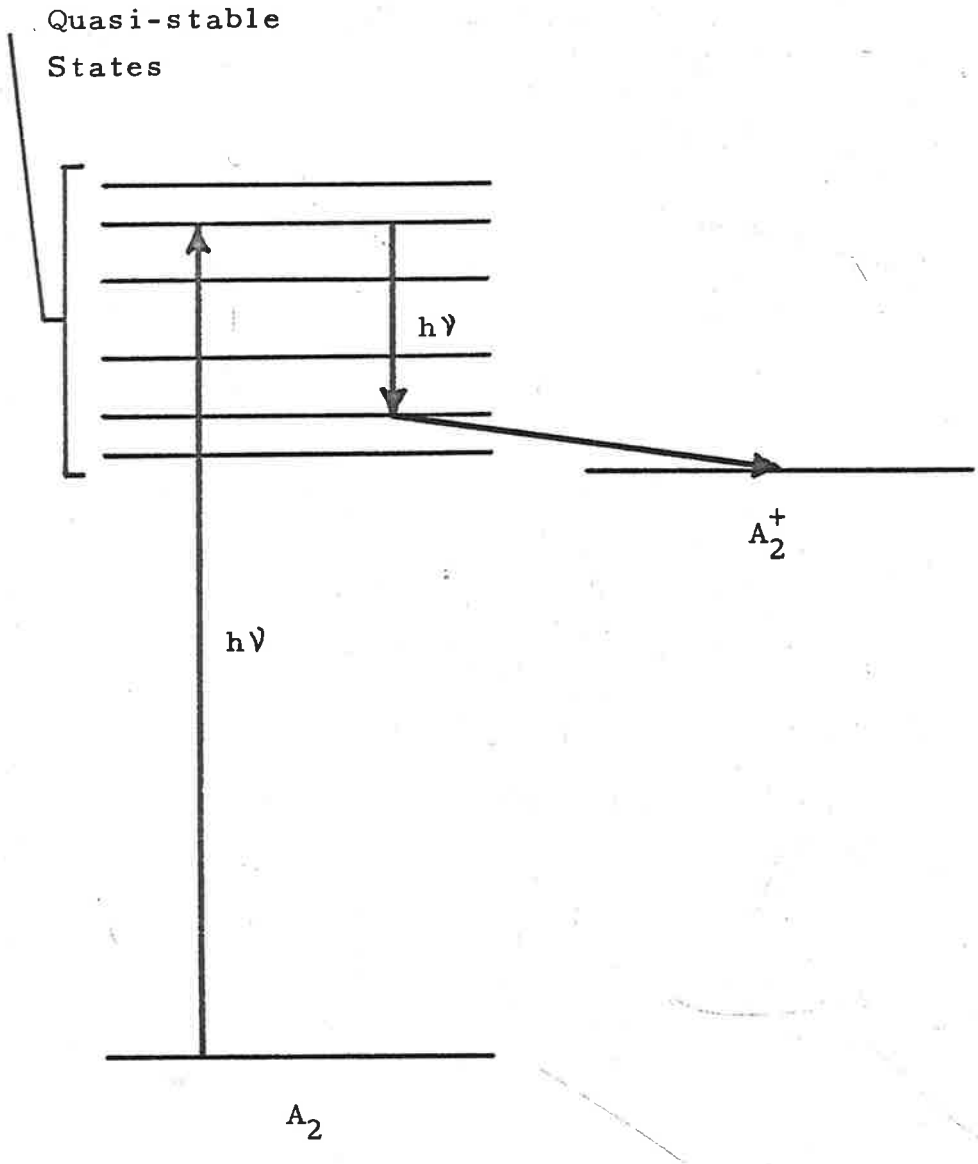

Fig.56. Energy level diagram of a hypothetical molecule A_2, illustrating a fluorescent autoionizing transition.

transition to the ionization continuum from several of the quasi-stable states. If a cascade of fluorescent transitions occurs in the region above 775 Å, then a transition to the continuum must be forbidden from all except the level which is 0.5 eV above the ground state of the ion, since only the peak at 0.5 eV appears in these spectra, apart from the main ground state peak. Present knowledge of the quasi-stable states does not allow an explanation of these effects on the basis of dipole selection rules.

Photoelectrons which result from processes of autoionization may have an angular distribution different from that of other photoelectrons. During the life of the quasi-stable state, the effect of the incident beam direction on the angular distribution may be partially lost, resulting in a smeared out distribution. This is analagous to the effect of collective excitation in the case of nuclear photodisintegration (Blatt and Weisskopf 1952). If this is so, then the cross-sections due to autoionization measured in the present experiment are slightly in error, because only a sample of the electrons, emitted in a direction perpendicular to the beam direction, were detected. Measurement of the angular distributions of photoelectrons may prove to be an important method of studying autoionization.

IV.2 Molecular Nitrogen

IV.2.1. Photoelectron energy spectra of molecular nitrogen

The partial photoionization cross-sections of molecular nitrogen were obtained from the analysis of photoelectron energy spectra recorded at 5 Å intervals in the region 615 Å to 745 Å, and also at 584 Å. These spectra were recorded under conditions identical to those under which the oxygen spectra were recorded. The oxygen free nitrogen was further purified with cold traps. Some typical photoelectron energy spectra from nitrogen are shown in Fig.57. The spectrum shown in Fig.57 (a) was recorded with an incident wavelength of 615 Å. It clearly shows three peaks, which were associated with the three energy states of the nitrogen ion which were accessible at this wavelength. These were the $X^2\Sigma_g^+$ (15.576 eV), $A^2\Pi_u$ (16.693 eV), and $B^2\Sigma_u^+$ (18.757 eV) states. (Mulliken 1957). The most energetic of the peaks, which was identified with the ground state of the ion, is interesting because it has a width almost equal to the instrumental resolution of 0.6 eV, indicating that there is little or no vibrational structure in the band. The position of the peak should, therefore, give the adiabatic value of the ionization potential of nitrogen. The position of the peak gives a value of 15.6 eV for the ionization potential, which agrees well with the accurate value of

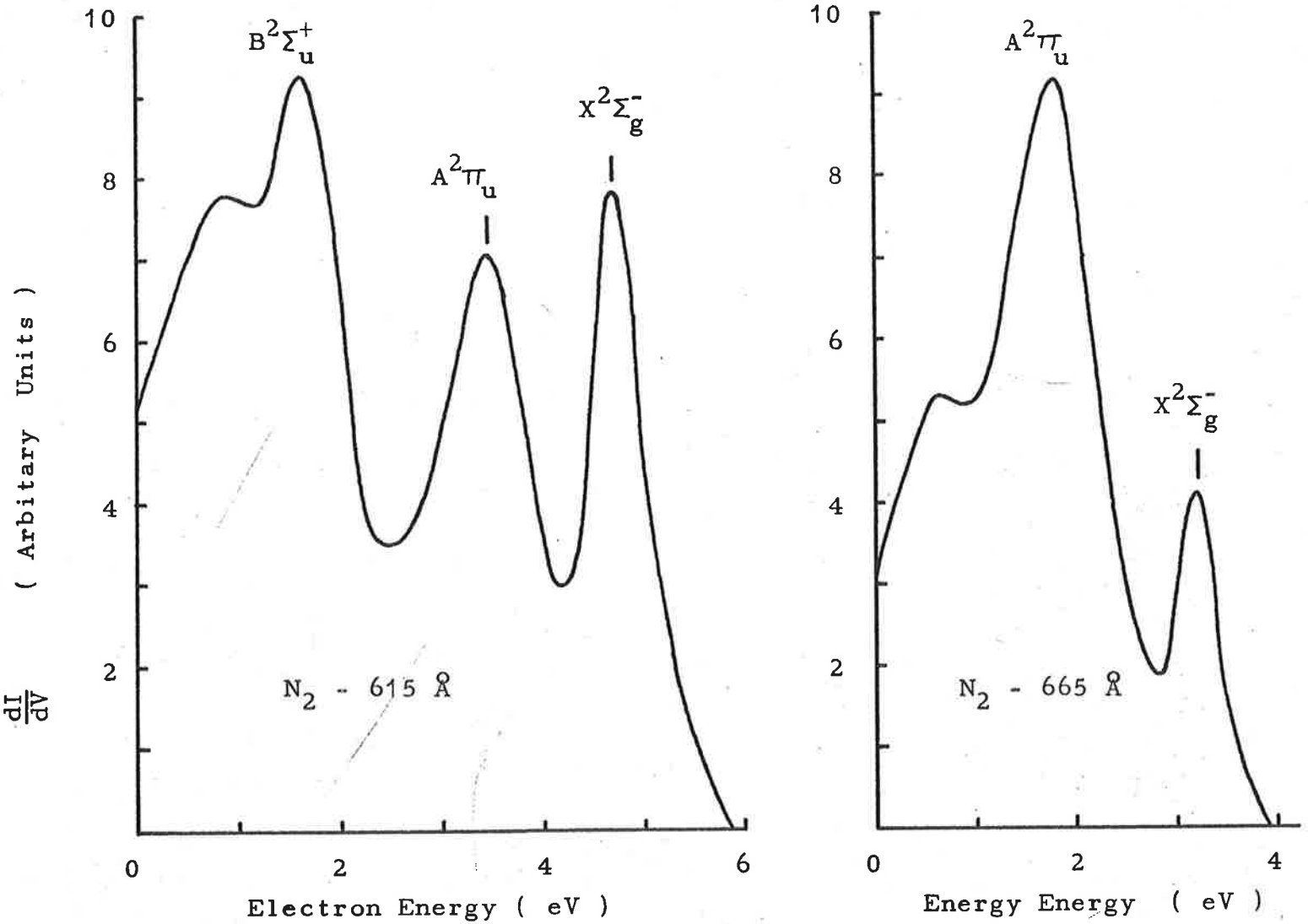

Fig.57. Photoelectron energy spectra from N_2.
(a) 615 Å (b) 665 Å

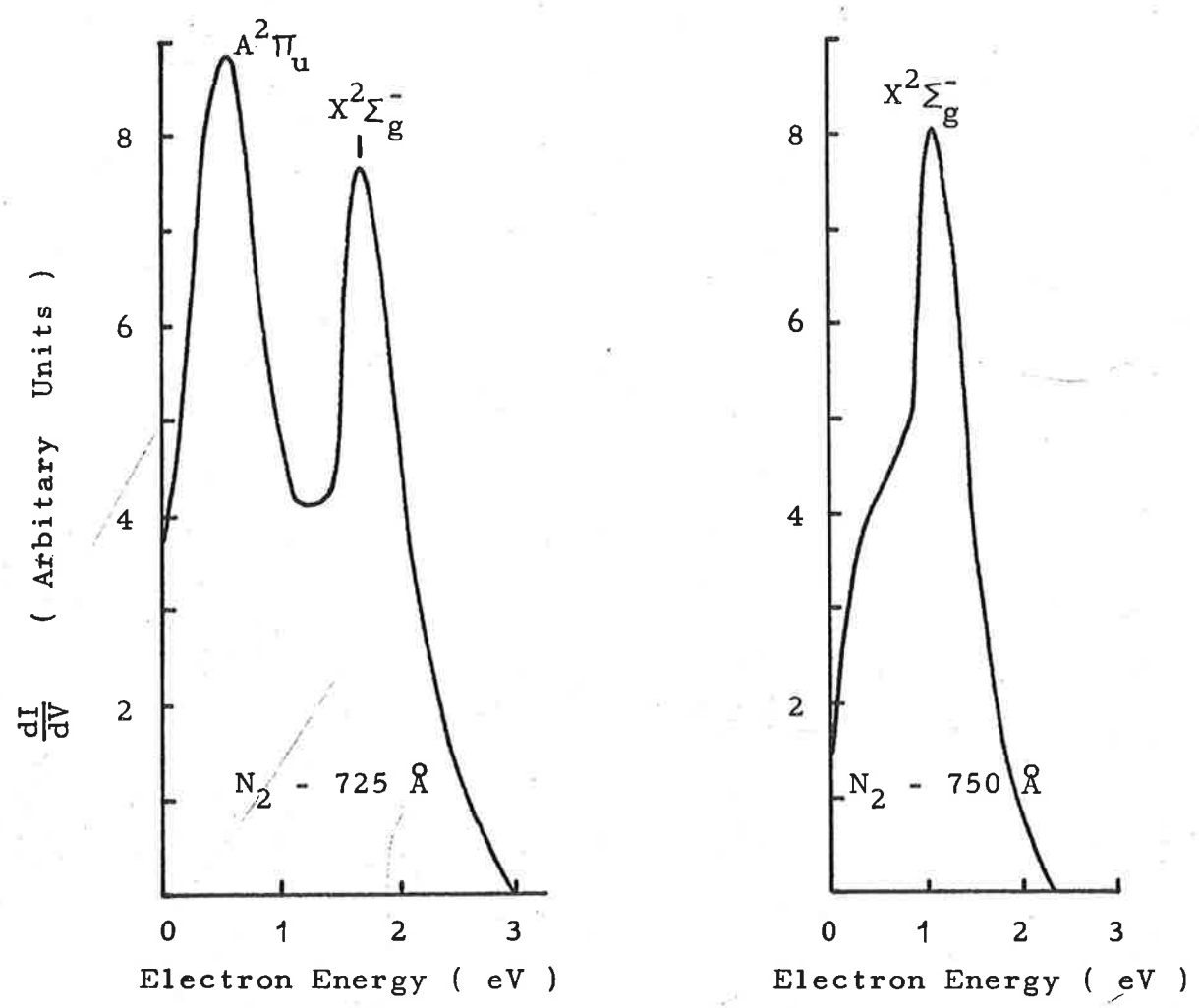

Fig.57. Photoelectron energy spectra from N_2.
(c) 725 Å (d) 750 Å

15.576 eV. This observation is in agreement with that of Al-Joboury and Turner, (Al-Joboury and Turner 1963) whose photoelectron spectrum from nitrogen at 584 Å is shown in Fig.58. No evidence of a fluorescent auto-ionization process was found in the nitrogen spectra.

IV.2.2 Variation of the partial photoionization cross-sections of molecular nitrogen with wavelength

The branching ratios for the three states of the nitrogen ion are shown as a function of wavelength in Fig.59. These were combined with the total photoionization cross-section of nitrogen given by Cook and Metzger, (Cook and Metzger 1964 a) and the total cross-section averaged over 10 Å intervals is shown in Fig.60. The partial photoionization cross-sections which were obtained are shown in Fig.61. Since the total photoionization cross-section shown in Fig.60 does not contain any gross features, and approximates to a step function, the branching ratio curves and the partial cross-section curves are similar in shape. The partial cross-sections for the photoionization of nitrogen contain little significant fine structure, but there does appear to be competition between the final states of the ion. The cross-section for the production of ions in the ground state ($X^2\Sigma_g^+$) rises from the threshold to a broad maximum, and decreases rapidly as the cross-section for the production

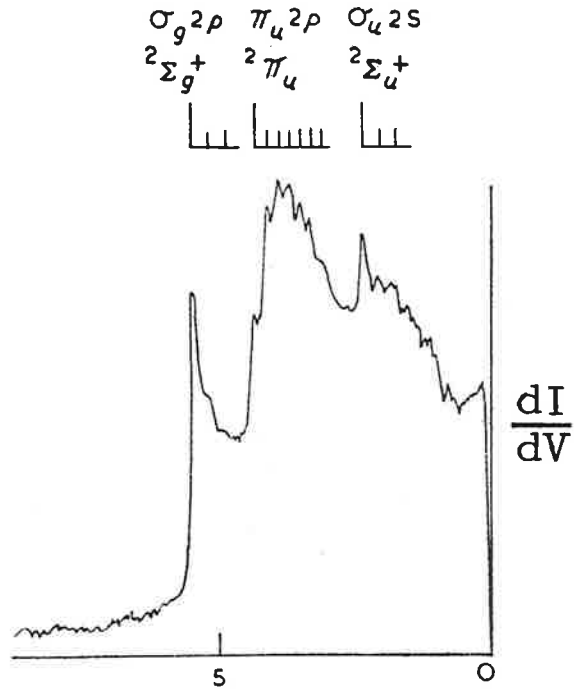

Electron Energy (eV)

Fig.58. Photoelectron spectrum from N_2 at 584 Å.
(Al-Joboury and Turner 1963)

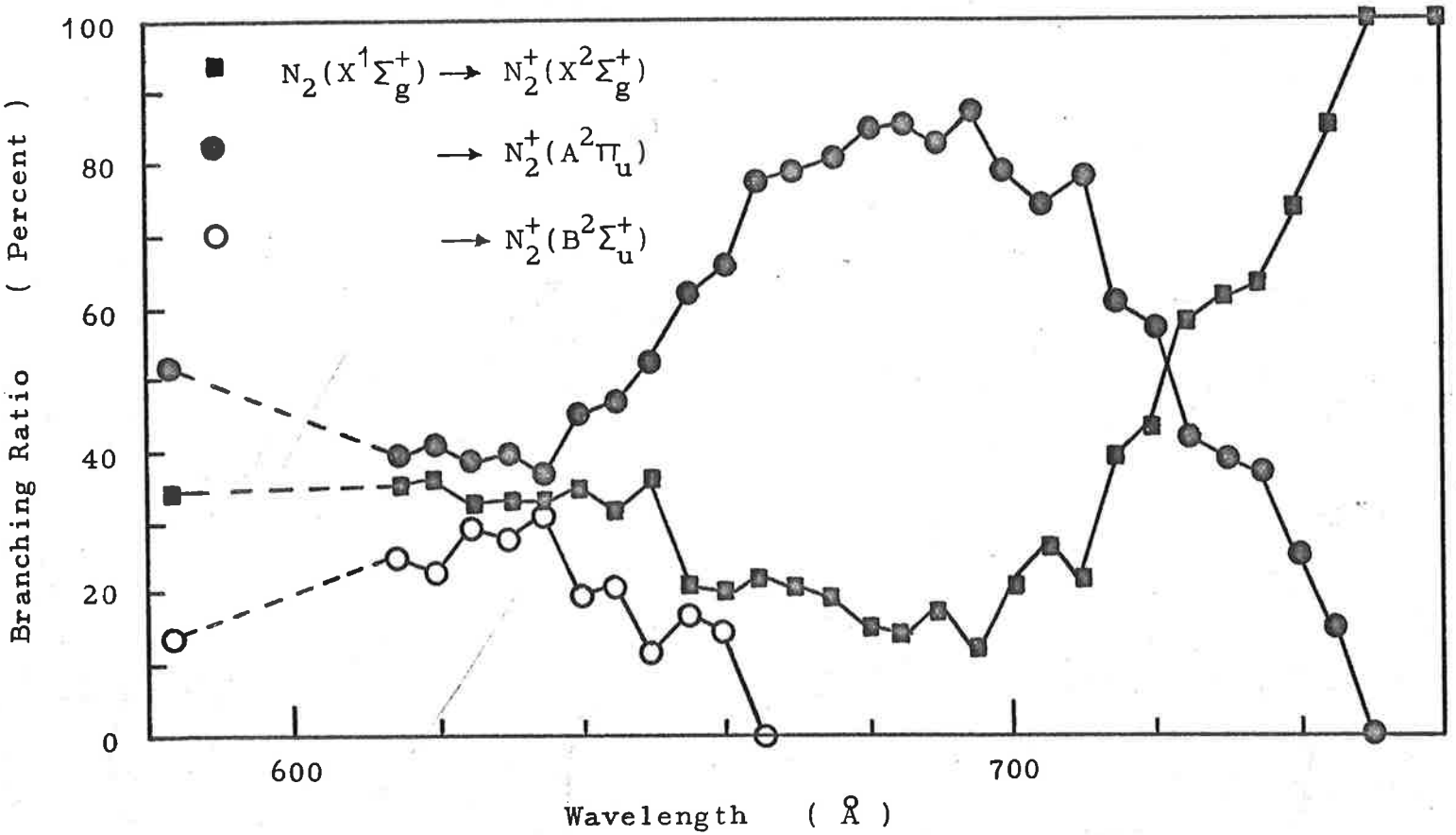

Fig.59. Branching ratios for the various photoionizing processes in N_2.

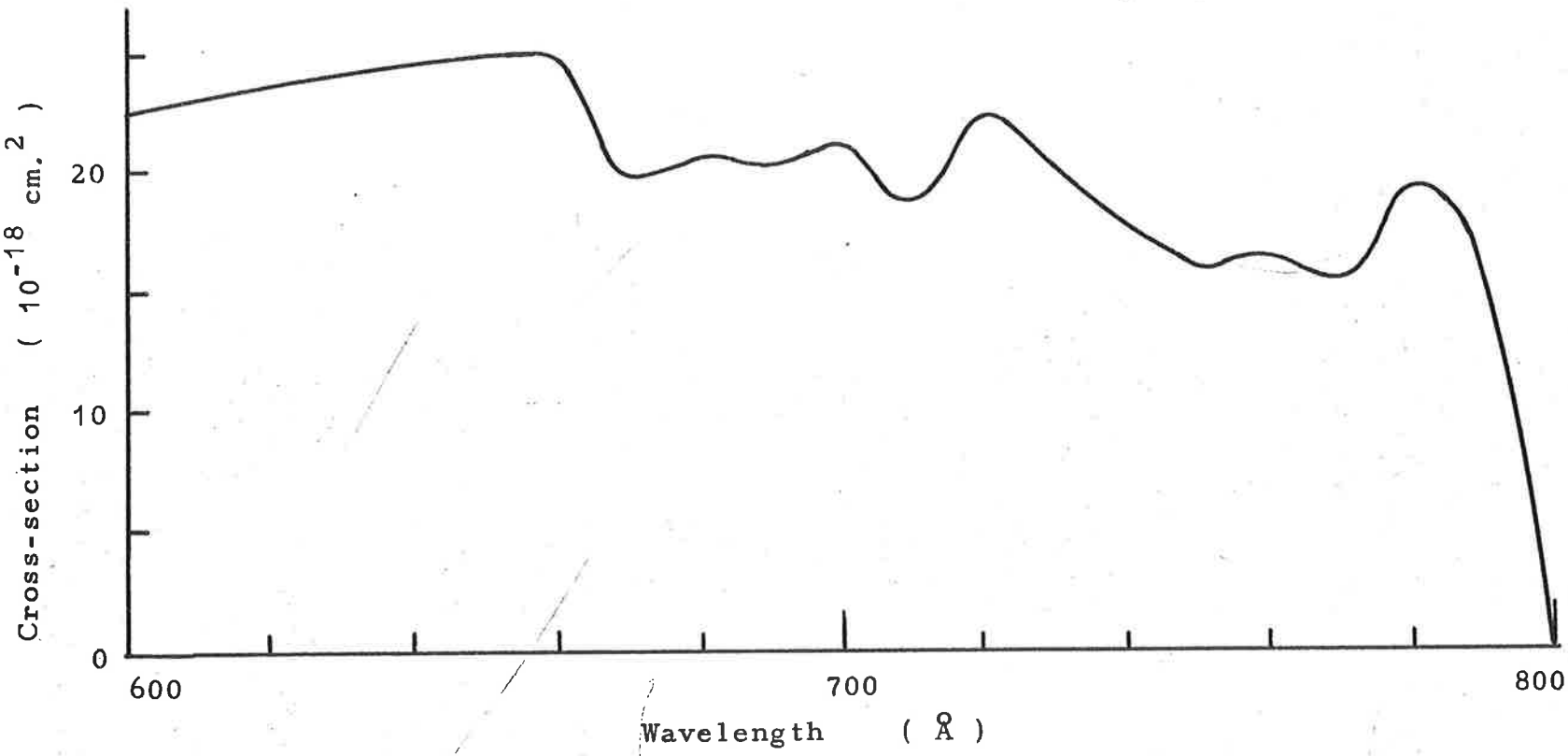

Fig.60. Total photoionization cross-section of molecular nitrogen (Cook and Metzger 1964a) reduced to 10 Å resolution.

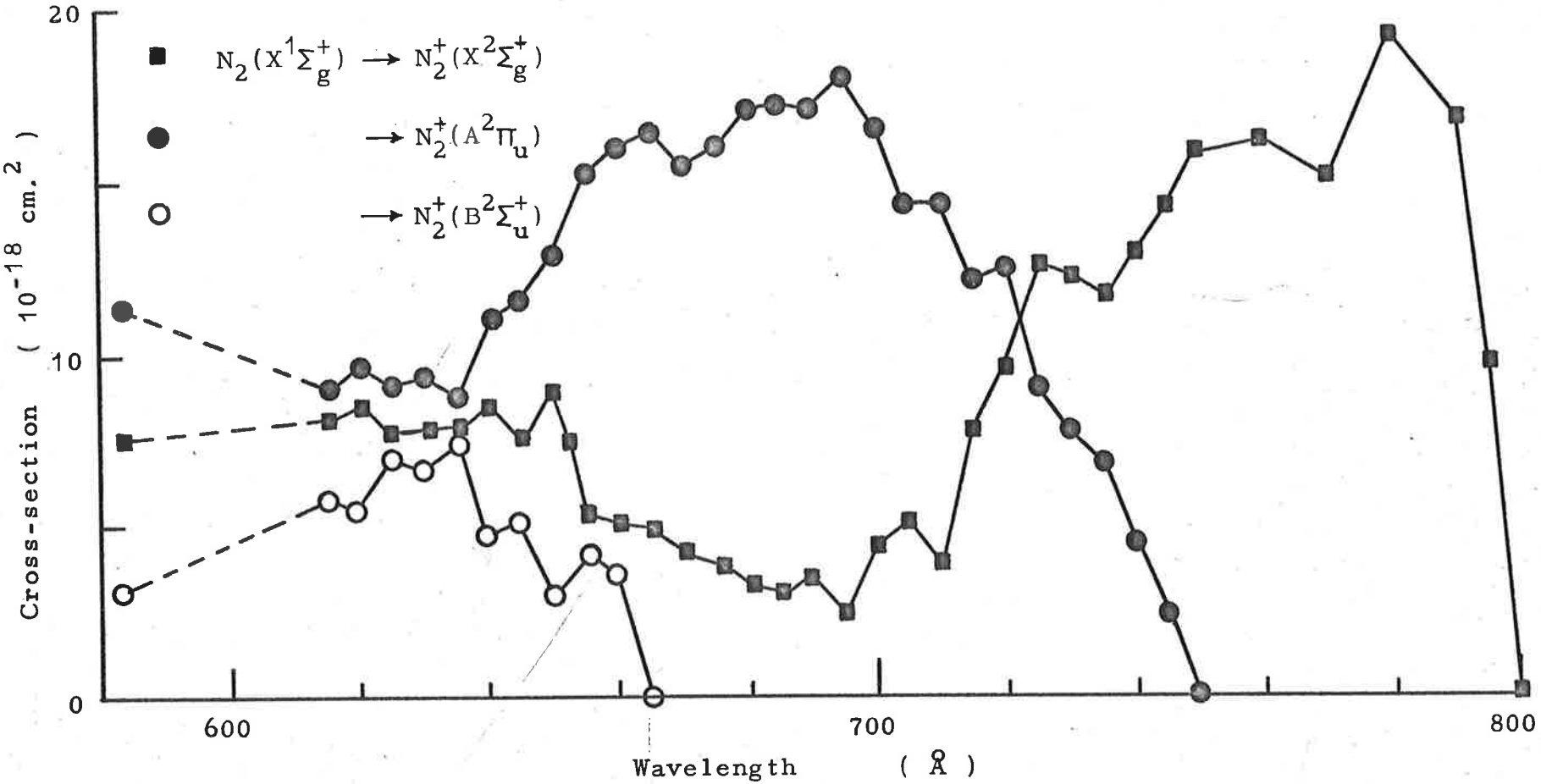

Fig.61. Partial photoionization cross-sections of molecular nitrogen.

of ions in the $A^2\Pi_u$ state increases from threshold. The $A^2\Pi_u$ cross-section in turn decreases from its maximum as the cross-section for the $B^2\Sigma_u^+$ state rises from its threshold. The $X^2\Sigma_g^+$ cross-section has a minimum coinciding in wavelength with the maximum of the $A^2\Pi_u$ cross-section, which appears to have a minimum value coinciding with the maximum of the $B^2\Sigma_u^+$ cross-section. All three curves have a similar shape, and the $X^2\Sigma_g^+$ and $A^2\Pi_u$ curves have roughly equal maxima which are about 2.5 times as large as the maximum of the $B^2\Sigma_u^+$ curve. The states have statistical weights in the ratio 1:3:1.

The results obtained by Schoen (Schoen 1964) are shown in Fig.62. The branching ratio for the $X^2\Sigma_g^+$ state given by Schoen is in good agreement with the average value of 32% obtained from the present results, but the average value of 20% for the $B^2\Sigma_u^+$ branching ratio in the present results is higher by a factor of two than the value indicated by Schoen.

IV.3 Water Vapor

IV.3.1 Photoelectron energy spectra of water vapor

The partial photoionization cross-sections of water vapor were obtained from the analysis of photoelectron energy spectra recorded at 10 Å intervals in the range 620 Å to 850 Å, and also at 584 Å. These spectra were recorded by allowing triple distilled water to evaporate

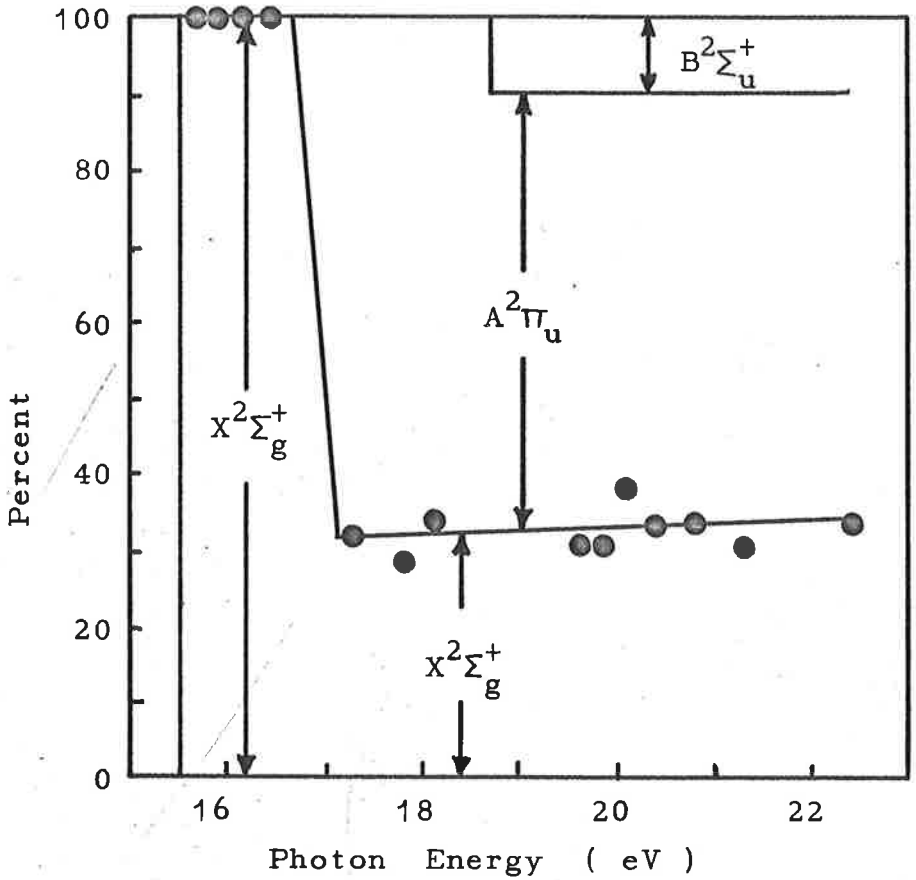

Fig.62. Percentage excitation to various states of N_2^+.
(Schoen 1964)

into the spectrometer chamber through a needle valve. Other conditions were identical to those for the experiments with oxygen and nitrogen. Typical photoelectron energy spectra from water vapor are shown in Fig.63.

The spectrum at 584 Å shown in Fig.63 (a) has three prominent peaks. The most energetic of these has a width of 0.7 eV, which is only slightly greater than the instrumental resolution. The position of the peak corresponds to an ionization potential of 12.7 eV, which is in good agreement with the value of 12.60 eV given by Frost and McDowell (Frost and McDowell 1958) for the ionization potential of water vapor. The peak was therefore associated with the $^2B_1$ ground state of H_2O^+. The second peak has a width of 1.7 eV, and the maximum corresponds to an energy state 14.9 eV above the ground state of H_2O. Frost and McDowell found that the $^2A_1$ state of H_2O^+ has an energy of 14.35 eV relative to the ground state of H_2O, and the second peak was associated with this state. The energy given by Frost and McDowell for the second excited state ($^2B_2$) of H_2O^+ is 16.34 eV. However, no peak corresponding to this state was distinguished in any of the spectra, but a small contribution may have been concealed in the broad peak associated with the $^2A_1$ state. The third peak in the spectrum at 584 Å is very broad and poorly defined. Two maxima can be seen which

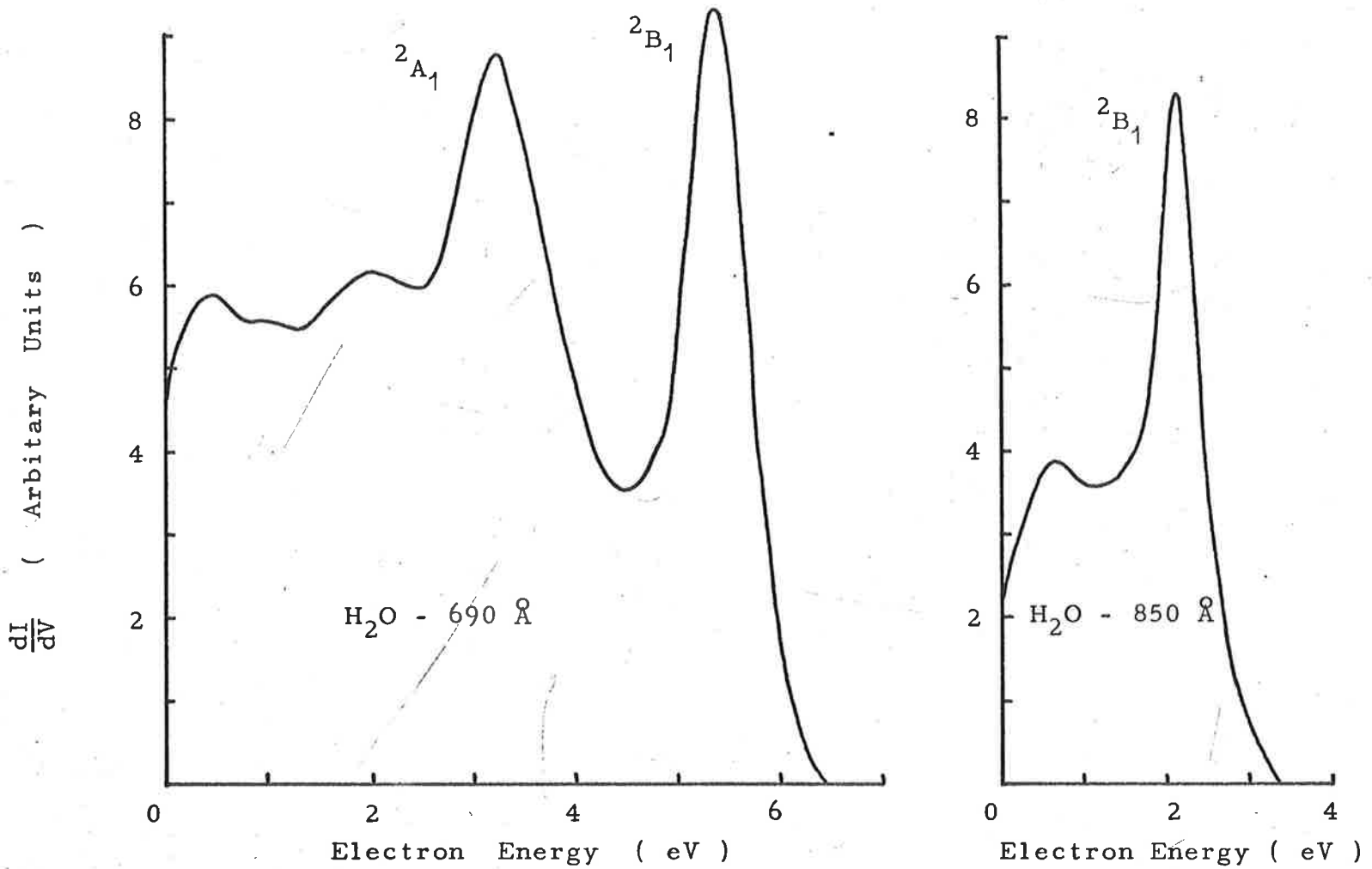

Fig.63. Photoelectron spectra from H_2O. (b) 690 Å, (c) 850 Å.

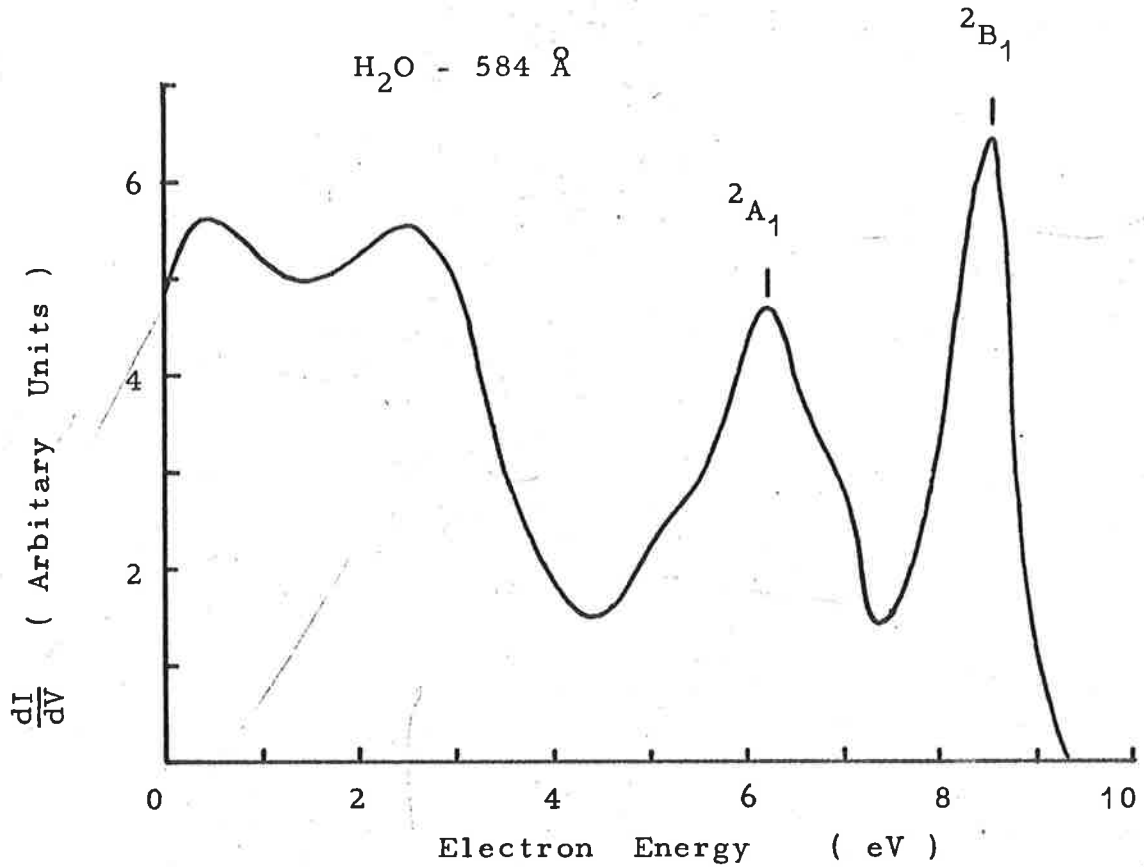

Fig.63 (a). Photoelectron spectrum from H_2O with an incident beam wavelength of 584 Å.

correspond to states with energies of 18.6 eV and 20.7 eV. Several dissociative ionization processes have thresholds in this region. These are thresholds for the production of OH^+ (18.3 eV), O^+ (18.8 eV), and H^+ (19.5 eV). (Field and Franklin 1957). The third peak was, therefore, associated with dissociative photoionization processes. The peak must have contained a large contribution from the production of OH^+, but no further identification of the processes was possible.

IV.3.2 Variation of the partial photoionization cross-sections of water vapor with wavelength

The branching ratios for the two states of H_2O^+ and dissociative photoionization are shown as a function of wavelength in Fig.64. This data was combined with the total photoionization cross-section measurements of Metzger and Cook, (Metzger and Cook 1964a) which are shown in Fig.65, to produce the partial photoionization cross-sections which are shown in Fig.66. The partial cross-sections contain very little structure, and increase gradually from threshold, in contrast to the partial cross-sections for the diatomic molecules. The $^2B_1$ cross-section has a maximum value at the threshold for the $^2A_1$ state, indicating some competition between these states.

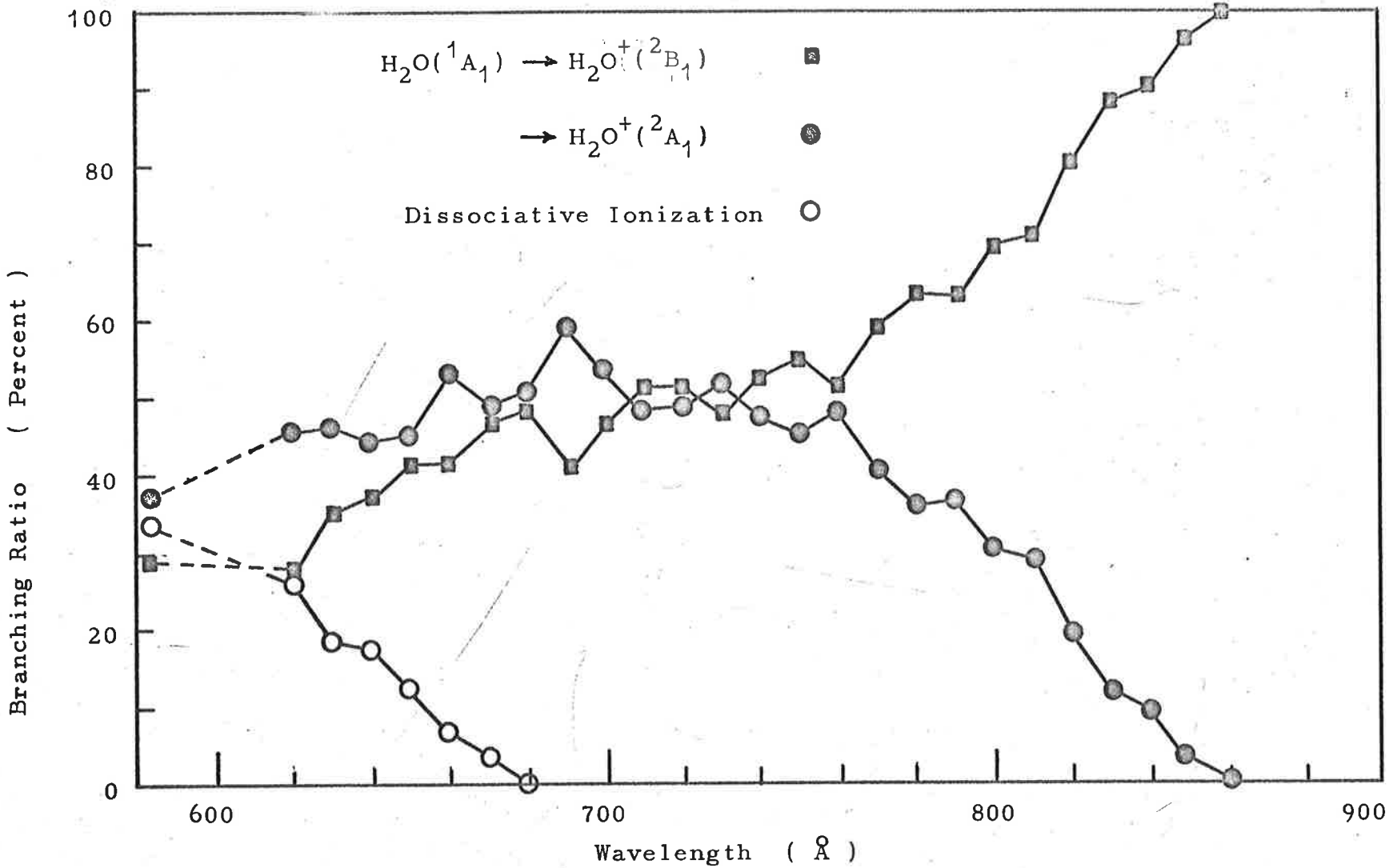

Fig.64. Branching ratios for the various photoionizing processes in H_2O.

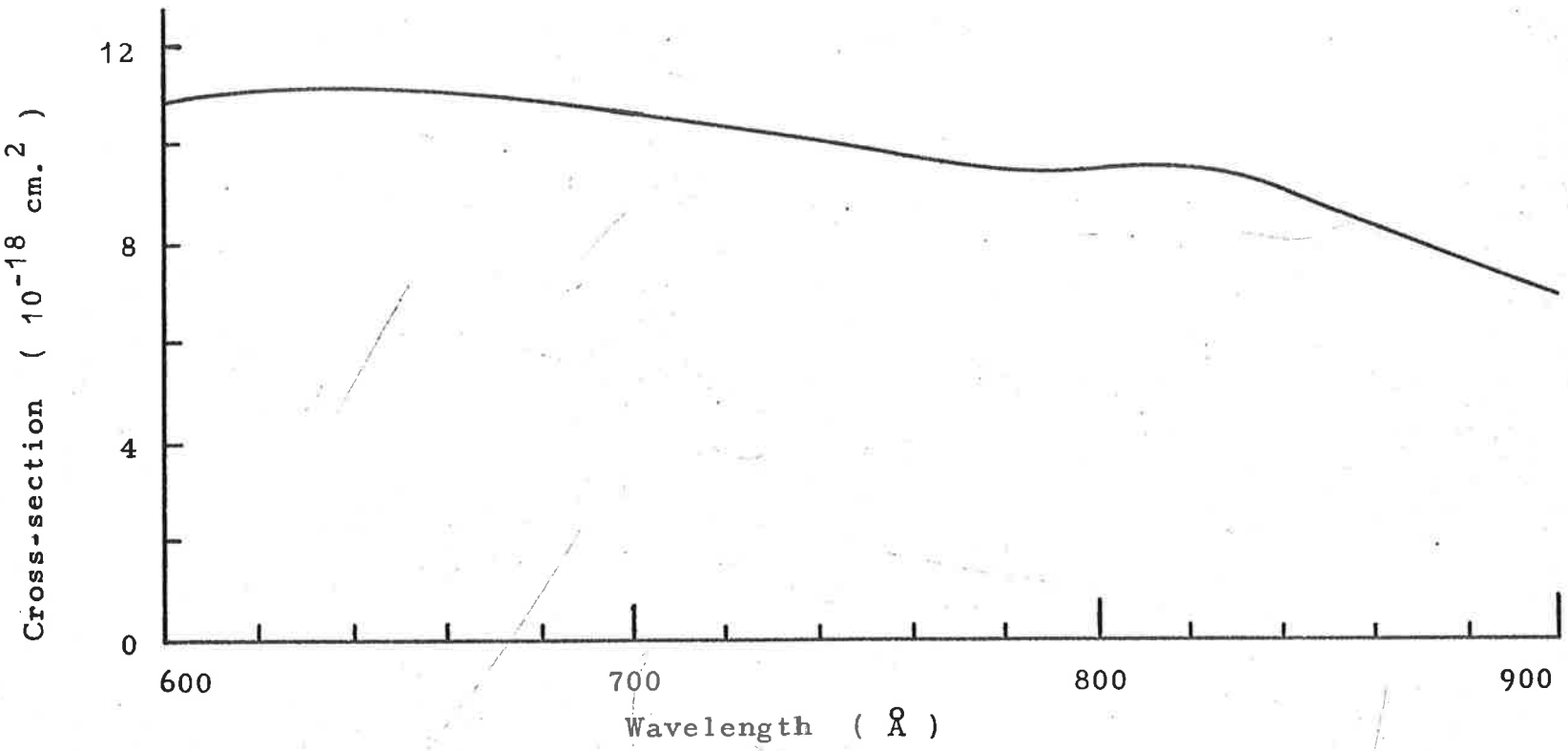

Fig.65. Total photoionization cross-section of water vapor.
(Metzger and Cook 1964a)

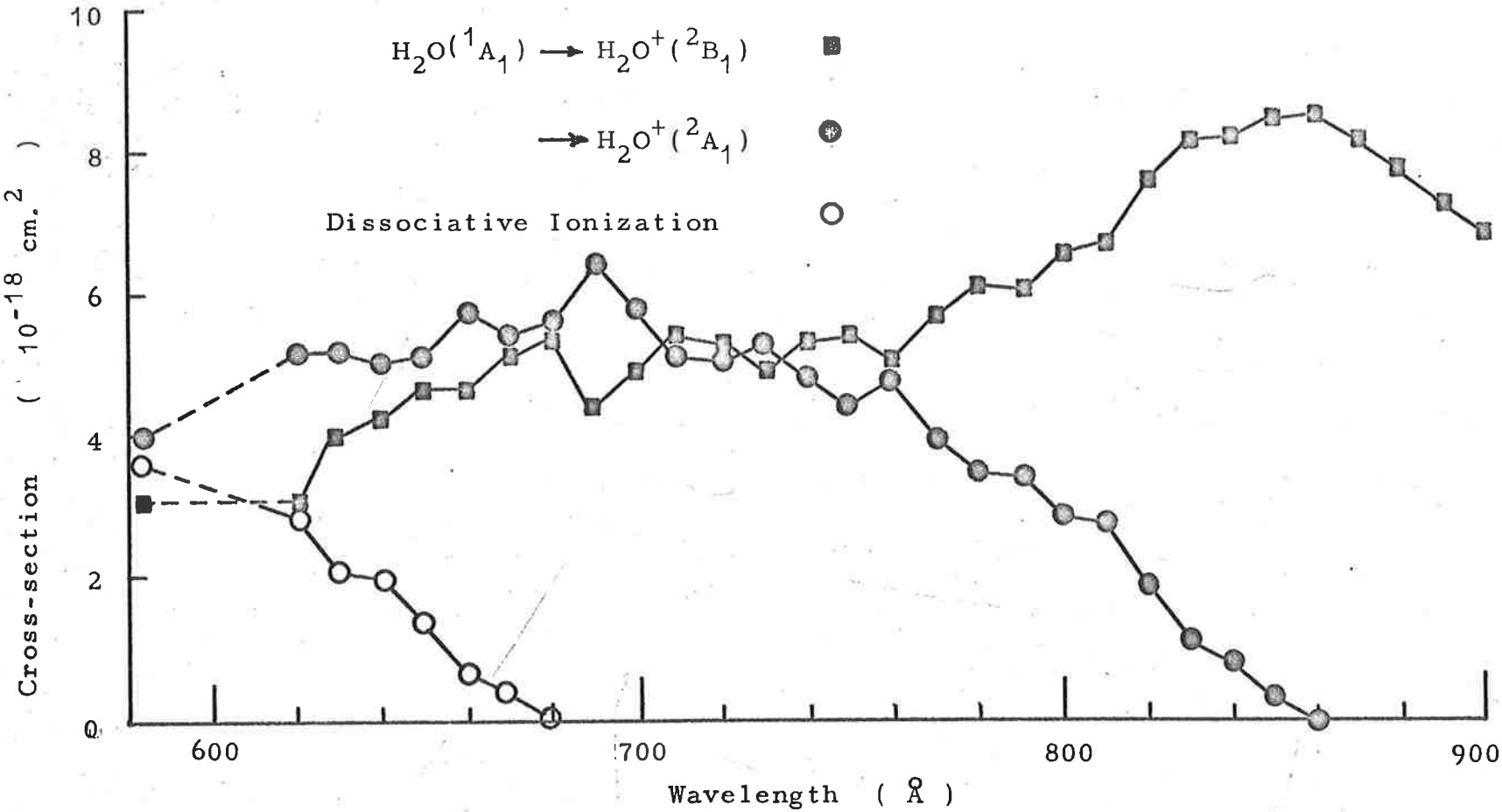

Fig.66. Partial photoionization cross-sections of water vapor.

CHAPTER V

PHOTOIONIZATION IN THE ATMOSPHERE

V.1 Introduction

The partial photoionization cross-section measurements which were presented in Chapter IV make possible a more accurate description of the production of photoelectrons in the ionosphere than has been possible in the past. The total photoionization cross-sections of the atmospheric gases are sufficient to account for the rate of production of photoelectrons, but in previous calculations of the energy distribution of the electrons, (Dalgarno et al 1963) inaccurate approximations to the partial photoionization cross-sections have been used. A knowledge of the energy distribution of the primary photoelectrons in the ionosphere is essential to a description of the subsequent dissipation of the kinetic energy of the electrons, and in the calculation of the equilibrium electron temperature. Another result of photoionization in the upper atmosphere is the emission of fluorescent radiation with an intensity which depends on the rate at which ions are produced in excited states. The partial photoionization cross-section measurements therefore make possible a detailed description of fluorescence in the ionospheric region of

the atmosphere.

V.2 Photoelectrons in the Ionosphere

The principal absorbers of extreme ultraviolet radiation in the ionospheric region of the atmosphere are atomic oxygen, molecular oxygen, and molecular nitrogen, and the photoionization of these is the main source of electrons. In order to calculate the rate of production and the energy distribution of the photoelectrons at a given altitude, the intensity distribution of the extreme ultraviolet spectrum of the sun and the number densities of the absorbers at that altitude, and the partial photoionization cross-sections must be known. The energy distribution has been calculated as a function of altitude by several workers. (Hanson and Johnson 1961, Dalgarno et al 1963, Tohmatsu et al 1965). In the absence of any experimental measurements of the partial photoionization cross-sections, Dalgarno et al assumed that these cross-sections were proportional to the statistical weight of the electronic state of the ion concerned, but the measurements made in the present experiments show that this assumption is inaccurate, particularly in regions of autoionization. In view of the present measurements of the partial photoionization cross-sections, the energy distribution of the primary photoelectrons in the ionosphere has been recalculated.

V.2.1 Calculation of the photoelectron energy distribution

The first stage of the calculation was the determination of the intensity distribution of the solar spectrum as a function of altitude. The number densities for O, O_2, and N_2 were taken from the COSPAR International Reference Atmosphere (1965). The model atmosphere corresponding to a mean solar activity at noon was chosen. (Model 5, hour 12). The atmosphere was divided into layers with a thickness (Δh) of 40 km. between the altitudes of 520 km. and 200 km., and a thickness of 20 km. in the region from 200 km. to 120 km. These layers were chosen so that the thickness was never greater than the scale height. It was assumed that the average density of each gas in such a layer was equal to the density at the centre of the layer. The incident solar fluxes assumed were those given by Hinteregger et al (Hinteregger et al 1965) in 62 wavelength regions between 1027 Å and 31 Å. The intensity in each wavelength region at the bottom of each successive layer was calculated using the equation:

$$I_h = I_{h-1} \exp -[\sigma(O)\, n(O) + \sigma(O_2)\, n(O_2) + \sigma(N_2)\, n(N_2)]\Delta h \quad (31)$$

The effective total absorption cross-sections listed by Hinteregger et al for each wavelength region were used,

and at wavelengths where the effect of radiation hardening is serious, the effective cross-section was varied linearly over the range of altitudes between the limits given by Hinteregger et al.

The production rates of O^+, O_2^+, and N_2^+ were calculated for each wavelength region at altitudes of 100 km, 110 km, 120 km, 160 km, and 280 km, using the equation:

$$P(X^+) = I_h \sigma_i(X)\, n(X) \qquad (32)$$

The photoelectron energy distribution was obtained by dividing the ion production rate according to the branching ratios for the various energy states of the ion. The branching ratios for the states of O_2^+ and N_2^+ at wavelengths longer than 584 Å were taken from Figs.49 and 59 respectively, and averaged over the wavelength regions. The branching ratios for the states of O^+ were taken from the cross-sections calculated by Dalgarno et al. (Dalgarno et al 1964). At wavelengths shorter than 584 Å the branching ratios for the states of O_2^+ and N_2^+ were extrapolated from the measurements in the region above 584 Å shown in Figs. 49 and 59. The branching ratios adopted were 20%, 35%, 25%, and 20% for the $X^2\Pi_g$, $a^4\Pi_u + A^2\Pi_u$, $b^4\Sigma_g^-$, and $^2\Sigma_g^-$ states of O_2^+, and 35%, 55%, and 10% for the

$X^2\Sigma_g^+$, $A^2\Pi_u$, and $B^2\Sigma_u^+$ states of N_2^+. These ratios were assumed to be constant at wavelengths shorter than 584 Å. In analogy with the partial cross-sections for atomic oxygen, (Dalgarno et al 1964) it was assumed that transitions corresponding to the removal of an inner shell electron had cross-sections much smaller than those for transitions corresponding to the removal of an outer electron.

The photoelectron energy scale was divided into regions of width comparable with the width of the wavelength regions into which the solar spectrum was divided. The regions had widths of 0.5 eV for energies between 0 and 10 eV, 2eV for energies between 10 eV and 30 eV, 5 eV for energies between 30 eV and 60 eV, 20 eV for energies between 60 eV and 100 eV, and 50 eV for energies greater than 100 eV. The photoelectrons were allotted to the energy regions occupied by the centres of the peaks in the energy spectrum at the wavelength corresponding to the centre of each wavelength region.

V.2.2 The primary photoelectron energy distribution

The primary photoelectron energy spectra at 120 km., 160 km., and 280 km., are shown in Figs.67-69. The spectra have a shape not unlike an exponential decay, with a number of superposed peaks which correspond to intense lines in the solar spectrum. At 280 km., the

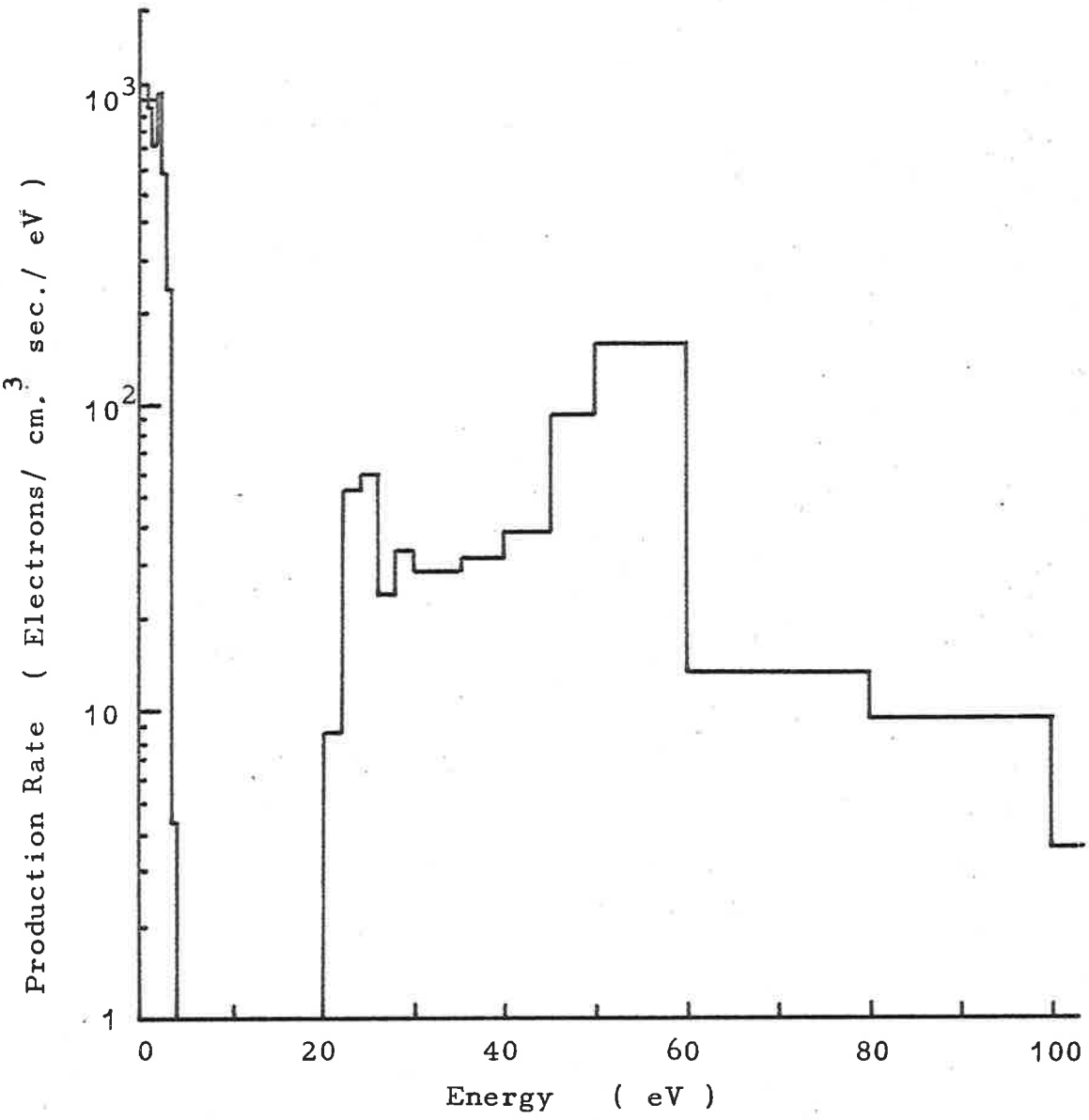

Fig.67 (a) Primary photoelectron energy distribution at 120 km.

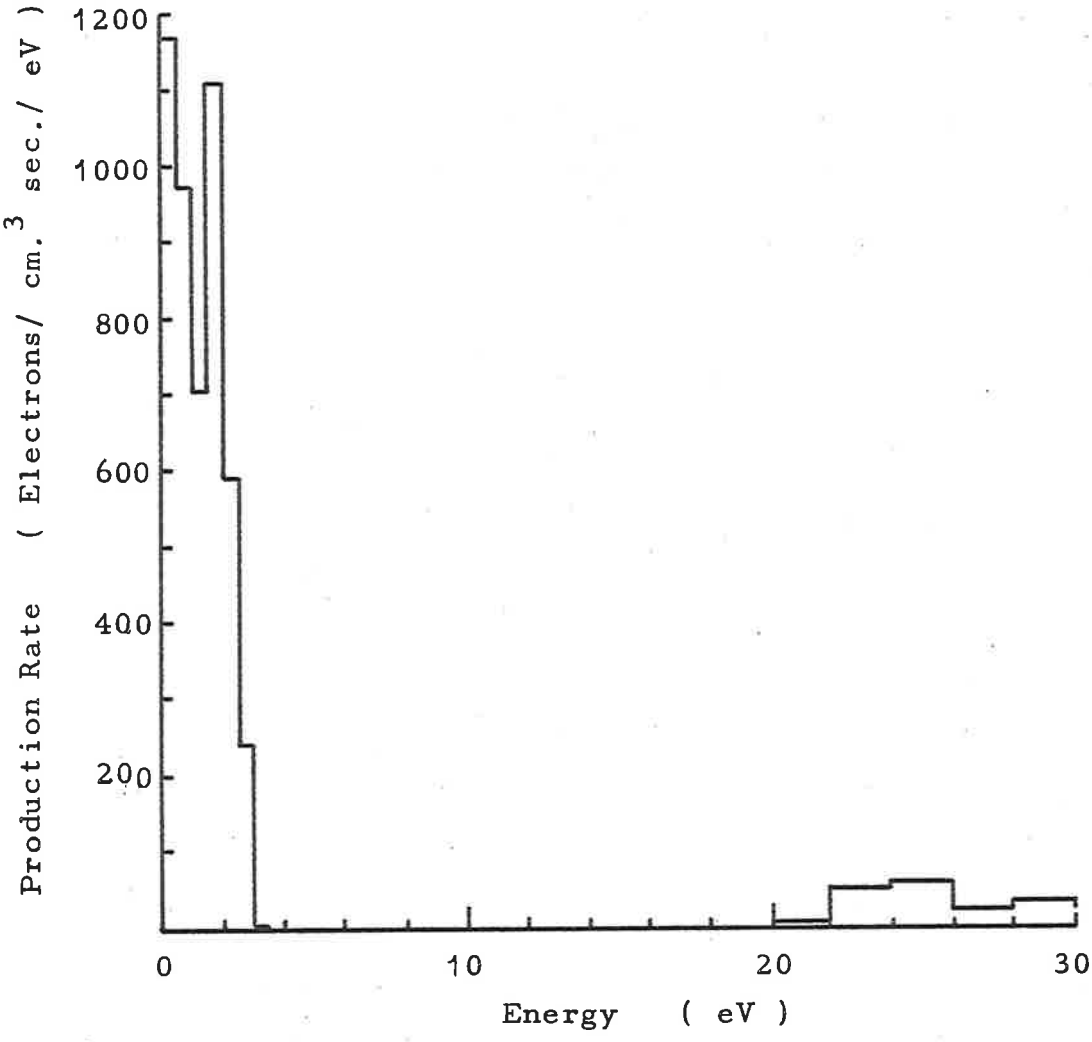

Fig.67 (b) Detail of primary photoelectron energy distribution at 120 km.

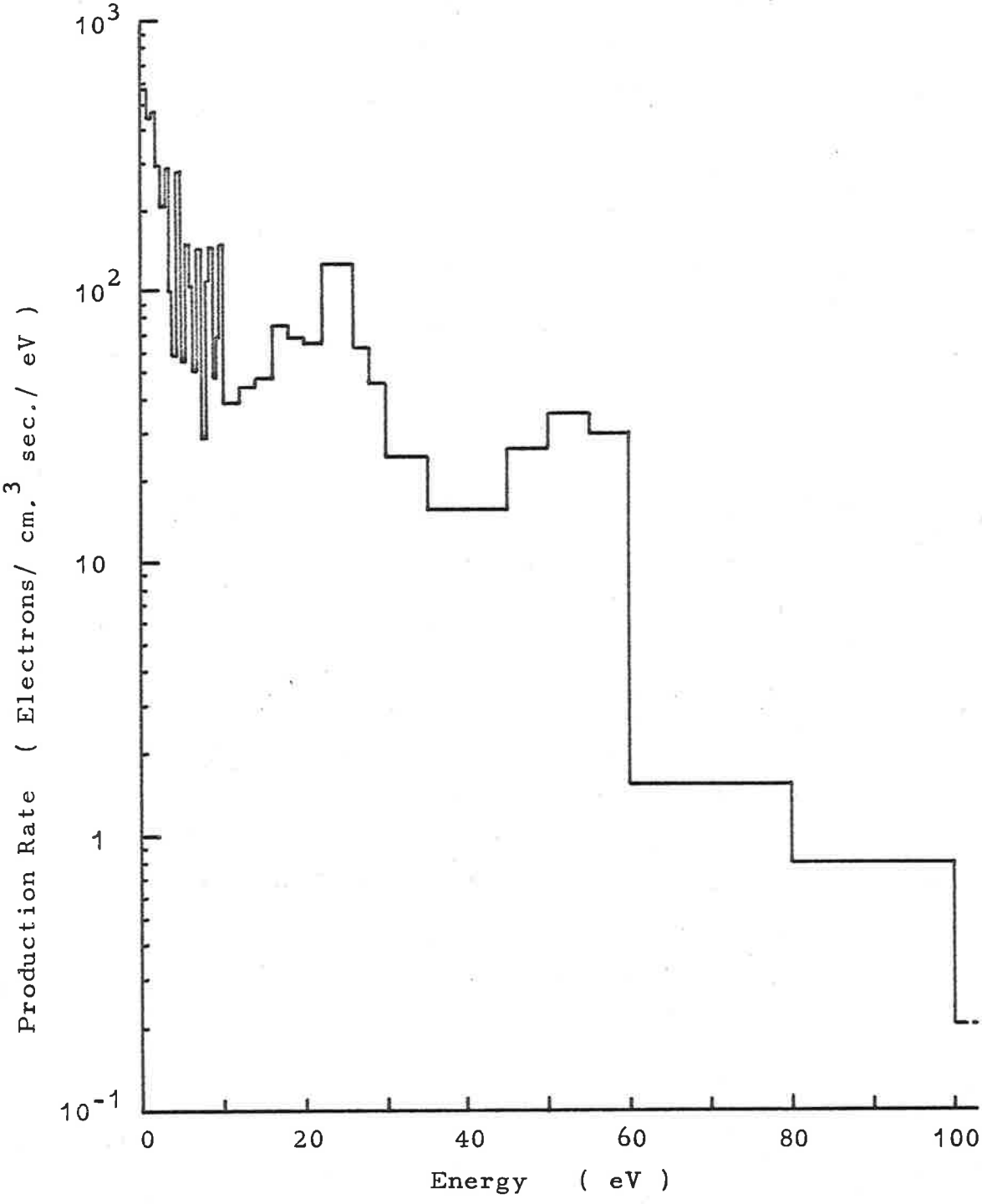

Fig.68 (a) Primary photoelectron energy distribution at 160 km.

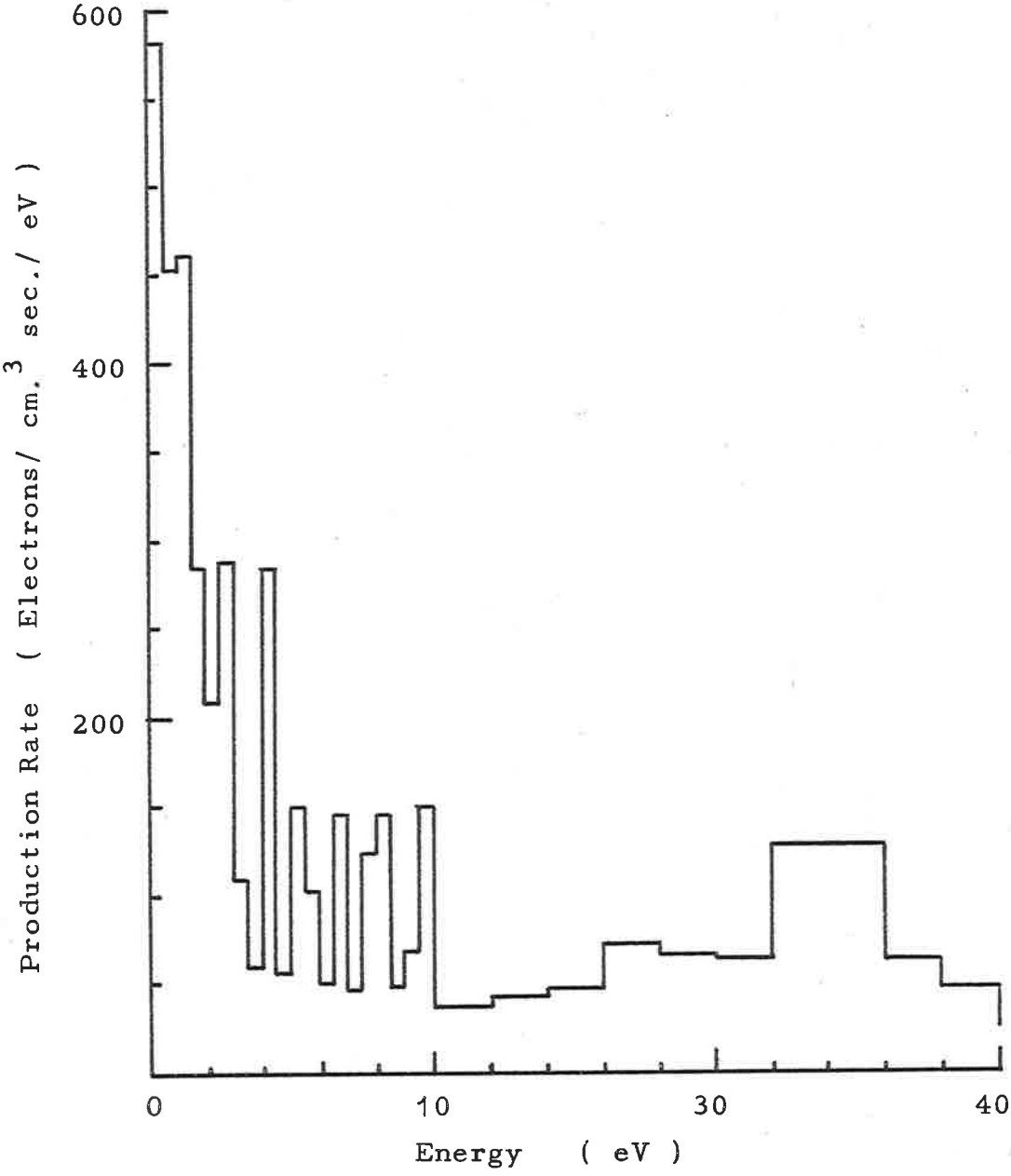

Fig.68 (b) Detail of primary photoelectron energy distribution at 160 km.

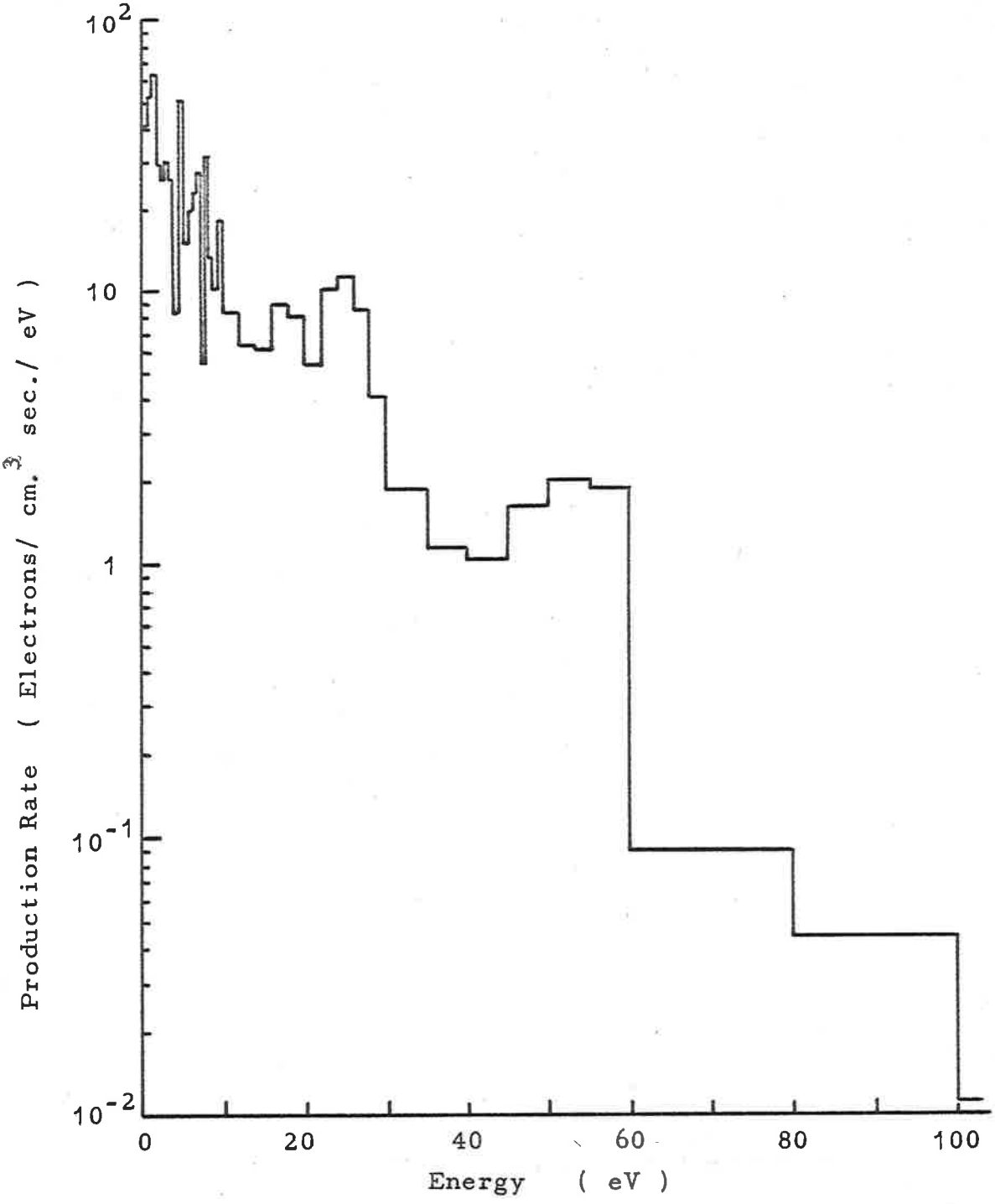

Fig.69 (a) Primary photoelectron energy distribution at 280 km.

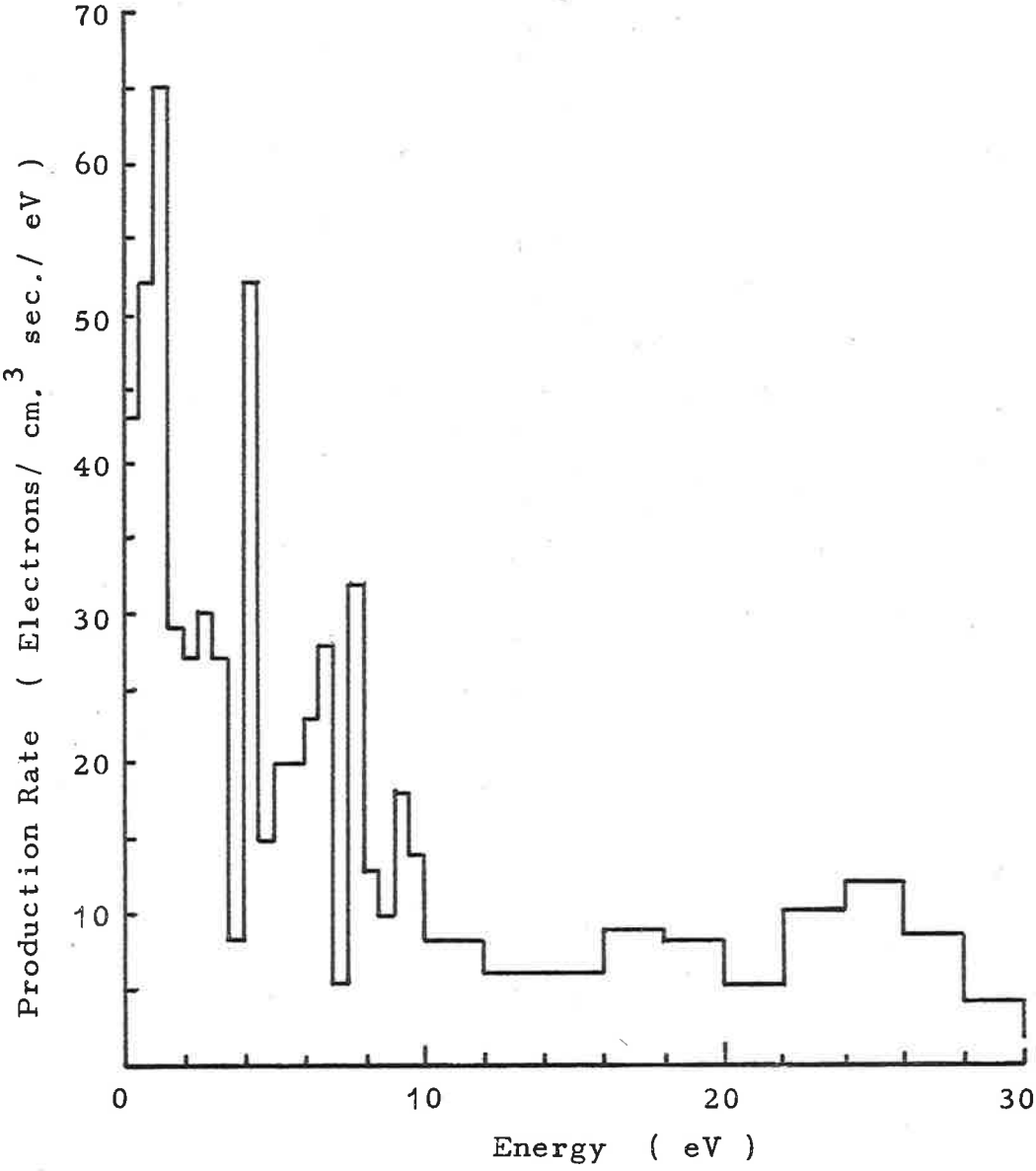

Fig.69 (b) Detail of primary photoelectron energy distribution at 280 km.

photoionization of atomic oxygen is the most important source of electrons, and the positions of the peaks are related to the energy levels of O^+. At lower altitudes the photoionization of molecular nitrogen and oxygen becomes more important, and the structure of the spectrum changes slightly. Maxima in the spectra at 25 eV and 55 eV correspond to large fluxes in the regions 310 Å - 280 Å and 205 Å - 165 Å respectively. The region from 310 Å to 280 Å includes the intense He II Ly-α line at 303.8 Å. The spectrum for 120 km., has a region from 4 eV to 20 eV in which there are very few electrons, because radiation of wavelength between 300 Å and 400 Å is absorbed at a higher altitude as a result of the larger absorption cross-sections in this region.

In Fig.70 some primary photoelectron energy distributions for a zero zenith angle given by Tohmatsu et al (Tohmatsu et al 1965) are shown. These spectra have a similar overall shape to those of the present results, but have different structure. The difference in the structure is most apparent in the maximum at 25 eV. At lower energy the results of Tohmatsu are less detailed than the present results, and a detailed comparison is not possible, but the structure does not appear to be in good agreement. These differences indicate that the partial photoionization cross-sections

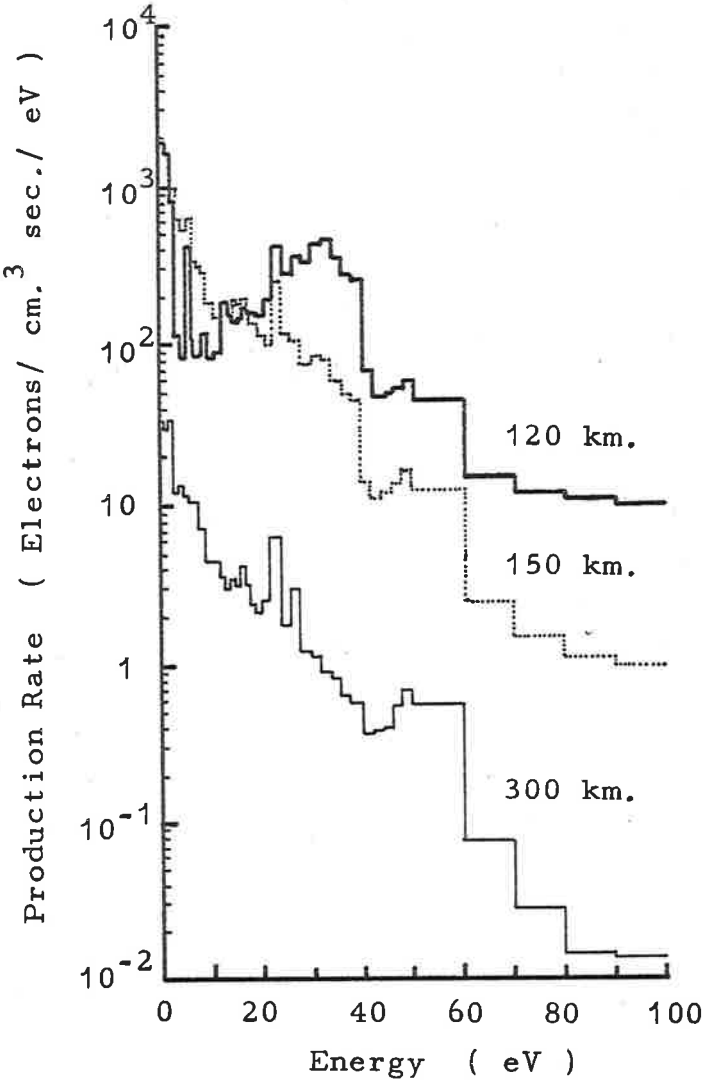

Fig.70. Source energy spectra of photoelectrons at solar zenith angle 0°.
(Tohmatsu et al 1965)

assumed by Tohmatsu et al were very different from those measured in the present work. The source of the partial photoionization cross-sections used by Tohmatsu et al is not clear, but the values listed by them are in very poor agreement with those of the present work. The spectrum at 120 km. obtained by Tohmatsu et al shows more electrons with energies in the range 4 eV to 20 eV than the spectrum shown in Fig.67, but this is probably a result of the different model atmospheres adopted for the two calculations, and represents an effective difference in altitude.

The total rate of deposition of kinetic energy at each altitude is compared in Table I with the corresponding values given by Dalgarno et al, and by Tohmatsu et al.

Table I

Total rate of deposition of primary photoelectron kinetic energy

Alt.(km)	Kinetic energy deposition rate (10^4 eV/cm.^{3}/sec.)		
	Present work	Dalgarno et al (1963)	Tohmatsu et al (1965)
280	0.67	0.36	0.43
160	7.6	5.9	9.6
120	22	2.7	40
110	18	-	40
100	11	-	30

The present results indicate a maximum energy deposition rate at an altitude close to 120 km., in better agreement with Tohmatsu et al than Dalgarno et al. The maximum is also much larger than that indicated by Dalgarno et al, as a result of the smaller solar flux below 500 Å assumed by Dalgarno et al.

V.3 Fluorescence in the Ionosphere

Fluorescence results when ions are produced in electronically excited states from which allowed transitions to a lower state can occur. The intensity of the fluorescence in the various band systems has been discussed previously, (Dalgarno and McElroy 1965, Tohmatsu et al 1965) but a rediscussion is necessary in view of the present measurements of the partial photo-ionization cross-sections.

V.3.1 Fluorescent transitions

Some discussion of the fluorescent transitions which occur is necessary before the expected intensity in the various band systems can be considered. Of the two excited states of the atomic oxygen ion which are important in the ionosphere, the ^2D state is metastable with a radiative lifetime of order 10^4 seconds. (Seaton and Osterbrock 1957). Ions in this state may be de-excited by superelastic collisions with electrons, and therefore act as a heating process in the ionosphere.

(Dalgarno et al 1963). The ^2P state of O^+ is also metastable, with a radiative lifetime of order 5 seconds. Although de-excitation by electron impact probably occurs, some radiation may also occur, (Dalgarno and McElroy 1965) and the production rate of atomic oxygen ions in the ^2P state provides an upper limit for the rate of emission of the four lines of the ^2P - ^2D multiplet at 7319-30 Å.

The fluorescence from molecular oxygen and molecular nitrogen will correspond to the transitions shown in Table II.

Table II

Fluorescent band systems in O_2 and N_2

Transition	Band System	Wavelength Region
$O_2^+(^2\Sigma_g^-) \rightarrow O_2^+(A^2\Pi_u) + h\nu$		3600 Å
$O_2^+(A^2\Pi_u) \rightarrow O_2^+(X^2\Pi_g) + h\nu$	2nd.Negative	2600 Å
$O_2^+(b^4\Sigma_g^-) \rightarrow O_2^+(a^4\Pi_u) + h\nu$	1st.Negative	5900 Å
$N_2^+(B^2\Sigma_u^+) \rightarrow N_2^+(X^2\Sigma_g^+) + h\nu$	1st.Negative	3900 Å
$N_2^+(A^2\Pi_u) \rightarrow N_2^+(X^2\Sigma_g^+) + h\nu$	Meinel	Infra-red

This list includes transitions from the $^2\Sigma_g^-$ state of O_2^+ which were not included in the calculations of previous workers. The $a^4\Pi_u$ state of O_2^+ is metastable, and is

probably de-excited through super-elastic collisions. Also, the Hopfield emission bands are not expected to be prominent, since it was assumed that the $c^4\Sigma_u^-$ upper state is not produced in significant numbers. Some additional fluorescence will result from the fluorescent autoionizing process, which was discussed in Sec.IV.1.6. However, the wavelength of the fluorescence cannot be predicted, since it is not known whether or not a cascade of fluorescent transitions occurs.

V.3.2 Intensity of fluorescent emission.

The rate of population of the upper state of each fluorescent transition is given in Table III for each of the five altitudes. The rate of population of the $A^2\Pi_u$ state of O_2^+ is supplemented by fluorescent transitions from the $^2\Sigma_g^-$ state, and the total rate of population is given in Table III.

Table III

Rates of population of the upper states of fluorescent transitions

	Rate of population (Ions/cm.^{3}/sec.)					
	O^+	O^+			N_2^+	
Alt.(km)	^2P	$^2\Sigma_g^-$	$b^4\Sigma_g^-$	$A^2\Pi_u$	$A^2\Sigma_u^+$	$B^2\Sigma_u^+$
280	63	3.4	6.0	5.2	81	20
160	250	96	140	140	990	210
120	140	230	280	310	1100	200
110	31	110	130	150	510	93
100	3.9	37	47	50	170	32

The values of the population rate were used to estimate the overhead intensity of each band system. A curve of production rate against altitude was drawn for the upper state of each fluorescent transition. Assuming that the emission rate for each fluorescent process was equal to the production rate of ions in the upper state of the transition, the area contained by the curves gave the overhead intensity by using the equation:

$$I = \frac{1}{10^6} \int_0^\infty R(h)\, dh \quad \text{Rayleighs} \qquad (33)$$

where R(h) is the rate of population of the particular state of the ion. The overhead intensity of each band system is given in Table IV, and compared with the results obtained by Dalgarno and McElroy, and by Tohmatsu et al.

Table IV

Overhead intensities of fluorescent band systems

Band System	Overhead Intensity (kR)		
	Present work	Dalgarno and McElroy 1965	Tohmatsu et al 1965
$O^+(^2P - {}^2D)$	3.0	1.5	3.0
O_2^+ Hopfield	-	0.6	-
O_2^+ 3600 Å	1.3	-	-
O_2^+ 1st. Neg.	1.9	2	5.5
O_2^+ 2nd. Neg.	2.0	0.4	1.2
N_2^+ 1st. Neg.	2.5	0.6	11.8
N_2^+ Meinel	12	9	12.8

The intensity given for the $O^+(^2P - {}^2D)$ multiplet is only an upper limit to the actual value, since some de-excitation of the metastable ^2P state occurs through super-elastic collisions. Dalgarno and McElroy estimate that the intensity of this multiplet is reduced by a factor of three by collisions with electrons and nitrogen molecules. The results of Tohmatsu et al give large values for the intensities of the O_2^+ first negative band system and the N_2^+ first negative band system, indicating large errors in the values they adopted for the partial photoionization cross-sections for the $b^4\Sigma_g^-$ state of O_2^+ and the $B^2\Sigma_u^+$ state of N_2^+. The large difference between the present value for the intensity of the O_2^+ second negative band system and the value given by Dalgarno and McElroy is a result of the transitions from the $^2\Sigma_g^-$ state of O_2^+ to the $A^2\Pi_u$ which were not included by Dalgarno and McElroy. The discrepancy in the values for the intensity of the first negative band system of N_2^+ is largely a result of the difference between the present measurement of the partial photoionization cross-section for the $B^2\Sigma_u^+$ state of N_2^+ and the value given by Schoen (Schoen 1964) which was assumed by Dalgarno and McElroy.

CHAPTER VI

SUGGESTIONS FOR FURTHER STUDY OF PHOTOIONIZATION

VI.1 Future Development of Photoelectron Spectroscopy

It is clear that the study of photoelectron energy spectra provides a valuable method of observing the process of photoionisation. The results presented in this thesis have shown the competition between the various photoionising processes, and the effect of autoionising energy states on the distribution of the cross-section among the competing processes. The photoelectron spectra from oxygen indicated that a fluorescent autoionising process occurs. Although the present results represent a considerable improvement over any previous measurement of the partial cross-sections, it is desirable that these phenomena be studied with better resolution than was achieved in the present work. The technique has the potential of providing data which will lead to a better understanding of the quasi-stable states which play an important part in the photoionization of molecular gases. It is also important that the observations should be extended to shorter wavelengths, where new photoionising processes have their threshold. These cross-sections are needed for the calculations of the energy distribution of the primary photoelectrons in the ionosphere.

VI.1.1 Improvements to the experimental technique

Before a more detailed study of the photoelectron energy spectra can be attempted, the experimental technique must be improved to allow spectra of higher resolution to be recorded. The most important of the factors limiting the resolution, which were considered in Sec.III.5.2, are the degree of collimation of the electrons, and the energy resolution of the beam from the monochromator. However, an improvement in each of these factors reduces the number of electrons collected, and a more sensitive method of detection is required in an improved apparatus. The most suitable method is the detection of individual electrons with one of the electron multiplying devices which have been developed. (Lassettre et al 1964, Goodrich and Wiley 1961). These devices require that the electrons should be accelerated to an energy sufficient to produce secondary electron emission from the dynode surfaces of the detector. The use of an electron accelerator also provides the possibility of focussing the photoelectrons into the detector from an ionization region larger than the detector. A new apparatus using this type of detector, with a plane parallel retarding potential analyser, is the next logical step from the present apparatus.

Although an improvement in the resolution of the spectrometer allows a more accurate unfolding of the spectra, the accuracy of the partial cross-sections is still limited by the low energy area in the spectra which results from the reflection of electrons from the surface of the collimating electrode. Further investigation of methods of producing a collimating electrode without this defect is needed.

The possibility of using a parallel plate electrostatic analyser, which was considered in Sec.III.2.1, warrants further investigation. Although the technical problems of using this analyser are very great because of the small number of electrons which may be detected, the advantage of being able to measure the angular distribution of the photoelectrons may also be considerable.

VI.1.2 Further experiments

There are several experiments which require the development of a photoelectron spectrometer with improved resolution and sensitivity. The first is a more detailed examination of the cross-sections which have been measured in the present work. In regions where the structure due to autoionization is strong, the partial cross-sections should be examined as a function of wavelength with a wavelength resolution smaller than

the width of the autoionized bands, thus building a detailed picture of the branching ratios from the quasi-stable states, from which variations in the properties of these states can be observed. The present results indicate that the autoionizing processes in oxygen favour the formation of ions in the ground state rather than the $a^4\Pi_u$ state of the oxygen ion. Improvement of the resolution to the point where the vibrational structure of the bands is resolved would allow accurate measurements of the energy levels to be made, and the relative excitation of the vibrational levels to be studied as a function of wavelength.

It is also desirable that the partial cross-section measurements should be extended to shorter wavelengths. For the purpose of calculating the energy distribution of the primary photoelectrons in the ionosphere, it was assumed that photoionizing processes which correspond to the removal of an inner electron make only a small contribution to the total photoionisation cross-section. This assumption was made in analogy with the calculated cross-sections for the corresponding transitions in atomic oxygen, (Dalgarno et al 1964) but it is necessary that these partial cross-sections should be measured. These measurements also require a more sensitive apparatus than the one used in the present

work, since the light sources which are available in the wavelength region below 600 Å are less intense than the Hopfield continuum source which was used in the present experiments.

Improved resolution is also required for further study of the process of fluorescent autoionization. Such a study would resolve the question of whether the upper quasi-stable state of the fluorescent transition can be associated with the autoionizing levels which appear in the total photoionization cross-section, or whether a much broader state is involved.

Measurement of the angular distribution of the photoelectrons would be valuable for at least two reasons. Firstly, the present measurements of the partial cross-sections are based on the measurements of a sample of the photoelectrons which are emitted in a direction perpendicular to the beam direction, under the assumption that this is a representative sample for all transitions. However, if the angular distribution is not the same for all transitions, then the partial cross-sections are in error, and a correction based on measurements of the angular distributions should be applied. Secondly, since the angular distribution depends on the angular momentum of the photoelectron, (Sec.III.5.1) the angular distribution of the photo-

electrons contains information about the nature of the transition. Photoelectrons emitted by processes of autoionization may be distinguished by a measurement of their angular distribution, which may be different from that of other transitions if the quasi-stable state is sufficiently long lived. (Sec.IV.1.6).

VI.2 Fluorescent Radiation

Some of the experiments which have been performed to study the fluorescence from gases induced by vacuum ultraviolet radiation were outlined in Sec.I.4.8. In the most useful of these experiments, (Judge et al 1963) the fluorescent radiation was dispersed with a low resolution monochromator, and the outlines of several band systems were recognised. The results of these experiments are valuable, and further improvement of the technique should be attempted. In particular, it is desirable that an experiment should be conducted to detect the radiation from fluorescent autoionizing transitions in molecular oxygen. (Sec.IV.1.6)

VI.2.1 Radiation from fluorescent autoionization

At an incident beam wavelength of 800 Å the amount of energy released as radiation in a fluorescent autoionizing transition in molecular oxygen corresponding to the ejection of a 0.5 eV photoelectron is 2.9 eV. If this energy is released as a single photon, then the

wavelength of the fluorescent radiation is in the region of 4300 Å. However, as discussed in Sec. IV.1.6, it is likely that a cascade of fluorescent transitions with an even number of steps occurs. If the number of transitions is two, then one of the photons must have a wavelength no longer than 8600 Å. The fact that previous experimenters have not observed fluorescence in oxygen at incident wavelengths longer than 770 Å may be explained if the radiation from the fluorescent autoionizing transition has a wavelength in the infra-red region where the detectors which were used are insensitive.

An initial experiment to investigate the emission of radiation through fluorescent autoionizing transitions should be conducted using an incident beam with a wavelength near 800 Å, which is intense and not necessarily of good resolution. The detector should be sensitive to infra-red radiation.

An improvement of the technique of dispersing fluorescent radiation would make possible the observation of the fluorescent radiation emitted by molecular oxygen ions in the $^2\Sigma_g^-$ state. If the radiation is produced by transitions to the $A^2\Pi_u$ state, then it has a wavelength in the region of 3600 Å.

This transition seems more probable than the transition to the $a^4\Pi_u$ state which was suggested by Judge et al (Judge et al 1963).

APPENDIX I

Ultraviolet Spectroscopy with a photoelectron spectrometer

Since the photoionization of argon by a monochromatic beam of radiation produces almost monoenergetic photoelectrons, (Sec.III.5) the energy spectrum of the photoelectrons produced by a non-monochromatic beam is the same as the photon energy spectrum of the beam. A photoelectron spectrometer may therefore be used as an ultraviolet spectrometer of moderate resolution, the present spectrometer having a resolution equivalent to 11 Å at a wavelength of 584 Å. It is suggested that an apparatus of this type may be useful as a low cost ultraviolet spectrometer.

Such a spectrometer may find application in rocket borne experiments, although there are several difficulties which must be overcome. An advantage of this spectrometer is the fact that it may have a large aperture if a method of restricting the gas flow from the spectrometer chamber can be devised. Difficulty may also be experienced in devising electronic circuits with time constants which are short enough to allow a sufficiently rapid rate of scan of the retarding potential. A variation of the spectrometer which detects only a fixed range of wavelengths may be constructed as shown in Fig.71. The

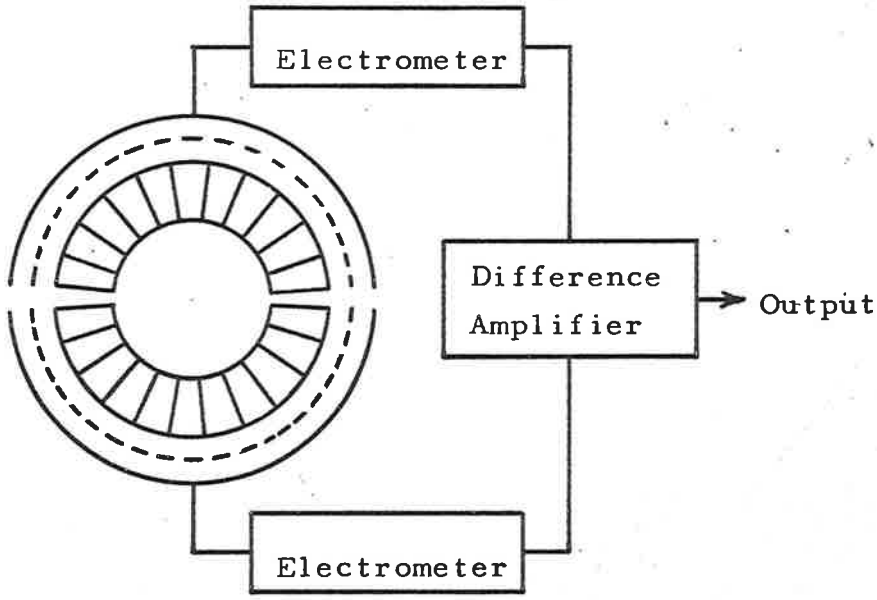

Fig.71. The differential photoelectron spectrometer.

cylindrical electrode structure is split into two sections, and each anode is connected to a separate electrometer. A fixed retarding potential is applied to each section of the spectrometer, each potential corresponding to a limit of the wavelength region which is to be detected. The difference between the electron currents measured by the two electrometers is proportional to the integrated intensity in the wavelength region defined by the difference between the two retarding potentials.

APPENDIX II

Resolution of the analysing grid.

When a wire grid is used as the analysing electrode of a retarding potential analyser, one of the factors which limits the resolution is the variation of the potential of the space between the grid wires from that of the wires. In the following calculation an expression is found for the potential midway between the wires of a grid consisting of parallel wires.

The electrode configuration is shown in Fig.72. The potentials of the cathode, grid, and anode are V_c, V_g, and V_a respectively. An analytic function $W = f(z) = U + iV$ is constructed, where $z = x + iy$. In this field, equipotentials are lines of constant V, and field lines are lines of constant U. The function is constructed by assuming that the grid wires can be simulated by line charges and dipoles placed along their axes. (Bunemann et al 1949). The field strength between the cathode and the grid is:

$$E_c = \frac{V_g - V_c}{a} \qquad (34)$$

and the field strength between the grid and the anode is:

$$E_a = \frac{V_a - V_g}{b} \qquad (35)$$

Thus E_c field lines per unit area arrive at the grid, and

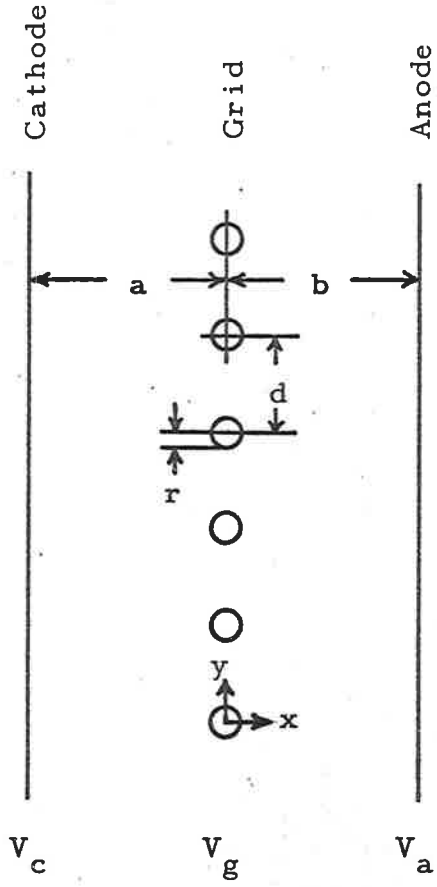

Fig.72. Configuration of the parallel wire analysing grid.

E_a lines per unit area leave it. The number of field lines per unit area arising from the grid is:

$$\Delta E = (E_a - E_c) \tag{36}$$

This implies that line charges of strength $\Delta Ed/4\pi$ are induced on the grid wires. The complex potential function for a unit line charge, periodic over the interval between the grid wires is:

$$W = 2i \log \sinh \frac{\pi z}{d} \tag{37}$$

This function gives approximately circular equipotentials in the vicinity of $z = 0, \pm id, \pm 2id$, etc. Neglecting terms in r^3, the mean potential around a circle of radius r is:

$$2 \log \frac{\pi r}{d} \tag{38}$$

The complex function corresponding to the grid wires at zero potential is:

$$W_L = \frac{\Delta E}{2\pi} id \left(\log \sinh \frac{\pi z}{d} - \log \frac{\pi r}{d}\right) \tag{39}$$

A uniform field E induces a dipole of intensity $\frac{1}{2}Er^2$ at the centre of the grid wires. The complex potential function for this series of dipoles is:

$$W_D = -Er^2 i\left(\frac{\pi}{d}\right) \coth \frac{\pi z}{d} \tag{40}$$

It can be shown (Bunemann et al 1949) that when combined with the uniform field function $W_E = iEz$ this function gives $|z| = r$ as a zero equipotential.

The complete potential function, which has

$|z| = r$, $|z \pm nid| = r$ as equipotentials, with $V=V_g$ is:

$$W = iV_g + W_L + W_D + W_E \tag{41}$$

The potential midway between two grid wires is found by putting $z = i\,d/2$, and evaluating the imaginary part of W. With $z = id/2$:

$$W_L = -\frac{\Delta E}{4}d - i\left(\frac{\Delta E}{2\pi}d \log \frac{\pi r}{d}\right)$$

$$W_D = 0 \tag{42}$$

$$W_E = -Ed/2$$

The potential midway between two grid wires is, therefore:

$$V = V_g - \frac{\Delta E}{2\pi}d \log \frac{\pi r}{d} \tag{43}$$

The point $z = id/2$ represents the minimum potential barrier (Fig.27) only when the fields E_c and E_a are equal and opposite. In general the relevant point lies on the line $z = x + id/2$, but in all cases the error calculated using the point $z = id/2$ is equal to, or bigger than the actual error. In Fig.73 the factor $\frac{d}{2\pi} \log \frac{\pi r}{d}$ is plotted as a function of the number of grid wires per inch for a number of grid wire diameters. The grid used in the photoelectron spectrometer described in Chapter III was constructed of wire mesh, and the potential fluctuation across the surface of the grid was less than that for a parallel wire grid with the same wire separation, and the above calculation provides an upper limit of the potential barrier spread. The potential

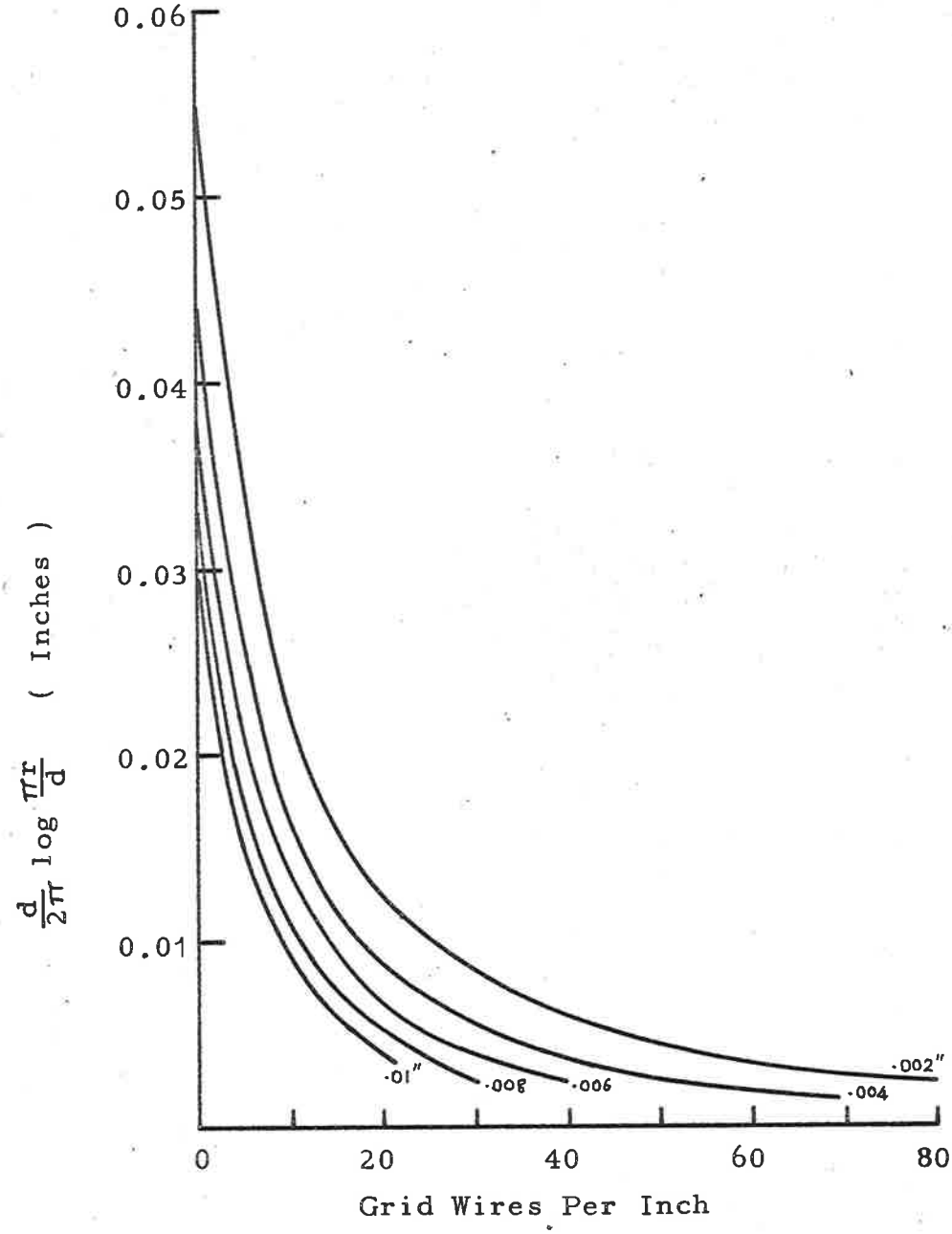

Fig. 73. The factor $\frac{d}{2\pi} \log \frac{\pi r}{d}$ as a function of the grid wire spacing for a number of grid wire diameters.

barrier spread given by this calculation for a peak energy of 5 eV is 0.04 eV.

APPENDIX III

Publications

The following papers have been written on the work described in this thesis;

A.J.Blake and J.W.Carver, 1965, "Partial Photoionization Cross-sections for Molecular Oxygen," Physics Letters 19, 387.

A.J.Blake, J.W.Carver, and G.H.Haddad, "Photo-absorption cross-sections of molecular oxygen between 1250 Å and 2350 Å," to be published 1966, J.Quant.Spectrosc.Radiat.Transfer.

BIBLIOGRAPHY

Al-Joboury, M.I., and Turner, D.W., 1963, J.Chem.Soc., p.5141.

Al-Joboury, M.I., May, D.P., and Turner, D.W., 1965, J. Chem.Soc., p.616.

Allison R., Burns, J., Tuzzolino, A.J., 1964, J.Opt.Soc. Am., 54, 747.

Axelrod, M.N., and Givens, M.P., 1959, Phys.Rev., 115, 97.

Baker, D.J., Beda, D.R., Tomboulian, D.H., 1961, Phys. Rev., 124, 1471.

Bates, D.R., and Massey, H.S.W., 1943, Phil.Trans., A239, 269.

Bethe, H.A., and Salpeter, E.E., 1956, Handbuch der Pysik, Vol.35, Ed.S.Flugge (Berlin: Springer-Verlag).

Beutler, H., 1933, Z.Phys., 86, 710.

Beynon, J.D.E., and Cairns, R.B., 1965, Proc.Phys.Soc., 86, 1343.

Blatt, J.M. and Weisskopf, V.F., 1952, 'Theoretical Nuclear Physics', (London: Chapman and Hall).

Bohr, N., 1913, Phil.Mag., 26, 1.

Bunemann, O., Cranshaw,T.E., and Harvey, J.A., 1949, Can. J.Res., 27, A191.

Cairns, R.B., and Samson, J.A.R., 1965a, J.Geophys.Res., 70, 99.

Cairns, R.B., Samson, J.A.R., 1965b, Phys.Rev., 139, A1403.

Carver, J.H., and Mitchell, P., 1964, J.Scient.Instrum., 41, 555.

Carver, J.H., and Mitchell, P., 1966, To be published, Space Research VI.

Cook, G.R., and Metzger, P.H., 1964a, J.Chem.Phys., 41, 321.

Cook, G.R., and Metzger, P.H., 1964b, J.Opt.Soc.Am., 54, 968.

Cook, G.R., and Ogawa, M., 1965, Can.J.Phys., 43, 256.

Cooper, J.W., 1962, Phys.Rev., 128, 681.

COSPAR INTERNATIONAL REFERENCE ATMOSPHERE, 1965, (Amsterdam: North Holland Pub.Co.)

Dalgarno, A., and Lynn, N., 1957, Proc.Phys.Soc.(Lond.), A70, 802.

Dalgarno, A., McElroy, M.B., Moffett, R.J., 1963, Planet. Space Sci., 11, 463.

Dalgarno, A., Henry, R.J.W., and Stewart, A.L., 1964, Planet.Space Sci., 12, 235.

Dalgarno, A., McElroy, M.B., 1965, Planet.Space Sci., 13, 947.

Dibeler, V.H., Reese, R.M., 1964a, J.Chem.Phys., 40, 2034.

Dibeler, V.H., Reese, R.M., 1964b, J.Res.Nat.Bur.Stds.Am., 68A, 409.

Dibeler, V.H., Reese, R.M., Krauss, M., 1965a, J.Chem.Phys., 42, 2045.

Dibeler, V.H., Krauss, M., Reese, R.M., Harllee, 1965b, J.Chem.Phys., 42, 3791.

Ditchburn, R.W., Bradely, J.T.S., Cannon, C.G., and Munday, G., 1954, 'Rocket Exploration of the Upper Atmosphere', ed. Boyd and Seaton, (London, Permagon Press).

Ditchburn, R.W., 1960, Proc.Phys.Soc. (Lond.), 75, 461 L.

Ditchburn, R.W., 1962, J.Quant.Spectrosc.Radiat.Transfer., 2, 351.

Ditchburn, R.W., and Opik, U., 1962, 'Atomic and Molecular Processes', Ed.D.R.Bates (London, Academic Press).

Ederer, D.L., and Tomboulian, D.H., 1964, Phys.Rev., 133, A 1525.

Fano, U., 1961, Phys.Rev., 124, 1866.

Fano, U., and Cooper, J.W., 1965, Phys.Rev., 137, A1364.

Field, F.H., and Franklin, J.L., 1957, 'Electron Impact Phenomena and Properties of Gaseous Ions', (New York: Academic Press).

Frost, D.C., and McDowell, C.A., 1955, Proc.Roy.Soc.A., 232, 227.

Frost, D.C., and McDowell, C.A., 1958, Can.J.Phys., 36, 39.

Frost, D.C., McDowell, C.A., Vroom, D.A., 1965, Phys. Rev.Letters, 15, 612.

Gilmore, F.R., 1965, J.Quant.Spectrosc.Radiat.Transfer, 5, 369.

Goodrich, G.W., and Wiley, W.C., 1961, Rev.Scient.Instrum. 32, 846.

Hanson, W.B., and Johnson, F.S., 1961, Mem.Soc.R.Sci., Liege, Series 5, 4, 390.

Hartree, D.R., 1957, The Calculation of Atomic Structures, (New York: Wiley).

Hasted, J.B., 1964, 'Physics of Atomic Collisions', (London, Butterworth), p.109.

Healey, R.H., and Reed, J.W., 1941, 'The behaviour of Slow Electrons in Gases', (Sydney: Amalgamated Wireless).

Heddle, D.W.O., 1962, J.Quant.Spectrosc.Radiat.Transfer, 2, 349.

Henry, 1897, Proc.Camb.Phil.Soc., IX, 319 (1897).

Herzberg, G., 1950, 'Molecular Spectra and Molecular Structure. I Spectra of Diatomic Molecules', (New York: Van Nostrand).

Hinteregger, H.E., Hall, L.A., and Schmidtke, G., Space Research V, 1175 (1964).

Hopfield, J.J., 1930, Astrophys J., 72, 133.

Huffman, R.E.H., Tanaka, Y., Larrabee, J.C., (1963a), J.Chem.Phys.39, 902.

Huffman, R.E., Tanaka, Y., Larrabee, J.C., (1963b), J. Chem.Phys., 38, 1920.

Huffman, R.E., Tanaka, Y., and Larrabee, J.C., (1963c), Appl. Opt. 2, 617.

Huffman, R.E., Larrabee, J.C., and Tanaka, Y., 1965, Appl. Opt., 4, 1581.

Hughes, A.L., 1910, Proc.Camb.Phil.Soc., 15, 483.

Hurzeler, Inghram, M.G., Morrison, J.D., 1957, J.Chem. Phys., 27, 313.

Johnson, F.S., Watanabe K., Tousey, R., 1951, J.Opt.Soc. Am., 41, 702.

Johnston, R.G., and Madden, R.P., 1965, Appl.Opt.4, 1574.

Judge, D.L., Morse, A.L., and Weissler, G.L., 1963, 'Sixth International Conference on Ionization Phenomena in Gases, (Paris), Vol.3, p.373.

Kunz, J., and Williams, E.H., 1920, Phys.Rev., 15, 550.

Kunz, J., and Williams, E.H., 1923, Phys.Rev., 22, 456.

Lassettre, E.N., Berman, A.S., Silverman, S.M., and Mrasnow, M.N., 1964, J.Chem.Phys., 40, 1232.

Lenard, P., 1900, Ann.Phys., 1, 486.

Lowry, J.F., Ederer, D.L., and Tomboulian, D.H., 1965, Phys.Rev., 137, A1054.

Losier, W.W., 1930, Phys.Rev., 36, 1285.

Madden, R.P., and Codling, K., 1963, Phys.Rev.Letters, 10, 516.

Madden, R.P., Codling, K., 1964, J.Opt.Soc.Am., 54, 268L.

Madden, R.P., and Codling, K., 1965, J.Appl.Phys., 36, 380.

Matsunaga, F.M., Jackson, R.S., Watanabe, K., 1965, J.Quant.Spectrosc.Radiat.Transfer, 5, 329.

McCowan, J.W., Clarke, E.M., Hanson, H.P., and Stebbings, R.F., 1964, Phys.Rev.Letters, 13, 620.

Metzger, P.H., and Cook, G.R., 1964a, J.Chem.Phys., 41, 642.

Metzger, P.H., and Cook, G.R., 1964b, J.Quant.Spectrosc. Radiat.Transfer, 4, 107.

Metzger, P.H., and Cook, G.R., 1965, J.Opt.Soc.Am., 55, 516.

Miescher, R., and Baer, P., 1952, Nature, 169, 581.

Migneron, R., and Levinger, J.S., 1965, Phys.Rev., 139, A646.

Moore, C.E., 1949, 'Atomic Energy Levels', Nat.Bur. Stand., Circ., 467, Vol.I.

Morrison, J.D., 1962, Institut International de Chimie, Douziemi Conseil de Chimie, Universite Libre de Bruxelles, p.397.

Morrison, J.D., 1964, J.Chem.Phys., 40, 2488.

Mulliken, R.S., 1957, Threshold of Space, (Permagon Press) p.175.

Namioka, T., and Tanaka, Y., 1962, Abstract Symposium on Molecular Structure and Spectroscopy, Science Council of Japan, Tokyo.

Newburgh, P.C., Heroux L., and Hinteregger, H.F., 1962, Appl.Opt.1, 733.

Nicholson, A.J.C., 1963, J.Chem.Phys., 39, 954.

Nicholson, A.J.C., 1965, J.Chem.Phys., 43, 1171.

Packer, D.M., and Lock, C., 1951, J.Opt.Soc.Am., 41, 699.

Perry-Thorne, A., Garton, W.R.S., 1960, Proc.Phys.Soc. (Lond.), B76, 833.

Piech, K.K., and Levinger, J.S., 1964, Phys.Rev., 135, A332.

Po Lee, and Weissler, G.L., 1952, J.Opt.Soc.Am., 42, 214 L.

Po Lee, 1955, J.Opt.Soc.Am., 45, 703.

Po Lee, Weissler, G.L., 1955, Phys.Rev., 99, 540.

Preston, W.M., 1940, Phys.Rev., 57, 887.

Price, W.C., and Collins, G., 1935, Phys.Rev., 48, 714.

Rudd, M.E., 1964, Phys.Rev.Letters, 13, 503.

Rustgi, O.N., 1964, J.Opt.Soc.Am., 54, 464.

Rustgi, O.N., Fisher, E.I., Fuller, C.H., 1964, J.Opt. Soc.Am., 54, 745.

Samson, J.A.R., 1963, Phys.Rev., 132, 2122.

Samson, J.A.R., 1964a, J.Opt.Soc.Am., 54, 876.

Samson, J.A.R., 1964b, J.Opt.Soc.Am., 54, 420 L.

Samson, J.A.R., 1964c, J.Opt.Soc.Am., 54, 842 L.

Samson, J.A.R., 1964d, J.Opt.Soc.Am., 54, 6.

Samson, J.A.R., and Cairns, R.B., 1964, J.Geophys.Res., 69, 4583.

Samson, J.A.R., 1965, J.Opt.Soc.Am., 55, 935.

Schoen, R.I., Judge, D.L., and Weissler, G.L., 1961, Fifth International Conference on Ionisation Phenomena in Gases (Munich), p.25.

Schoen, R.I., 1964, J.Chem.Phys., 40, 1830.

Seaton, M.J., 1951, Proc.Roy.Soc.(Lond.), A208, 418.

Seaton, M.J., and Osterbrock, D.E., 1957, Astrophys.J. 125, 66.

Sewell, K.G., 1965, Phys.Rev., 137, A418.

Smith, A.M., 1961, Thesis, Institute of Optics, University of Rochester.

Sommerfeld, A., 1930, 'Wave Mechanics' (London:Methuen), p.181.

Stewart, A.L., and Webb, T.G., 1963, Proc.Phys.Soc. (Lond.), 82, 532.

Tanaka, Y., 1942, Sci.Pap.Inst.Phys.Chem.Res.(Tokyo), 39, 465.

Tanaka, Y., and Takamine, T., 1942, Sci.Pap.Inst.Phys. Chem.Res.(Tokyo), 39, 437.

Tanaka, Y., Jursa, A.S., and Le Blanc, F.J., 1958, J.Opt.Soc.Am., 48, 304.

Tanaka, Y., Huffman, R.E., and Larrabee, J.C., 1962, J.Quant.Spectros.Radiat.Transfer, 2, 451.

Tohmatsu, T., Ogawa, T., and Tsuruta, H., 1965, Rep. Ionos.Space Res. Japan, 19, 482.

Vilesov, F.I., Kurbatov, B.L., and Terenin, A.N., 1961, Soviet Physics - Doklady, 6, 490.

Wacks, M.E., and Krauss, M., 1961, J.Chem.Phys., 35, 1902.

Wainfan, N., Walker, W.C., Weissler, G.L., 1955, Phys. Rev., 99, 367.

Wannier, G.H., 1955, Phys.Rev., 100, 1180.

Watanabe, K., Inn, E.C.Y., 1953, J.Opt.Soc.Am., 43, 32.

Watanabe, K., Marmo, F.F., Inn, E.C.Y., 1953a, Phys.Rev. 91, 1155.

Watanabe, K., Inn, E.C.Y., and Zelikoff, M., 1953b, J. Chem.Phys., 21, 1026.

Watanabe, K., 1954, J.Chem.Phys., 22, 1564.

Watanabe, K., Marmo, F.F., 1956, J.Chem.Phys., 25, 965.

Watanabe, K., 1957, J.Chem.Phys., 26, 542.

Watanabe, K., 1958, Adv.Geophys., 5, 157.

Watanabe, K., and Matsunaga, F.M., 1961, Hawaii Inst. Geophys., Contrib.27, Honolulu.

Watanabe, K., and Jursa, A.S., 1964, J.Chem.Phys., 41, 1650.

Waugh, J.B.C., Lovering, J.F., and Graf, G.R., 1964, Proc. I.R.E.E. Aust., 25, 174.

Weissler, G.L., 1956, Handbuch der Physik, Vol.21, Ed. S.Flugge (Berlin: Springer-Verlag).

Weissler, G.L., Samson, J.A.R., Ogawa, M., and Cook, G.R., 1959, J.Opt.Soc.Am., 49, 338.

Wigner, E.P., 1948, Phys.Rev., 73, 1002.

Wilkinson, P.G., and Byram, E.T., 1965, Appl.Opt., 4, 581.

Wilson, C.T.R., 1899, Phil.Trans.Roy.Soc.Lond., A192, 403.

Wood, R.W., 1911, Phys.Opt., p.513.